TIME-DEPENDENT NEUTRON AND PHOTON DOSE-FIELD ANALYSIS

A Thesis

Presented to

The Academic Faculty

By

Hasani Omar Wooten

In Partial Fulfillment

Of the Requirements for the Degree

Doctor of Philosophy in Nuclear and Radiological Engineering

Georgia Institute of Technology

August 2005

TIME-DEPENDENT NEUTRON AND PHOTON DOSE-FIELD ANALYSIS

Approved by:

Dr. Nolan E. Hertel, Advisor
Nuclear and Radiological Engineering
Georgia Institute of Technology

Dr. C.-K. Chris Wang
Nuclear and Radiological Engineering
Georgia Institute of Technology

Dr. Ratib Karam
Nuclear and Radiological Engineering
Georgia Institute of Technology

Professor Emeritus Donald J. Dudziak
Nuclear Engineering
North Carolina State University

Professor Eva K. Lee
Industrial Systems Engineering
Georgia Institute of Technology

Dr. Drew E. Kornreich
Los Alamos National Laboratory

Date Approved: June 22, 2005

Dedicated to my aunt,

Beulah “Bea” Payne Lax

and

in memory of

Professor Julia Ann Thompson

ACKNOWLEDGEMENT

I am extremely appreciative of my academic advisor and good friend during graduate school, Dr. Nolan Hertel. His experience, intuition, and knowledge have been tremendous resources for me over the past six years, and I am grateful to have had the opportunity to work with and learn from him.

Throughout this research, a number of individuals have been of great assistance. Drs. John Hendricks, Bob Little, and Kent Parsons at Los Alamos often dropped what they were doing to explain concepts, look at my data, and make suggestions. I also wish to thank Dr. Tom Farish for his interest and support of this work, and the members of the Systems Modeling and Analysis group at Los Alamos for making me feel more like a colleague than a student. Dr. Drew Kornreich, the author of the original Pandemonium code, has been invaluable help for this entire project, and I continually admire his intellect, and his ability to remain calm in stressful situations. To Drs. Chris Wang, Ratib Karam, and Eva Lee, I thank you for taking an interest in this research and participating on my thesis committee.

A very special thanks goes to my Los Alamos mentor and good friend, Dr. Donald Dudziak and his wife Judy for all of their support, technical and beyond, for the past two years. Thanks Don for sharing your knowledge and wisdom, postulates on life and politics, unforgettable lunch discussions, your patience during my learning process, and for so many trips to visit while I sat at TA-52. This thesis would be nonexistent without your valued help.

There is no way I would have made it this far without the support of my friends at Georgia Tech and Los Alamos. Special thanks to Carmen Greene for our countless conversations on everything and nothing, neologisms, and your friendship. To the other NRE students who made study sessions and Friday night penny poker so much fun, I extend my thanks for being pleasant and welcome distractions during the rigorous graduate school experience. To recently-graduated Drs. Jeremy Sweezy, Michele Sutton-Ferenci, and Karen Kelley, thank

you all for allowing me to help you guys with your projects, for always answering my many questions, and for providing inspiration over the years.

To Mom, Dad, Tiffany, and all of my extended family, for all your love and support over the years, thank you so much. Though not specifically listed, I sincerely appreciate the support I have received from many other friends, colleagues, and family. Your contributions are not forgotten.

Lastly, for their investment in this young researcher, I gratefully acknowledge the Georgia Institute of Technology and the National Science Foundation.

TABLE OF CONTENTS

LIST OF TABLES

LIST OF FIGURES

SUMMARY

A unique tool is developed that allows the user to model physical representations of complicated glovebox facilities in two dimensions and determine neutral-particle flux and ambient dose-equivalent fields throughout that geometry. The Pandemonium code, originally designed to determine flux and dose-rates only, is improved to include realistic glovebox geometries, time-dependent source and detector positions, time-dependent shielding thickness calculations, time-integrated doses, a representative criticality accident scenario based on time-dependent reactor kinetics, and more rigorous photon treatment.

A primary benefit of this work has been an extensive analysis and improvement of the photon model that is not limited to the application described in this thesis. The photon model has been extended in energy range to 10 MeV to include photons from fission and new photon buildup factors have been included that account for the effects of photon buildup at slant-path thicknesses as a function of angle, where the mean free path thickness has been preserved.

The overall system of codes is user-friendly and it is directly applicable to facilities such as the plutonium facility at Los Alamos National Laboratory, where high-intensity neutron and photon emitters are regularly used. The codes may be used to determine *a priori* doses for given work scenarios in an effort to supply dose information to process models which will in turn assist decision makers on ensuring as low as reasonably achievable (ALARA) compliance. In addition, coupling the computational results of these tools with the process model visualization tools will help to increase worker safety and radiological safety awareness.

CHAPTER 1 INTRODUCTION

1.1 Background

The handling of plutonium and uranium remains an integral component of the U.S nuclear stockpile stewardship program. Prior to 1946, plutonium purification at Los Alamos National Laboratory was performed in open-faced hoods and workers were protected by means of respiratory equipment and protective clothing. Not until a number of workers showed evidence of internal contamination via urine samples were the chemical processes moved to enclosed gloveboxes. Enclosed gloveboxes resulted in additional worker protection and provided an enclosed environment for plutonium sources [1]. Over the next eight years, glovebox designs proceeded through several iterations, each of which attempted to balance space and convenience for the worker. By 1956, a somewhat modular design was implemented that allowed for project-dependent configuration.

As plutonium processing increased through the latter half of the 20th century, improvements in chemical separation technology led to further developments in glovebox design to support new equipment and environmental controls. Safety measures such as bell-jars were introduced into gloveboxes that allow workers to quickly extinguish fires, and airflow was designed with negative pressure to prevent the escape of harmful fumes.

Today, plutonium processing continues much in the same manner. Large plutonium R&D facilities exist that contain rooms of glovebox "trains" manned by workers. The work done at such facilities is limited by several factors, most importantly worker safety, and in particular, radiological safety. The radiation dose received by the worker depends on the source characteristics (nuclides, emitted radiation types and energies, material form, and density) and the shielding between the worker and the sources. Dose originates not only from sources in the worker's glovebox but potentially from all other sources in the facility. To further complicate the problem, it must be recognized that any such facility is transient in nature. Thus, between any given points in time, the source characteristics may be different (due to radioactive decay, or as a result of the work done upon the source during a process),

and the shielding parameters may differ (due to source and detector motion about the room). Radiation exposure within such facilities can be minimized if specific tasks can be analyzed from a radiation dosimetry perspective prior to commencement. Thus, facility managers devote substantial resources toward process modeling in efforts to keep worker doses below ALARA (As Low As Reasonably Achievable) limits. The development of tools to model radiation facilities and complex radiation fields is not new.

A variety of radiation transport codes exist with which such modeling can be performed. The Monte Carlo N-Particle (MCNP) [2] and MCNPX [3] codes use stochastic methods to simulate particle transport using libraries of particle interaction cross sections. The benefit of MCNP is its ability to model complex geometries and source configurations. Other codes use deterministic methods based on solving the neutron transport equation numerically. For example, the code ONEDANT [4] solves the one-dimensional Boltzmann equation using the discrete-ordinates method. The major benefit of deterministic codes is their ability to completely describe neutron fluxes and currents at every point in the modeled system. Unfortunately, the aforementioned codes and others often require the user to master the operation of the code itself; that is, years may be spent developing the skills needed to fully understand the code's inputs, outputs, and methods so that the user can interpret the results in relation to the user's intent. Furthermore, the complexity of the input files and the length of time required for these codes to run are often proportional to the complexity of the problem.

This thesis develops a method that accurately predicts time-dependent neutral particle dose fields using two-dimensional physical and one-dimensional calculational models. The method produces reliable calculations of sufficient accuracy for planning and training purposes within a fraction of the time needed by sophisticated three-dimensional methods. The method is designed to compute doses in glovebox processing facilities, and it also addresses the scenario of accidental criticality for use in training glovebox workers in the safe handling of nuclear materials.

It should be mentioned that references to "dose" are more accurately described as dose equivalents, determined by multiplying the particle flux by a flux-to-dose equivalent

conversion coefficient. For ease of presentation, future references to "dose" will be understood to imply ambient-dose equivalent.

1.2 Current modeling techniques

Experts in radiation transport in both industry and government worldwide have developed modeling codes for every aspect of nuclear design and technology. As a result, there is no shortage of general purpose shielding software that could indeed be applied to the problem of determining dose fields given a room full of sources and gloveboxes. For such a particular application, a brief analysis of the components of the problem is presented.

The question is posed: how does one successfully model a transient nuclear processing facility from a radiation dose perspective? Several key components are identified. First, one must have sufficient detail about the facility's geometric layout. The physical model is an important consideration given that facilities can range in size from several feet to several hundred feet in length and width, and such details often play a substantial role in deciding which currently-existing tools one may employ. Of equal significance to layout is how the work is done. For example, a glovebox facility differs greatly in its processes than does a waste or recycling plant, and therefore the contents of the facility may add considerable complexity to its geometry. One also needs information regarding radiation type, source strengths, and energy spectra of source material. Several codes in existence are useful where primary radiological hazards exist from photons only, such as the point kernel codes MicroShield [5] and QAD [6], which both analyze photon transport. But such codes would be insufficient for areas where neutron fluxes are major contributor to total dose. Further, details as to shielding materials located throughout the facility and information on the transient nature of the facility are needed for typical calculations, particularly in determining time scales upon which calculations are to be based. Two examples of facilities requiring different methods and tools would be (a) a radiation detection laboratory on a university campus (b) a fuel reprocessing plant. Both examples contain vastly different radiological conditions requiring different tools to conveniently model the radiation fields.

MCNP or MCNPX offers users the most general usage capability in terms of geometry and source definitions. However, it requires extensive familiarity with transport phenomena, cross sections, geometry specifications, variance reduction techniques, and tally estimators. The time required to perform calculations using MCNP can reach hours, days, and even weeks in computer time for complex problems (such as rooms full of gloveboxes and sources). Deterministic transport equation solvers, such as ONEDANT, that discretize space for the purpose of solving the Boltzmann equation are excellent tools for analysis of critical dimensions and flux determinations of regular geometry systems. More complex systems can be modeled, but this also requires extensive effort. Although somewhat computationally faster than Monte Carlo, deterministic methods are limited to cruder geometric representations. In addition, deterministic codes, when modeling systems that contain areas of low density (such as air) in 3-dimensional geometry, are very susceptible to abnormalities inherent within the calculational techniques, such as ray effects.

1.3 Pandemonium 1.0

To answer the posed question, Kornreich and Dooley developed a modeling system that reasonably predicts neutral particle dose rates in a complicated glovebox facility [7-8]. The code, Photon and Neutron Dose Equivalent Model of Nuclear Materials in Uncomplicated Geometry Models (Pandemonium) is a time-independent modeling system that determines dose rates in a facility based upon user-supplied source characteristics and geometrical layout of gloveboxes. The code was shown to compare well with Monte-Carlo simulations and experiments given the level of approximation. Features of Pandemonium such as many of the applied theories for neutron and photon transport support the need for the code to obtain answers quickly when compared to the code's more widely used and rigorous counterparts. As a time-independent model, Pandemonium 1.0 calculates dose-equivalent rates for both neutrons and photons. Thus, the model substitutes a stationary situation for what is, in reality, a dynamic scenario. A complete description of the physics included in Pandemonium is provided in the above references. Herein, however, a summary of major features is presented and details pertinent to this research are thoroughly discussed in later chapters.

For neutrons, the code uses one-group diffusion theory to determine the neutron current at the surface of spherical sources, where the neutrons originate from spontaneous fission and (α,n) reactions between decaying transuranic isotopes and low-Z materials (i.e., many sources are mixtures such as PuO_2). Other sources of neutrons such as (n,2n) are not considered. For neutronic calculations in Pandemonium, cross-section data are chosen under the assumption that (α,n) neutrons exist at an energy between 4 and 5 MeV, while spontaneous fission neutrons are created at an energy of 2 MeV. For shielding materials available in the code (lead, steel, and air), neutrons are assumed to retain their initial energy. However, for water shielding, moderation effects are accounted for by the application of numerical fits relating neutron dose to thicknesses of water shields based upon discrete-ordinates calculations.

An extensive photon model was developed in Pandemonium for photons between the energies of 10 keV and 1 MeV. Although not formally a multigroup model in the traditional use of the term, Pandemonium's photon group structure consists of 17 'bins' in which photon calculations occur. The major difference between this code and others is that Pandemonium includes no intra-group communication. That is, photons originating in one energy bin remain in that bin for the length of the calculation. Photon attenuation occurs in each bin to reduce the numbers of photons surviving as they pass though shielding, and photon buildup factors are applied to account for scattered photons. Photon sources are determined from a library of mass-normalized photon source strengths for the various transuranic isotopes that compose the source. With an upper limit of 1 MeV, the code ignores higher energy fission photons.

1.4 Purpose and scope of study

For Pandemonium to be of greater practical use, several improvements to Pandemonium have been implemented which more accurately represent the particle fluxes and dose rates at detector positions, and that make the code more useful in the planning of radiological work. These items may be categorized as follows:

(1) geometry improvements,

(2) time-dependence, and

(3) photon model improvements,

each of which will be individually discussed in this thesis.

Pandemonium 1.0 represented gloveboxes as two-dimensional rectangular shells of lead, stainless steel, and hydrogenous shielding. Sources are modeled as solid spheres and spherical shells of user-defined radii, and modeling is done at the plane of work, defined to be the height above the floor where the worker's dosimeter is located (assumed to be the same for all workers). Detectors, or positions in 2-D space, are located in the same plane through the room. The 2-D modeling translates into one-dimensional spherical and slab geometry calculations. This work introduces a series of more realistic 2-D glovebox models based on blueprints of gloveboxes in use at Los Alamos. As a result, more accurate estimates of shielding thicknesses between sources and detectors are possible, as new models account for realistic features of gloveboxes such as windows and gloveports.

Work included in this thesis creates a time-dependent version of Pandemonium such that calculations can support the dynamic and transient nature of nuclear facilities. By introducing time as a variable, sources and detectors are allowed to change positions throughout the scenario, and corresponding changes in shielding are determined. Furthermore, in addition to dose rates, a time-integrated total dose calculation is performed, allowing the user to obtain valuable information about doses received during a specific process, rather than at a particular instant in time. Also, a simple criticality model has been implemented for the sole use of exemplifying to radiological workers the basics of criticality safety, and what happens to one's dose in the presence of a criticality accident.

The photon modeling capability of Pandemonium has been extensively improved and builds upon previous efforts in the scientific literature. The maximum energy range has been expanded from 1 MeV to 10 MeV, allowing for the inclusion of highe energy fission photons. An exhaustive literature review of thin-shield angular photon buildup factors has been conducted and the results included in the new version of the code. The study includes the most recent photoatomic cross-section data available and includes comparisons of

photon buildup for different transport calculation techniques. The results of this study, slant-path buildup factors, are of interest not only to users of Pandemonium but to the larger radiation shielding community.

The Pandemonium system includes a more user-friendly and extensive interface. The code, originally composed in FORTRAN 77, has been translated into C++ so that it can be coupled with another simulation suite under development at Los Alamos. Throughout this work, a number of minor modifications have been performed that allow the code to make use of newer data for cross sections, mass-normalized source strengths, and flux-to-dose equivalent conversion coefficients.

CHAPTER 2 GEOMETRIC IMPROVEMENTS TO PANDEMONIUM

The modeling capabilities of Pandemonium are two-fold. First, physical representations of a glovebox layout, source specifications, and detector locations are modeled in Cartesian 2-D geometry, and the plane of the model is assumed to be roughly equal to the height of the worker's external dosimeter. This allows for the calculation of shield layers and thicknesses between each source-to-detector pair. Once this model is designed, Pandemonium 1.0 uses a 1-D spherical diffusion theory model to calculate neutron current at the source surface and point-kernel techniques to determine neutron/photon fluxes at the detectors.

Version 1.0 of the code has been modified in Version 2.0 to include more realistic (i.e., blueprint based) geometrical glovebox models. The improvements include the introduction of a separate 2-D geometry calculator, ShieldCALC. This chapter outlines a description of version 1.0 geometry, thereby introducing reasons for why geometry improvements are needed. A detailed description of ShieldCALC calculations is followed by explanations of updates in the Pandemonium source code and Visio® Visual BASIC macro.

2.1 Justification for improvements in the physical geometry

In version 1.0 of Pandemonium, gloveboxes were represented by rectangular slabs of lead and steel, arranged as shown in Figure 2.1a, with the total length and width dimensions being decided by the user. The most important benefit from using such a model is that shield thickness calculations for this simple case are straightforward, especially given that all gloveboxes are the same, save for the width and height dimensions and thicknesses of lead and steel. Unfortunately use of this simple glovebox model results in serious overestimates in shielding and generally has little resemblance to an actual glovebox.

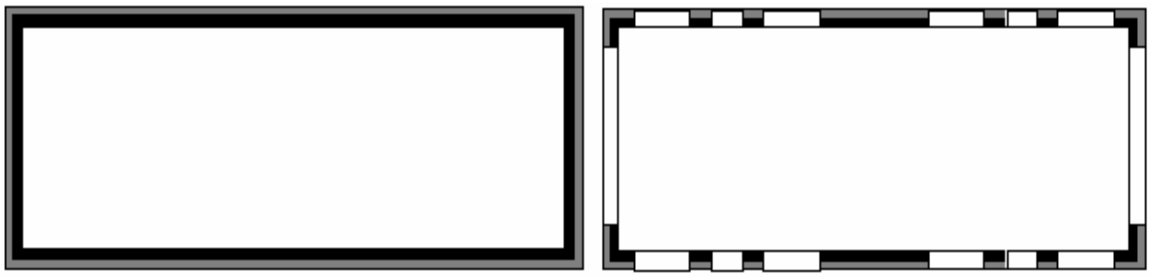

Figure 2.1. (a) Glovebox geometry in Pandemonium 1.0, and (b) more realistic proposed glovebox geometry accounting for gloveports and windows.

Kornreich and Dooley compared Pandemonium calculations with prior measurements at Los Alamos and they found that Pandemonium calculations can be up to an order of magnitude lower than measured neutron and photon dose rates. In addition to the errors introduced by the lack of detail available about the source characteristics, the authors note their glovebox model inherently overestimates the shielding.

In most gloveboxes, gloveports provide the worker with access to the inside of the glovebox and, depending on the use of the glovebox, the ports may be closed with leaded rubber gloves. Furthermore, windows composed of leaded glass allow the worker to observe the activities inside of gloveboxes. A typical realistic glovebox is shown in Figure 2.2.

Figure 2.2. Example of a collection of gloveboxes upon which proposed model is based. Windows and gloveports represent material inhomogeneities not previously modeled.

Most gloveboxes are much more complicated than shown in Figure 2.1a, and they are made of more materials than just lead and steel. It is expected that improving the geometry calculations to include gloveports and windows will reduce calculated lead and steel thicknesses.

2.2 The ShieldCALC geometry calculator

For the new version of Pandemonium, the geometry calculating portion of the code has been removed and developed as a separate code, ShieldCALC. ShieldCALC performs shielding thickness calculations for each source-to-detector pair not only for the original geometry shown in Figure 2.1a, but for the entire revised glovebox models shown in Figure 2.1b and Figure 2.3.

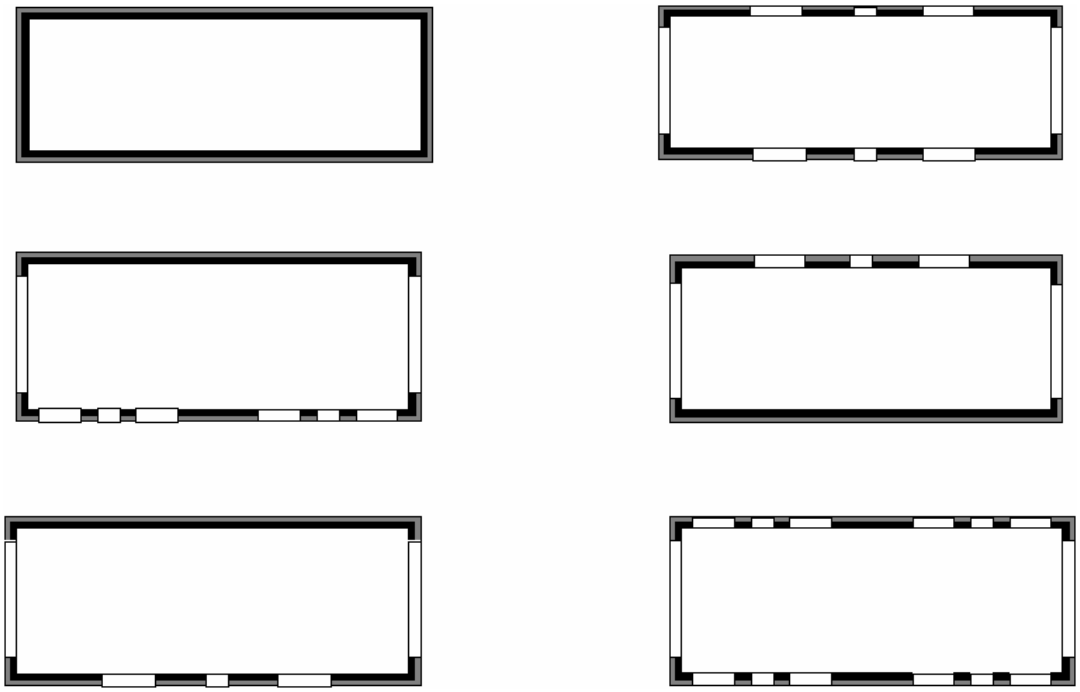

Figure 2.3. Realistic glovebox options for Pandemonium 2.0. Not shown is the 'trunk-line' glovebox that has three workstations on either side.

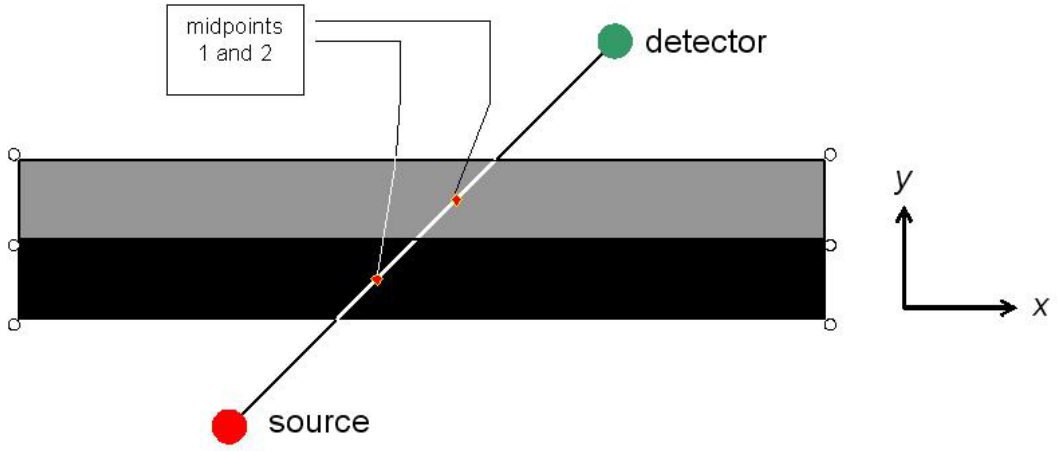

Figure 2.4. Coordinate system, vertices, and midpoints used in new geometry.

Glovebox details such as window and gloveport positions and widths are calculated directly from blueprint drawing of gloveboxes in use at Los Alamos [9]. Gloveboxes can be rotated in increments of 90° in either direction, and this angle is used by ShieldCALC to rotationally

transform the necessary gloveboxes. Lead shielding is assumed to be always located on the inner side the stainless steel layer of the glovebox. ShieldCALC uses the following procedure to determine widths and materials of shields between each source-to-detector pair.

A vertex (shown as small circles in Figure 2.4) is defined to be the intersection of two segments comprising a physical surface of the glovebox (see below). For each glovebox, ShieldCALC uses the position (defined to be the x and y coordinates of the glovebox center), dimensions, type, and lead and steel thicknesses to calculate the x and y positions of each vertex of the glovebox of that specific type. The number of vertices range from 12 for the windowless glovebox to 180 vertices for the trunkline type glovebox.

For those gloveboxes with an angle of rotation (increment of ± 90°), ShieldCALC converts the angle to radians, then performs the following transformation on all vertices.

$$x' = R\cos(\theta_{rot} + \theta_o) + x_{GB} \qquad (2.1)$$
$$y' = R\sin(\theta_{rot} + \theta_o) + y_{GB}$$

where,

R = $\sqrt{(x_o - x_{GB})^2 + (y_o - y_{GB})^2}$

x_{GB}, y_{GB} = glovebox position

x_o, y_o = vertex position

θ_{rot} = specified angle of rotation

θ_o = $\tan^{-1}\left[\frac{y_o - y_{GB}}{x_o - x_{GB}}\right]$

Segments exist between certain vertices where physical material boundaries exist. ShieldCALC determines the endpoint coordinates (x and y positions) of all horizontal and vertical segments and writes this data to file for later use. Segments play an important role in the geometry calculations as they can be intersected by source-to-detector lines. In the event that gloveboxes are rotated by

$$\pm n \cdot \left(\pi/2\right) \text{ for odd } n,$$

horizontal segments become vertical, and vice-versa. ShieldCALC recognizes this situation and reclassifies the vertices as horizontal or vertical as appropriate. The number of segments per glovebox ranges from 12 (windowless glovebox) to 208 (trunkline).

When a source-to-detector line (Figure 2.4) intersects two segments, the midpoint between these intersections is calculated. The coordinates of this midpoint are compared to pre-defined "space declarations" determined by ShieldCALC to identify the material in which the midpoint is located. Glovebox shielding is represented by multiple rectangular slabs of lead and stainless steel. In addition, window and gloveport regions have been included such that a given source-to-detector line may intersect multiple regions of lead, stainless steel, air, and window material and gloveport material (both of which are currently, air). In Cartesian coordinate systems, a rectangular region in space is uniquely defined by two opposite corners, $(x_{\min}, y_{\min})$, and $(x_{\max}, y_{\max})$. Consequently, the rectangular slabs of shielding are also defined by the appropriate vertices. For the given glovebox type, ShieldCALC uses the appropriate vertices as the two points required to declare the slab and material type. If a midpoint is found to lie outside of the declared spaces (including lead, steel, window, gloveport, and polyshield), the midpoint is assumed to be located in air.

The prior explanations form the information foundation that ShieldCALC uses to calculate shielding thicknesses. Knowledge of the vertices, segment, and spatial regions allow the code to calculate any segment intersections along the source-to-detector line. Elementary point-slope formulism is extensively used to determine which segments are intersected for each source-to-detector line, and to determine the coordinates of these intersections. All calculated intersections are either in order of increasing x, or in the event that the source and detector have the same x coordinate, calculations are performed in order of increasing y.

Following the calculation of the n intersection points, for all n, the n^{th} and n^{th}+1 intersections coordinates are used to determine the distances between intersections. The midpoints coordinates are also calculated using Equation (2.2).

$$x_{mid,n} = \left(\frac{x_n + x_{n+1}}{2} \right), \quad y_{mid,n} = \left(\frac{y_n + y_{n+1}}{2} \right) \qquad (2.2)$$

All midpoints are compared to the spatial declarations, and the end result is a series of shield thicknesses and materials that is readable by Pandemonium.

Although ShieldCALC tracks the ordering of shielding, this ordering is not considered in Pandemonium calculations, where the total shielding of each material is used. Future work should consider the impacts of shielding order or buildup factors, but this is beyond the scope of this study.

The input file that ShieldCALC uses to calculate the geometry and shielding thicknesses is supplied by the user via one of two ways. The first, and less often used method, would be for the user to create the input file using a text editor. This requires the user to be familiar with the input file format. Alternatively, the user may use the supplied Microsoft Visio® template files which contain a macro written in Visual BASIC. The user then simply draws the glovebox, source, and detector arrangement using classic Microsoft Windows® drag-and-drop techniques, supplies the appropriate source characteristics, and then runs the macro. An example layout is shown in Figure 2.5. The macro output consists of an ASCII text file that forms the input for ShieldCALC and Pandemonium 2.0 (Figure 2.6). This method has several advantages. Of course, the user requires no details about the file format, thereby saving time and effort in learning this material. Secondly, drag and drop, resizing, and altering icons save a great deal of time, saving the user from performing coordinate calculations on a separate spreadsheet. It is recommended that users refrain from writing their own files, thus, allowing the macro to perform this task. The format of the Visio® macro output is presented below.

After the user draws the geometry in Visio®, the supplied macro converts the glovebox dimensions, positions of the sources and detectors, and source details into an ASCII text file

readable by both the ShieldCALC and Pandemonium executables. The format of this output is relatively simple. The Visio® output consists of five general data fields: General, Glovebox, Polyshield, Detector, and Source.

The General Data field consists of two lists. The first contains the number of gloveboxes in the given scenario, the number of hydrogenous shields, the number of sources, and number of detectors. The second lists an integer representing the type of glovebox for each glovebox being modeled. Currently, gloveboxes consist only of lead and steel, i.e., leaded rubber gloves and leaded glass have not yet been modeled. Regions inside and outside the glovebox, as well as gloveports and windows, are assumed to consist of air.

The Glovebox Data field consists of three sub-fields. For each glovebox, its x and y center coordinates are listed, followed by its angle of rotation. Next, for each glovebox, the outer dimensions (width and depth) are listed in units of feet. The third sub-field lists, for each glovebox, the lead and stainless steel shielding thicknesses in centimeters. These units, though different, are consistent with facility layouts and blueprints used to design glovebox models.

The Polyshield Data field lists, for each hydrogenous shield, the x and y coordinates for the shield, followed by the shield's dimensions (width and depth). The Detector Data field lists, for each detector, its position (x, y) in feet.

The Source Data field begins with a description of the field contents and it is provided for those who wish to manually create their own input files. For each source, its position coordinates are followed by the source outer and inner radii. Next, the number densities for the nine source nuclides (^{238}Pu, ^{239}Pu, ^{240}Pu, ^{241}Pu, ^{242}Pu, ^{241}Am, ^{233}U, ^{235}U, ^{238}U) are followed by atomic numbers and number densities for four low-Z target nuclides (for [α,n] neutrons). Lastly, in the event the source is surrounded by a low-Z shield, two source-shield atomic numbers and thicknesses are listed.

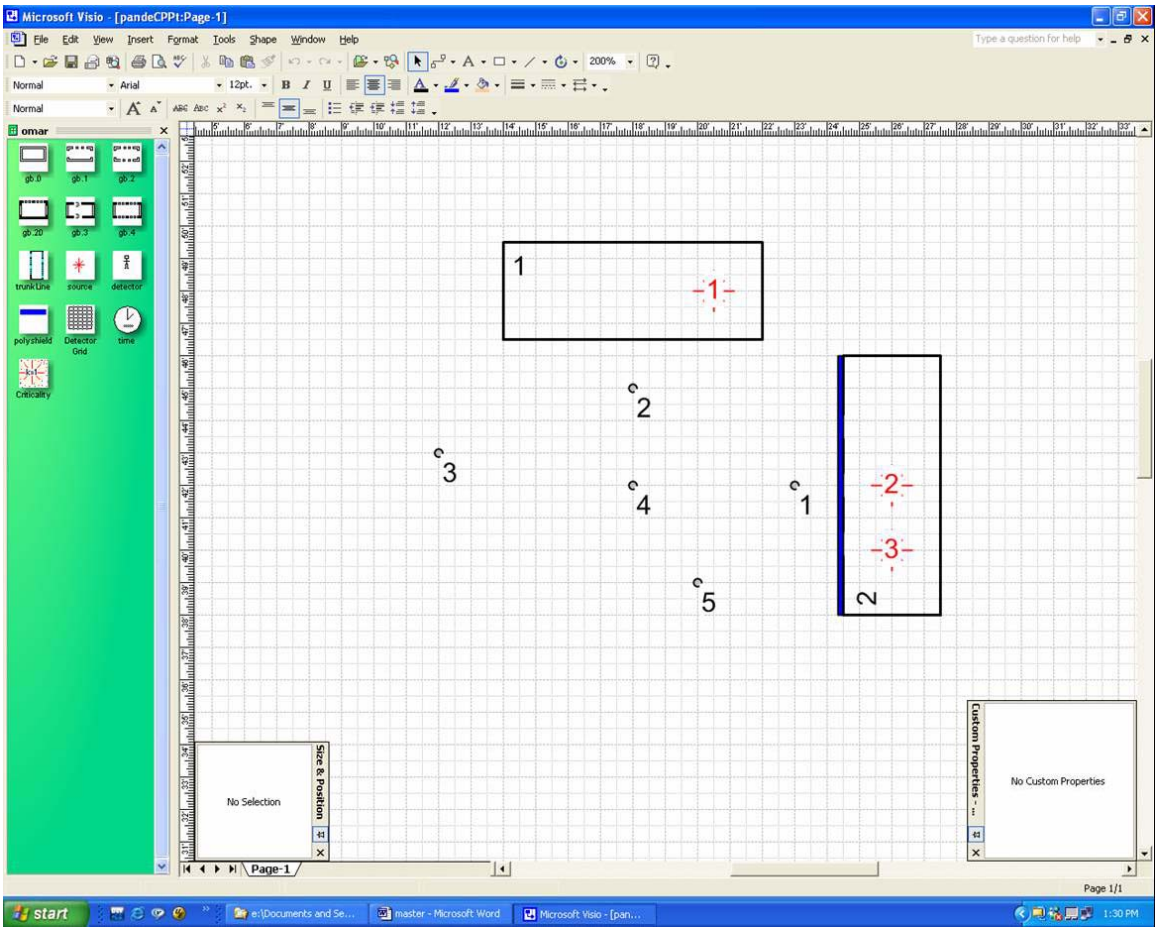

Figure 2.5. Screen capture of a typical Pandemonium input scenario in Visio® showing two gloveboxes, two sources, one detector, and one polyshield.

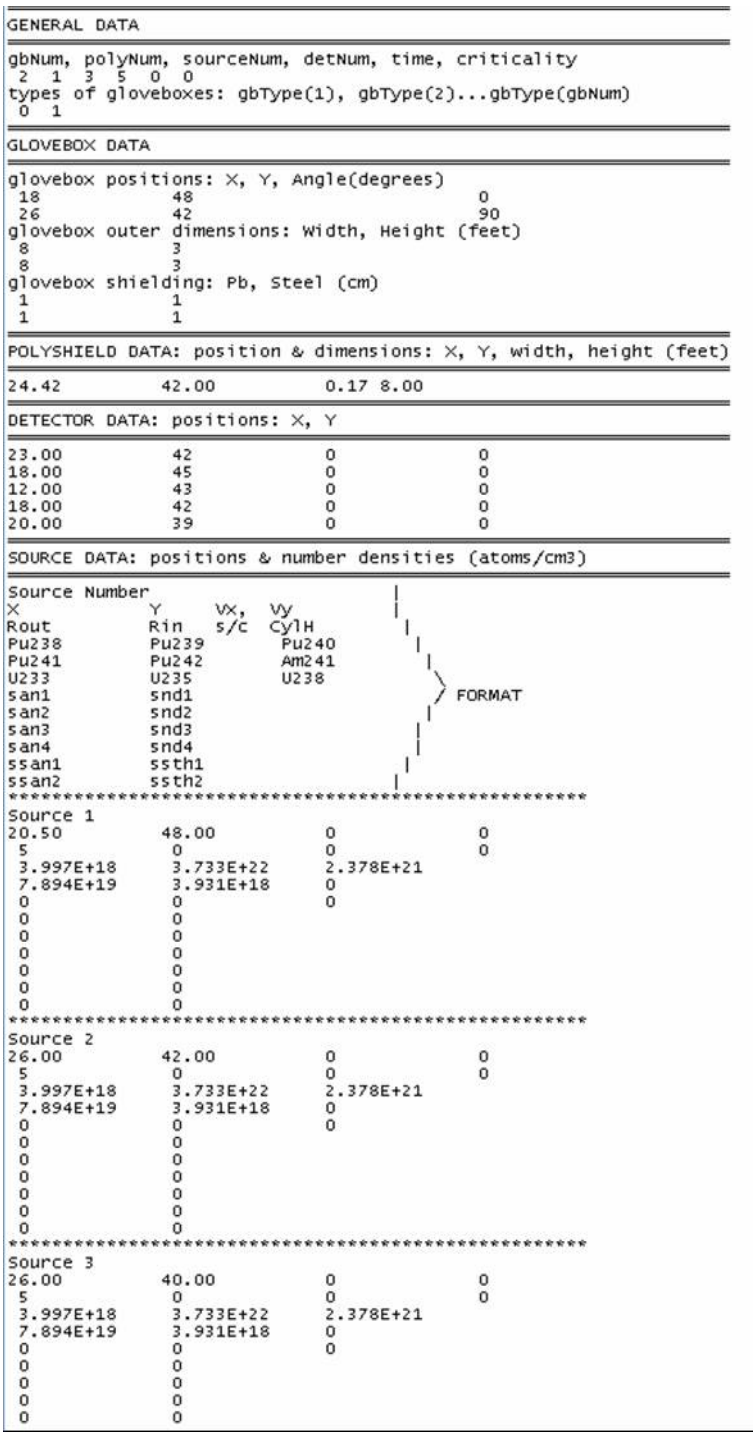

```
GENERAL DATA
gbNum, polyNum, sourceNum, detNum, time, criticality
 2  1  3  5  0  0
types of gloveboxes: gbType(1), gbType(2)...gbType(gbNum)
 0  1
GLOVEBOX DATA
glovebox positions: X, Y, Angle(degrees)
 18             48                      0
 26             42                      90
glovebox outer dimensions: Width, Height (feet)
 8              3
 8              3
glovebox shielding: Pb, Steel (cm)
 1              1
 1              1
POLYSHIELD DATA: position & dimensions: X, Y, width, height (feet)
24.42          42.00          0.17 8.00
DETECTOR DATA: positions: X, Y
23.00           42             0              0
18.00           45             0              0
12.00           43             0              0
18.00           42             0              0
20.00           39             0              0
SOURCE DATA: positions & number densities (atoms/cm3)
Source Number                          |
X              Y     Vx,  Vy           |
Rout           Rin   s/c  CylH          |
Pu238          Pu239        Pu240        |
Pu241          Pu242        Am241         |
U233           U235         U238           \
san1           snd1                         / FORMAT
san2           snd2                        |
san3           snd3                       |
san4           snd4                       |
ssan1          ssth1                     |
ssan2          ssth2                     |
*****************************************************
Source 1
20.50          48.00          0              0
 5              0              0              0
 3.997E+18      3.733E+22      2.378E+21
 7.894E+19      3.931E+18      0
 0              0              0
 0              0
 0              0
 0              0
 0              0
 0              0
 0              0
*****************************************************
Source 2
26.00          42.00          0              0
 5              0              0              0
 3.997E+18      3.733E+22      2.378E+21
 7.894E+19      3.931E+18      0
 0              0              0
 0              0
 0              0
 0              0
 0              0
 0              0
 0              0
*****************************************************
Source 3
26.00          40.00          0              0
 5              0              0              0
 3.997E+18      3.733E+22      2.378E+21
 7.894E+19      3.931E+18      0
 0              0              0
 0              0
 0              0
 0              0
 0              0
```

Figure 2.6. Using the Visio® macro produces the above ShieldCALC/Pandemonium ASCII input file.

CHAPTER 3 TIME DEPENDENCE

In the original version of Pandemonium, the calculated quantities for neutral particles are flux (units of cm^{-2}-s^{-1}) and effective-dose-equivalent rate (mrem-hr^{-1}). As a result, calculations using the original version were limited to static arrangements of sources and detectors, which is clearly a simplistic representation of what is actually a dynamic radiological environment. During a work process in a glovebox facility the movement of sources within or in between different gloveboxes results in continuous changes in shielding parameters (i.e., materials and thickness) as a function of time. As the photon flux calculation hinges upon point-kernel and photon buildup methods, the materials and thicknesses at any given moment in time have significant impacts on the calculated quantities. In addition, if we model personnel as hydrogenous shields, the dynamic nature of the situation becomes even more apparent.

The only way to determine a "total dose" estimate for a given work scenario using the code's original version is to obtain dose rates for a given static situation, manually change the detector and source positions, rerun the code, and repeat for a selected number of static cases. Obviously, this method, in addition to being cumbersome to the user, has the disadvantage of leaving the user to analyze the data and interpret it into a total dose form, thereby increasing the user's workload significantly. Also, the original Pandemonium does not address any neutron multiplication from nearby sources. As Pandemonium's major utility is to increase worker safety, it would be incomplete without at the very least a rudimentary analysis of what neutron and photon dose rates might be expected if an excursion were to occur.

To address these issues, Pandemonium has been improved to allow for dynamic positioning of sources and detectors through the geometry. The code, in addition to determining static dose rates, now integrates dose rate with respect to time to provide a total dose for the given scenario. As it is anticipated Pandemonium will be used in training workers, a specific criticality scenario is provided that will identify the time-profile of radiation doses as the excursion occurs.

This chapter details the time-dependent behavior of Pandemonium, including descriptions of techniques used to update source and detector positions, dose integration, some limitations and possible solutions of the methods used, and the criticality model.

3.1 General time dependence in pandemonium

Pandemonium requires the user to create a two-dimensional model using the computer aided design tool, Microsoft Visio®. The user identifies locations of gloveboxes and the initial positions (and x and y components of velocity, if applicable) of detectors and sources. This information is translated by ShieldCALC using Newton's equations of motion and the result is a description of all shielding materials between each source-to-detector pair at each timestep in the scenario.

Given a scenario, the user also identifies time variables that describe the total time of the scenario and the number of intervals during that time in which the code will perform shielding calculations. It then follows that:

$$t_i = t_o + i \cdot t_{step} \qquad i = 1, 2, \ldots, N \tag{3.1}$$

where,

$$t_{step} = \frac{t_{total}}{N} \tag{3.2}$$

and,

t_i = the i^{th} timestep (s)

t_o = initial time of scenario (s)

t_{total} = total time in scenario (s)

N = number of user-chosen timesteps.

If N represents the number of intervals into which the total time is split, the total number of calculations necessary is $N+1$. In choosing N, the user must be aware that in general, the larger N, the better the calculation, especially when the total scenario time is on the order of

a few minutes. This also implies that a more dense calculation will require more computer time than a calculation in which N is relatively small.

At each time-step calculation, source and detector positions are updated, shielding thicknesses and materials are recalculated, and the neutron and photon fluxes are determined, as are the ambient dose equivalents at each detector due to each source. According to basic Newtonian physics, the source/detector positions are described as

$$x_i = x_o + v_{ox} t_i$$
$$y_i = y_o + v_{oy} t_i \qquad (3.3)$$

where,

x_o, y_o = initial x and y positions

v_{ox}, v_{oy} = x and y velocities

x_i, y_i = positions at i^{th} timestep.

Velocities are assumed to be constant in Pandemonium 2.0 and a source or detector moves in the same direction for the length of the calculation unless a special situation arises in which the sources are determined to pass through glovebox walls. An analysis of this situation is presented later in this chapter. This, however, is a limitation of the code. One recognizes that such straight-line motion of sources, and even more so, detectors, which represent people in the facility, are highly unlikely. Thus, the user must run multiple scenarios if large velocity changes are expected. However, this capability will be invaluable for benchmarking coupled dose estimation/process models that include time-dependent behavior.

ShieldCALC determines total material thicknesses at each timestep based on the above discussion. The information is stored in an interim file that Pandemonium later uses in calculating fluxes and doses. The benefit of this method lies in its automation, thereby reducing the workload required by the user. Of course, the user must still provide thoughtful and appropriate parameters. For example, in a scenario with a total time of 1 hour, choosing N to be 10 would be inappropriate unless sources and detectors are moving

very slowly. Conversely, a choice of N = 100 would be wasteful for a scenario of 10 seconds unless the source or detector is moving extremely fast.

3.2 Ghost sources

In the Pandemonium model, gloveboxes remain stationary, yet detectors and sources are free to move during the course of the scenario. During the development of the code, it was observed that without special attention being paid to the source position at each timestep, it was possible for a source to be located inside a glovebox wall, or outside a glovebox entirely (when it was not intended to be so). Likewise, detectors may also be located in regions where steel, lead, or some other material is already present. To address these issues, the following decisions were made. Because Pandemonium is an attempt to somewhat accurately model reality, sources located inside a glovebox at the start of the model are always confined to that glovebox. Detectors may be located anywhere in the geometry, either within or outside of gloveboxes, as the user may be interested in doses inside of gloveboxes. Also, obtaining a dose profile of a facility requires detector points located regularly throughout the geometry, regardless of whether that point is inside or outside of a glovebox. Thus, given a source initially within a glovebox, assuming its velocity will take the source outside of the glovebox during the scenario, the "ghost source" position is at each timestep compared with the inner glovebox walls. If the source is determined to be located outside of a glovebox, or in a wall, its position is reset to that of the previous timestep.

One limitation of this method regarding "ghost sources" is that in a given facility, sources are routinely transferred between gloveboxes as work performed upon them is completed. To handle this situation, the user would need to run several scenarios depending upon how many gloveboxes the source is to encounter along its voyage. Another limitation that is closely related to choice of N and total time involves resetting the source position if at any timestep the source is found to be outside of the glovebox. For a situation with large total time and few N, the source travels a significant distance between any two timesteps. If this source is determined to be a "ghost source," resetting the source position to the previous timestep can have dramatic consequences for the calculation, as the source may be located

somewhere where the shielding characteristics may be completely different. Ultimately, the goal is to marry dose calculation capability with process modeling tools.

3.3 Dose integration

The new version of Pandemonium includes time-dependent source and detector positions and therefore time-varying shielding parameters. The result of these improvements is the ability for the code to provide not only dose rates at each timestep, but a cumulative dose calculation that predicts a total dose received by a detector during a scenario. This allows a user to identify the best course of action for limiting dose in any given scenario. Although the dose calculations are performed *N+1* times, as aforementioned, only *N* doses are both reported and used in the cumulative dose as described in the following approximation (the trapezoidal rule for integration).

$$D_{cumulative} = \int_0^T \dot{D}(t)dt \approx \sum_{i=1}^{N} \dot{D}(t_i)\Delta t \qquad (3.4)$$

$$\dot{D}(t_i) = \left(\frac{\dot{D}_{t_{i-1}} + \dot{D}_{t_i}}{2} \right) \qquad (3.5)$$

Here, $\dot{D}(t)$ quantities represent dose rates, whereas $D_{cumulative}$ is the total time-integrated dose. To further explain, consider the following example. Given a scenario with *N* timesteps, each of width Δt, the total dose in the *first* timestep would be the average of the dose rates at t = 0 and $t = \Delta t$, multiplied by Δt. Note that in the above equation it has been tacitly assumed that Δt is a constant, and therefore independent of which timestep is being calculated.

Although beyond the scope of this work, it is recognized that more efficient calculations may be achieved by introducing a variable timestep width, and certainly this method would be needed in future versions of the code in which source and detector velocities may become time-dependent. For the case where timesteps are wide enough such that "spikes" in dose rate may occur, say for example, when a fast-moving detector passes in close proximity to a

high-intensity source, it is possible that such spikes may be invisible to Pandemonium. A solution to this problem would be to allow the code to automatically adjust timestep widths once rapidly changing dose rates are observed. This would add a new level of complexity to the code, but may be worthwhile in some applications, and should therefore be investigated as further development of Pandemonium continues.

3.4 Neutron sources in Pandemonium 1.0

Pandemonium determines dose rates from neutral particles in a glovebox facility based on user-supplied information about the source. The accuracy of such calculations depends upon the quality of the source details. A brief discussion of how Pandemonium determines the total neutron source strength is presented and followed by the improvements made during this work. Also discussed is a simple criticality scenario model added to the code.

3.4.1 Source strength

To identify a source in Pandemonium, the user simply drags the source template onto the facility layout in Visio®. The user must then, as prompted, supply pertinent details regarding the source atomic components, number densities, and source shield details. The densities of the source components (fissile and non-fissile) are determined as:

$$\rho_i = \frac{N_i A_i}{A_v} \qquad (3.6)$$

where,

ρ_i = density of atomic component i (g/cm^3)

N_i = user-supplied number density (atoms/cm^3)

A_i = molecular weight for i^{th} component (g/mol), and

A_v = Avagardo's number (atoms/mol).

For non-fissile low-Z elements within the source, Pandemonium determines an (α,n) source component based upon a matrix of calculations by the SOURCES [10] code. SOURCES data are computed in accordance with typical plutonium mixes common to work at Los Alamos such as, for example, plutonium oxide compounds. The (α,n) component is given by:

$$S_{(\alpha,n)} = \sum_{j=1}^{Q} \sum_{k=1}^{M} Y_{j,k} \rho_k N_j \qquad (3.7)$$

where,

$S_{(\alpha,n)}$ = (α,n) source strength (neutrons/s cm^3)

$Y_{j,k}$ = SOURCES calculated neutron yield for fissile component j and low-Z component k (neutrons/s-g), and

ρ_k = density of non-fissile component k (g/cm^3), and

N_j = number density of fissile component j (atoms/cm^3).

The remaining neutron source component is spontaneous fission, found by,

$$S_{sf} = \sum_{j=1}^{Q} \lambda_{1/2,j} P_{sf,j} \upsilon_j N_j \qquad (3.8)$$

where,

S_{sf} = neutrons from spontaneous fission (neutrons/s- cm^3)

$\lambda_{1/2,j}$ = decay constant for fissile component j (1/s)

$P_{sf,j}$ = probability of spontaneous fission (unitless), and

υ_j = number of neutrons per spontaneous fission (unitless).

In Equations (3.7) and (3.8), Q represents the total number of fissile components of the source and M represents total number of low-Z elements. It follows that the total neutron source strength is then

$$S_{neutron} = S_{(\alpha,n)} + S_{sf} \qquad (3.9)$$

3.4.2 k_{eff} Estimate

The neutron flux model in Pandemonium is based on one-group time-independent diffusion theory. This method of determining neutronic distribution in sources in the code is ideal for its simplicity and ease of implementation. This method also prevents Pandemonium from becoming bogged down in detailed multi-group calculations, with the result that it maintains the code as a quick estimate of neutron fluxes throughout a facility. Although the new version of the code is time-dependent, Pandemonium in essence integrates a series of time-independent calculations, i.e., it is quasi-static. One-group diffusion theory details are available in most introductory texts for nuclear engineering and in the original Pandemonium manual, but a concise summary for the purpose of explaining features of Pandemonium is presented.

Beginning with the time-independent diffusion equation, we note that

$$\frac{1}{k}\upsilon\Sigma_f\phi(\vec{r}) = \Sigma_a\phi(\vec{r}) - D\nabla^2\phi(\vec{r}) \qquad (3.10)$$

where

$\phi(\vec{r})$	=	spatial flux distribution
υ	=	number of neutrons released per fission (unitless)
Σ_f	=	macroscopic fission cross section (1/cm)
D	=	diffusion coefficient (cm)
Σ_a	=	absorption macroscopic cross section (1/cm)
k	=	eigenvalue ensuring balance (production of neutrons to equal loss of neutrons).

Rearranging Equation (3.10) gives

$$\nabla^2\phi(\vec{r}) = \frac{1}{D}\left(\frac{1}{k}\upsilon\Sigma_f - \Sigma_a\right)\phi(\vec{r})$$

which implies that,

$$\nabla^2\phi(\vec{r}) = -B_g^2\phi(\vec{r}) \qquad (3.11)$$

where B_g^2 is defined as geometric buckling. Substituting Equation (3.10) into Equation (3.8) and solving for k gives,

$$k = \frac{\upsilon\Sigma_f}{DB_g^2 + \Sigma_a}. \qquad (3.12)$$

All sources in Pandemonium are assumed to be spherical (solid or shells) with the exception of the criticality model, in which the source is a cylindrical bucket being filled over time with an aqueous plutonium mixture.

The buckling, B_g^2, for spherical geometry is

$$B_g^2 = \left(\frac{\pi}{R_{ex}}\right)^2, \qquad (3.13)$$

where R_{ex} is the extrapolated radius. For subcritical scenarios, k_{eff} is estimated according to Equation (3.12), where the B_g have been determined using Equation (3.13). Although not explicitly used in Pandemonium, k_{eff} is provided as an output if the user wishes to compare its value to other methods of calculation.

3.4.3 Criticality scenario

In an effort to present Pandemonium as not only a dose estimator but also as an educational tool for radiological workers, an example of a hypothetical criticality accident has been implemented into the code. The goal is to provide a time-dependent visual aid explaining a rapid increase in dose as a worker stands next to a bucket filling beyond criticality with an aqueous plutonium solution.

Because the scope of this model is out of the range of calculations within Pandemonium, a generic model based on k_{eff} calculations by the Monte Carlo code MCNPX is presented to the user. MCNPX was used to simulate a 1 cm-thick, 30 cm tall polyethylene bucket with a radius of 15 cm at different stages of being filled. From these data, a curve was created relating k_{eff} vs. fill volume. The scenario assumes the bucket is completely full and supercritical at the end of the calculation, arbitrarily chosen as 5 minutes long. A 4^{th}-order polynomial is fit to the data, and the x-axis of the curve is divided by a constant fill rate of $(\pi r^2 h)/T$, thereby producing an empirical equation for k_{eff} vs. time. Physical properties for the criticality model are listed in Table 3.1.

Table 3.1. Physical and material properties used to construct the criticality model. Specific variables are defined on the following page.

Scenario Parameter	*Value*
Radius	15 cm
Height	30 cm
Time	300 s
Solution Density (200g Pu/L)	1.19 g/cm^3
α	5.5E-05 1/ ^{o}C
K	0.2825 g-^{o}C/J
l	1.56E-7 s
ρ	0.00344
β	0.00212

4th Order Polynomial Coefficients: $k_{eff}(t) = at^4 + bt^3 + ct^2 + dt + e$	
a	-1.1947E-10
b	1.2769E-07
c	-5.5642E-05
d	1.2475E-02
e	2.1299E-01

Aqueous Plutonium Solution Number Densities (atoms/cm^3)	
^{238}Pu	5.56E+17
^{239}Pu	4.75E+20
^{240}Pu	2.93E+19
^{241}Pu	6.58E+17
^{242}Pu	1.01E+17
^{241}Am	1.11E+18
H	6.60E+22
O	3.30E+22

When required to perform this calculation, Pandemonium resorts to the empirical formula described above instead of the diffusion estimate of k_{eff}. As Pandemonium is only designed for spherical sources, at each timestep the bucket is modeled as an equivalent-mass sphere for dose rate calculations. In the final timestep of the criticality scenario, k_{eff} becomes slightly greater than 1, and it is also greater than the value required for prompt-criticality, at which point a modified Nordheim-Fuchs model is applied. Hetrick's text on reactor dynamics [11] provides an analysis of neutron pulses for fast and thermal reactors, and his results are applied to the criticality scenario. According to Hetrick, the time-varying neutron population is described by

$$n(t) = \frac{\ell}{\alpha K}\frac{\omega^2}{2} sech^2 \frac{\omega t}{2} \qquad (3.14)$$

where the parameters are determined from the isotopic components, cross sections, and reactivity increases, and

ℓ = neutron generation time (s)

ω = inverse period (1/s) = $\frac{\rho - \beta}{\ell}$

α = negative of temperature coefficient of reactivity (1/°C)

K = inverse heat capacity (g-°C/J)

ρ = reactivity (unitless)

β = delayed neutron fraction (unitless).

As shown, this equation actually yields the assembly power in Watts. To obtain the number of fissions produced during the pulse, Equation (3.14) is integrated over time, and conversion factors and the solution's mass are multiplied along with the assumption that each fission produces 200 MeV of recoverable energy. Values for α for the solution and K for plutonium are obtained from References 12 and 13. The heat capacity, K^{-1} for the plutonium solution is obtained using a simple mass weighting according to Equation (3.15),

$$K^{-1}{}_{Pu-H_2O} = W_{H_2O} K^{-1}{}_{H_2O} + W_{Pu} K^{-1}{}_{Pu}, \tag{3.15}$$

where the W's are the weight fractions of water and plutonium.

The polynomial used to model $k_{eff}(t)$ predicts a step reactivity insertion of \$1.62 in the final timestep of the simulation. The discrete-ordinates code PARTISN, using 16-group Hansen-Roach neutron cross sections [14-15], was used to perform a time eigenvalue search, α_{time}, on a physical model identical to that used by MCNPX. From the time eigenvalue, ℓ is obtained,

$$\ell = \frac{k_{eff} - 1}{\alpha_{time}}. \tag{3.16}$$

In this scenario, once ρ exceeds \$1, the Nordheim-Fuchs model can be applied. We assume that the reactivity insertion that takes the system supercritical is rapid enough to be modeled as a step insertion. Equation (3.14) is integrated with respect to time to obtain the total energy (and hence, number of fissions) produced during the pulse,

$$\int_0^\infty n(t)dt = \int_0^\infty \frac{\ell}{\alpha K} \frac{\omega^2}{2} sech^2 \frac{\omega t}{2} dt = \frac{2\ell\omega}{\alpha K} \tag{3.17}$$

This value is then converted to units of neutrons/cm^3-second by dividing by the volume and width of the timestep. Recalling that Pandemonium treats neutrons from both (α, n) and spontaneous fission reactions, the fission neutrons produced are explicitly assigned to the spontaneous fission source. Noting that in an aqueous solution, neutrons are mostly thermal upon exiting the solution, during the criticality model Pandemonium approximates this by performing the flux calculations at 2 MeV source energy, then by multiplying that flux by the dose coefficient at 0.0253 eV.

As shown in Table 3.2, Pandemonium predicts a total dose of 1.65 $\times 10^4$ rem (neutron) and 9 $\times 10^3$ rem (photon), and for comparison, it also presents dose results from major criticality

accidents involving fissile material in both solid and solution form. The amount of shielding in Pandemonium's criticality model is significantly less than that which may exist in a realistic situation, and this most likely results in an increased dose. Also, in this model, the total distance between the source sphere and the detector is less than 1 meter (91.4 cm), whereas in most accidents, the distance is slightly larger. The end result produces a dose somewhat higher than estimated from past criticality accidents. Although this is positive, that is, Pandemonium conservatively over predicts dose, it suggests that a more refined model may produce better results.

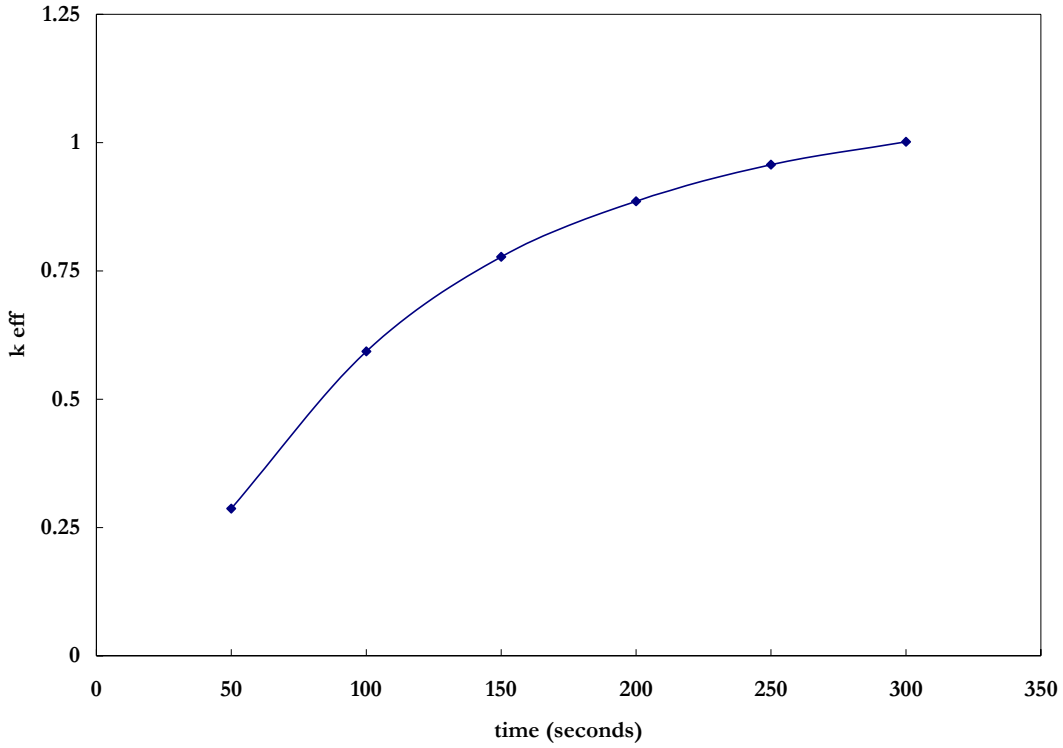

Figure 3.1. MCNPX calculations and curve fit of time dependent k_{eff} for the criticality scenario.

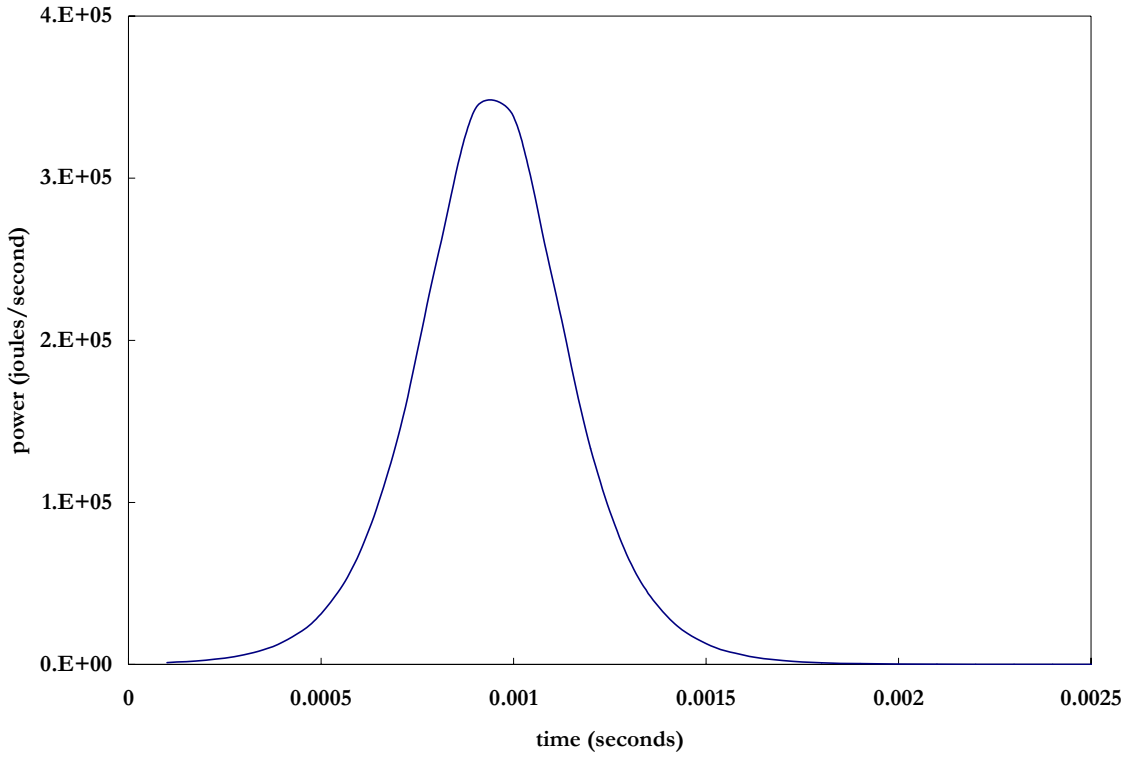

Figure 3.2. Nordheim-Fuchs model predicts the above power pulse for the Pandemonium criticality model.

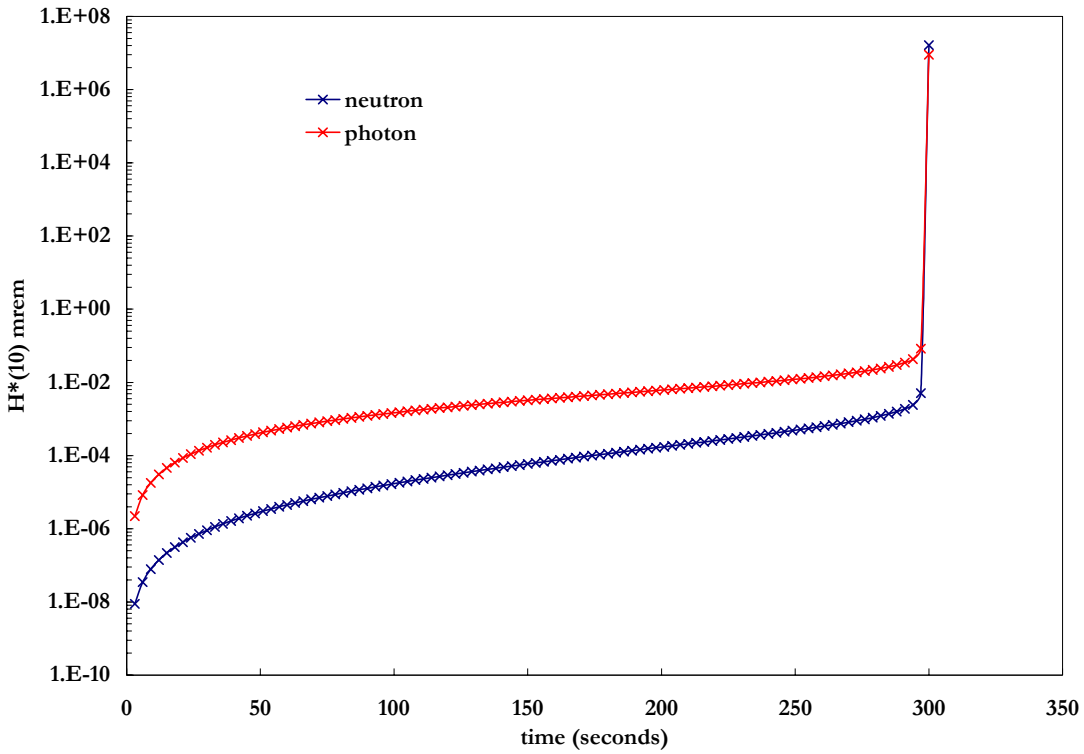

Figure 3.3. Cumulative ambient dose equivalent calculated by Pandemonium during criticality scenario.

Table 3.2. Comparison of Pandemonium criticality scenario results to major criticality accidents within the last 60 years [16].

Year	*Location/Facility*	*Material & Geometry*	*Yield (fissions)*	*Maximum Reported Dose*
		solid spheres		
1945	Los Alamos	solid Pu sphere/tungsten bricks	1.00E+16	510 rem
1946	Los Alamos	solid Pu hemisphere / Be ref.	3.00E+15	2100 rem
1968	Chelyabinsk (RFNC)	solid U sphere/ U reflector	6.00E+16	4000 rem
		aqueous solutions		
1968	Mayak Prod. Fac.	Pu solution / cylindrical	1.00E+17	2450 rem
1999	Tokai-mura, Japan	uranyl nitrate solution / cylindrical	8.00E+16	20 GyEq
	PANDEMONIUM	**Pu solution / cylindrical**	**1.34E+17**	**25500 rem**

CHAPTER 4 THE PANDEMONIUM PHOTON MODEL

A major focus, and the most in-depth component, of this work is an extensive expansion in Pandemonium's photon modeling capability. Several modifications have been included that make the code more robust and rigorous in its calculation of photon ambient dose equivalent, including an expanded energy range to account for higher energy fission photons, and the inclusion of results from an original study into buildup factors and their angular relationships to photon beams incident on thin slabs. First, however, an overview of the photon modeling originally in Pandemonium is presented, that will provide the basis upon which will follow a discussion of the improvements made during this work.

4.1 Energy structure

Pandemonium 1.0 has a photon energy structure spanning the two decades between 10 keV and 1 MeV. Seventeen energy bins provide for a multigroup calculation in the sense that calculations are performed in each of the 17 bins (see Table 4.1). In radiation transport, multigroup methods imply that particles' energies are tracked and changes in energy result in cross-group communication within different groups. In discrete-ordinates simulations, this detailed energy treatment often drives the computation time required. In Pandemonium, the group structure is maintained, but cross-group communication is neglected. Instead, the code performs calculations in each group, and buildup factors account for photons whose energies have changed as a result of interactions within shields. The usually conservative approach is taken that all photons in a bin exist at the higher upper energy limit of that bin.

Table 4.1. Energy group structure for photon calculations in Pandemonium 1.0

Bin	*Energy (MeV)*		
	lower limit		*upper limit*
1	0	-	0.01
2	0.01	-	0.015
3	0.015	-	0.02
4	0.02	-	0.03
5	0.03	-	0.04
6	0.04	-	0.05
7	0.05	-	0.06
8	0.06	-	0.08
9	0.08	-	0.1
10	0.1	-	0.15
11	0.15	-	0.2
12	0.2	-	0.3
13	0.3	-	0.4
14	0.4	-	0.5
15	0.5	-	0.6
16	0.6	-	0.8
17	0.8	-	1

Because of the 1-MeV upper energy limit in version 1.0, source photons originate only from the decay of isostopes that compose the source. Nuclear decay data from the Evaluated Nuclear Data File (ENDF) [17] are used to construct mass-normalized photon source strengths for each energy bin (Table 4.2) according to the following formula,

$$S_i(E_j) = \frac{Y_i(E_j) N_x \lambda_i A_v C}{A_i} \qquad (4.1)$$

where

$S_i(E_j)$ = mass normalized source strength at energy E_j for isotope i (Ci/g)

$Y_i(E_j)$ = decay yield at energy E_j (decays/atom)

N_x = normalization factor for radiation of type x, where = gamma- or x-ray (unitless),

λ_i = decay constant for isotope i (1/s),

A_v = Avogadro's number (atoms/mole),

A_i = molecular weight of isotope i (g/mole), and

C = conversion coefficient – 2.703×10^{-11} (Ci/Bq).

The volumetric source strength is obtained by multiplying Equation (4.1) by the density of isotope i and dividing by C as shown

$$S_{V,i}(E_j) = \frac{\rho_i S_i(E_j)}{C}, \qquad (4.2)$$

where

$S_{V,i}(E_j)$ = volumetric source strength (photon/cm^3-s).

It follows that for a given energy bin, the total photon source strength is

$$S_V(E_j) = \sum_{i=1}^{N} S_{V,i}(E_j), \qquad (4.3)$$

where there are N isotopes composing the source.

Table 4.2 Mass normalized source strengths used for transuranics photon sources.

Energy [MeV]	*Pu-238*	*Pu-239*	*Pu-240*	*Pu-241*	*Pu-242*	*Am-241*
			[Ci/g]			
0.015	7.41E-01	1.20E-03	9.13E-03		1.31E-04	4.82E-01
0.02	1.00E+00	1.34E-03	1.10E-02	1.45E-03	1.64E-04	6.61E-01
0.03	2.37E-01	3.42E-04	2.72E-03		4.27E-05	1.66E-01
0.04		6.51E-04				4.71E-03
0.05	6.78E-03	7.30E-05	1.01E-04	5.21E-06	1.47E-06	2.62E-03
0.06		1.76E-03		3.60E-06		7.99E-04
0.08	5.15E-09	7.49E-05		2.43E-05		1.39E-04
0.1	1.30E-03	8.23E-05	4.54E-07	8.67E-04		7.28E-04
0.15	1.72E-09	5.12E-04	1.62E-05	5.55E-04	1.01E-07	9.62E-04
0.2	1.61E-04	3.27E-05	9.13E-07	6.80E-06	1.19E-08	1.33E-05
0.3	7.38E-07	5.00E-05	9.13E-07			3.10E-05
0.4		2.64E-04				4.30E-05
0.5		1.14E-04				2.90E-06
0.6		2.22E-07	2.27E-10			6.73E-07
0.8	7.89E-06	5.13E-06	3.75E-08			2.57E-05
1	1.39E-06	7.42E-08	1.36E-09			2.43E-07

4.2 Photon flux and buildup

Once the photon sources for each energy bin have been determined, Pandemonium 1.0 calculates the flux contribution from each source at each detector by applying the scalar flux solution for a self-absorbing sphere in air. This flux, when multiplied by a flux-to-dose response function and a buildup factor and attenuated through the shields, yields a dose contribution from each source in each energy bin. Because the detector positions in Pandemonium are arbitrary, a detector may be located inside a source, on the surface, or exterior to the source. In the first and third cases, the reader is referred to the original derivation in the Appendix of the Pandemonium manual. The middle case is somewhat simpler, the solution to the flux being,

$$\phi(R, E_j) = \frac{S_V}{2\mu_s(E_j)}\left(1 - \frac{1 - e^{-2\mu_s(E_j)R}}{2\mu_s(E_j)R}\right), \tag{4.4}$$

in which case,

$\phi(R, E_j)$	=	flux at the surface of a source of radius R ($1/\text{cm}^2$), and
$\mu_s(E_j)$	=	photon attenuation coefficient at energy E_j ($1/\text{cm}$). Subscript s refers to the 'source.'

Photons that escape the source sphere are then radially attenuated through the Pandemonium 1.0 physical model, and scattered photon contributions are described by the use of ANSI/ANS [18] standard exposure buildup factors.

Applying buildup factors and conversion coefficients, and accounting for attenuation through shields present between a source and detector, Pandemonium 1.0 gives the following result for dose at a detector:

$$D(E_j) = B_{\exp}(E_j)\phi(E_j)R_D(E_j)\prod_{i=1}^{N} e^{-\mu_i(E_j)\Delta_i} \qquad (4.5)$$

where

$B_{\exp}(E_j)$ = exposure buildup at energy E_j (unitless),

$R_D(E_j)$ = fluence-to-dose conversion coefficient,

$\mu_i(E_j)$ = photon attenuation coefficient of the i^{th} shield at energy E_j (1/cm), and

Δ_i = linear thickness of the i^{th} shield (cm).

Photon buildup factors in Pandemonium 1.0 are determined from elemental data to be used in the Geometric-Progression empirical formula [18],

$$B(E,x) = 1 + \frac{(b-1)(K^x - 1)}{K-1}, \quad K \neq 1$$

$$B(E,x) = 1 + (b-1)x, \quad K = 1 \qquad (4.6)$$

$$K(E,x) = cx^a + \frac{d\left(\tanh\left(\frac{x}{X_k} - 2\right) + \tanh 2\right)}{1 + \tanh 2}$$

where

x = mean free path thickness of shield (unitless), and

a, b, c, d, X_k = are energy and material dependent coefficients tabulated in the reference.

Although the above description provides a reasonable estimate of photon buildup effects at the detector, a number of reasons exist as to why this method should be replaced with results from a more in-depth study into buildup factors. First, dose in Equation (4.5) is determined by using infinite-media *exposure* buildup factors. A better result will make use of finite-media *ambient dose equivalent* buildup factors. Secondly, with the continued development and improvements in cross-section measurements and data archiving, use of

the latest available cross sections will provide the best assessment of photon buildup. Such improvements include accounting for coherent scattering between photons and the collective atomic electrons, and incoherent scattering between photons and individual electrons bound to the atom. Buildup factors in the referenced ANSI standard, and photon attenuation coefficients in version 1.0, do not include the bound electron effects of incoherent scattering. Third, generic buildup factors may not always be appropriate for their planned use. In Pandemonium, photons originate within a spherical source, exit the source, and transport through slabs of material that represent walls of gloveboxes. Many photon buildup calculations (including those listed in the ANS/ANSI standard) are performed under point-isotropic (i.e., spherical) and infinite-media geometries. The Pandemonium model would be better represented in slab geometry.

Lastly, Pandemonium determines the linear thickness of each shield between every source-to-detector pair along with the angle relative to normal with which the line-of-sight intersects each shield. Such angles can have a wide variety of values due to the arbitrary positions of both sources and detectors at any point in time. However, by applying point-isotropic buildup factors, version 1.0 ignores the angle by which the source-to-detector line-of-sight intersects shields. Previous studies [19, 20, 21] show that the angle by which a beam of photons is incident upon a slab can have significant impacts on photon transmission and reflection probabilities and photon buildup factors.

In a review of the literature to be discussed in the next chapter, it is noted that the previous angular buildup factor studies keep the normal slab thickness constant as incident angle is varied. To date, no studies have shown a relationship between incident angle and buildup while keeping the uncollided (or, slant-path) photon slab thickness constant as shown in Figure 4.1. Given the method in which Pandemonium applies buildup factors, such a relationship is necessary. We therefore aim to identify the 'purely-angular effect' of photon buildup by comparing the buildup factor result from Figure 4.2a to that of Figure 4.2b.

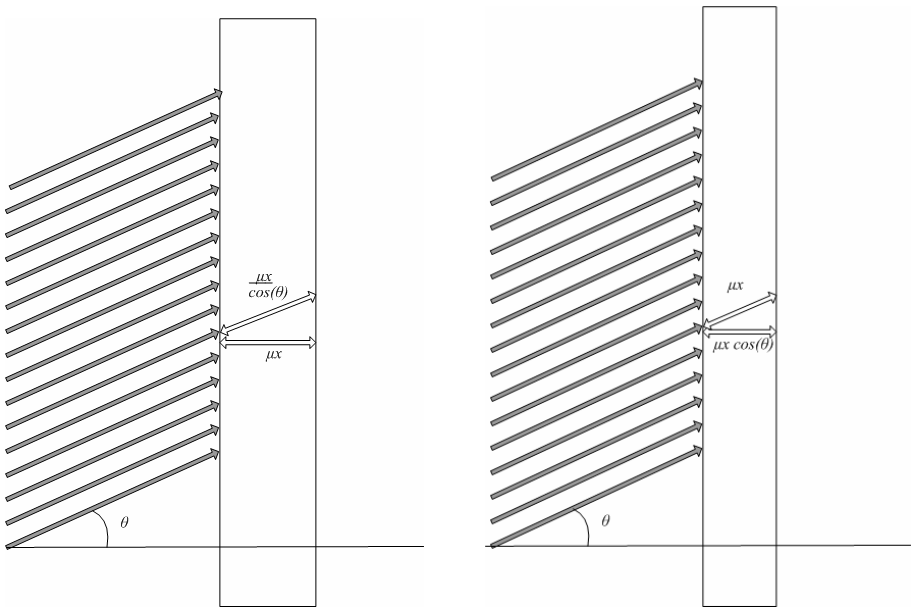

Figure 4.1. Historical geometry for previous angular buildup factors keeping normal slab thickness constant (a) and proposed geometry for identifying purely angular effect on buildup (b). In (b) we maintain the slant-path thickness by adjusting the normal-path thickness as incident angle is varied.

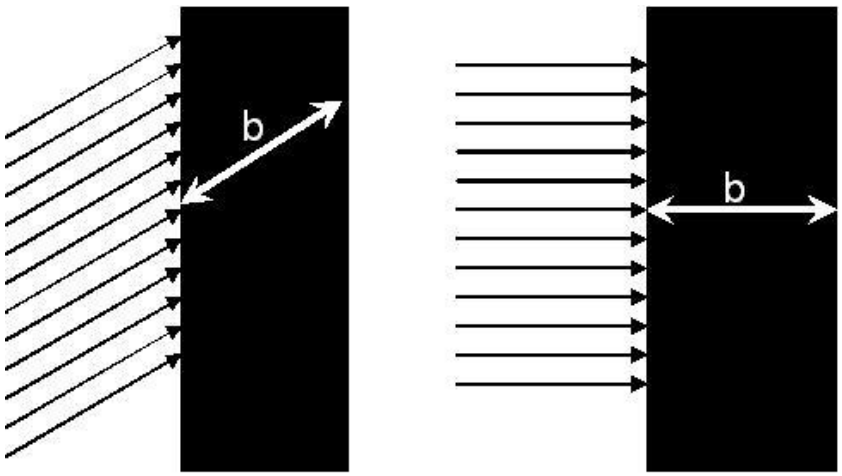

Figure 4.2. The purely-angular effect of photon buildup is determined by comparing the slant-path result (a) to the normally-incident case (b). In both cases the uncollided photon path-length is the same.

These reasons suggest the need for a new detailed analysis of photon buildup factors, one that uses the most recent photon cross sections available. Of interest to the general radiation shielding community are the purely angular buildup factors due to the above geometry, since to date, there has been no direct comparison of purely-angular effects of buildup, defined as such because the only variable between the two buildup factors in Figure 4.2 is the angle of incidence; the uncollided photon contribution remains the same.

Based on the overview of Pandemonium's photon model given above, a number of improvements have been implemented: extension of the energy range, the inclusion of fission photons, and improved and more appropriate photon buildup factors. The energy range and fission photon improvements are discussed in this chapter, while the photon buildup factor study is presented in the following chapters.

4.3 Photon model improvements

4.3.1 Energy range extension

Penetrating photons with higher energies are now accounted for in Pandemonium. Shown in Table 4.3 is the expanded energy bin structure. An additional eight energy bins have been added to nuclear data libraries and are used by the code for photon calculations. This energy extension includes additions to photon mass attenuation coefficients, original geometric-progression buildup factor formula coefficients for each element, and original dose-equivalent conversion coefficients within the code. Because the photon mass attenuation coefficients in version 1.0 are from the 1991 ANSI standard, new values from the National Institute of Standards and Technology (NIST) [22] that include the effects of coherent scattering have replaced former values.

Table 4.3. Extended energy range of photon model in Pandemonium 2.0.

Bin	*Energy (MeV)*		
	lower limit		*upper limit*
1	0	-	0.01
2	0.01	-	0.015
3	0.015	-	0.02
4	0.02	-	0.03
5	0.03	-	0.04
6	0.04	-	0.05
7	0.05	-	0.06
8	0.06	-	0.08
9	0.08	-	0.1
10	0.1	-	0.15
11	0.15	-	0.2
12	0.2	-	0.3
13	0.3	-	0.4
14	0.4	-	0.5
15	0.5	-	0.6
16	0.6	-	0.8
17	0.8	-	1
18	1	-	1.5
19	1.5	-	2
20	2	-	3
21	3	-	4
22	4	-	5
23	5	-	6
24	6	-	8
25	8	-	10

4.3.2 Fission photons

The main advantage of extending the photon energy range to 10 MeV is to account for higher energy penetrating photons produced during fission. Peele and Maienschein [23] obtained by experiment a prompt-fission photon spectrum that is suitable to be used for both ^{235}U and ^{239}Pu. To their data they fit the following empirical formula:

$$N_{p\gamma}(E) = \begin{cases} 6.6 & 0.1 < E < 0.6 \\ 20.2e^{-1.78E} & 0.6 < E < 1.5 \\ 7.2e^{-1.09E} & 1.5 < E < 10.5 \end{cases}, \qquad (4.7)$$

where

$N_{p\gamma}(E)$ = number of prompt fission photons (photons/MeV-fission),

E = energy (MeV).

To obtain a fission spectrum per fission in the expanded Pandemonium energy structure (Table 4.4), the above equation is integrated for each bin between 0.1 MeV and 10 MeV, the results of which are then summed as follows:

$$N_{p\gamma} = \sum_{i=10}^{25} \int_{E_{low,i}}^{E_{high,i}} N_{p\gamma}(E)dE, \qquad (4.8)$$

where $E_{high,i}$ and $E_{low,i}$ are the high and low energy limits for bin *i*. When multiplied by the fission rate within a source, the normalized fission photon spectrum (per fission) is used to determine the number of photons produced from fission within each bin. Reference 8 derives the neutron flux within a solid sphere as

$$\phi(r) = \frac{S}{B^2 D}\left[\frac{R+d}{r}\frac{\sin Br}{\sin B(R+d)} - 1\right], \qquad (4.9)$$

where

S = neutron source (neutrons/cm^3),

B^2 = material buckling (1/ cm^2),

D = diffusion coefficient (1/cm),

d = extrapolation distance (cm), and

R = source radius (cm).

Since the reaction rate is defined as $R_{fiss} = \int_V \Sigma_f \phi(r) dV$, assuming a constant fission cross section, it follows that the total fission rate in a solid source of radius R is,

$$R_{fiss} = \frac{4\pi\Sigma_f S}{DB^2}\left[\frac{R+d}{\sin B(R+d)}\left(\frac{\sin BR}{B^2} - \frac{R\cos BR}{B}\right) - \frac{R^3}{3}\right], \qquad (4.10)$$

where R_{fiss}, the reaction rate, has units of (fissions/cm^3-s).

To account for decay photons from fission fragments, Pandemonium makes use of the commonly-used shielding approximation that decay photons are in equilibrium with fission photons, and that the energy spectra are equal. Applied to Pandemonium, this means the fission photon spectrum is simply multiplied by a factor of 2.

For those bins whose upper energy limits are less than 1 MeV, the total photon source is the sum of those from decay of fissile isotopes and those from prompt fission and decaying fission fragments. Those bins with energies above 1 MeV have total sources from fission (prompt and delayed) alone. Thus, the photon model includes photons from decaying fissile isotopes, those produced by subcritical fissions, and those produced from the decay of fission fragments.

Table 4.4. Normalized fission spectrum in expanded energy bin structure.

bin	*normalized spectrum (photons/fission)*
10	3.300E-01
11	3.300E-01
12	6.600E-01
13	6.600E-01
14	6.600E-01
15	6.600E-01
16	1.168E+00
17	8.183E-01
18	1.128E+00
19	5.411E-01
20	4.956E-01
21	1.666E-01
22	5.603E-02
23	1.884E-02
24	8.463E-03
25	9.567E-04

CHAPTER 5 PHOTON BUILDUP FACTORS – METHODS

It has been previously noted that a thorough improvement of the photon model in Pandemonium must include the use of buildup factors that are determined from transport calculations taking advantage of the most recent cross sections. Because the code applies point-isotropic buildup factors to situations in which the source-to-detector line of sight intersects slab shields at oblique angles, improvements must include the angular effect of buildup factors in slab geometry. A set of photon buildup factors that address the above issues is presented in the next two chapters. A purely-angular effect of buildup factors for thin shields is also explored which, to date, has not been identified in the literature but that should be of interest to the larger community involved in radiation protection and shielding. An exhaustive literature review of buildup factors is followed by a description of the present buildup-factor calculations. Results and analysis of the calculations follow in the next chapter.

Since photon buildup factors were introduced by White [24], their use in radiation shielding analysis and design has been extensive. As more detailed cross sections have become available, new theoretical techniques have been developed, and vast improvements in computing power have been realized, photon buildup factors have been studied both experimentally and even more so calculationally [25]. Methods have been developed to calculate particle flux densities by a variety of techniques. The moments method [26] solves for the angular moments of the flux density in simple geometries. Discrete-ordinates methods determine flux density by directly integrating a form of the transport equation in which energy, angle, and space are discretized. The Monte-Carlo method does not explicitly solve the transport equation, but instead obtains answers by simulating individual particles and recording aspects of their average behavior. Both discrete-ordinates and Monte-Carlo methods have been used in buildup factor studies by Hirayama, Harima and others [27] in which the effects of secondary photons from bremsstrahlung and fluorescence were identified. Hirayama [28], using plane geometry and Monte Carlo, and Kitsos [29], who used spherical geometry and discrete-ordinates, both demonstrated that the inclusion of incoherent and coherent scattering phenomena in cross sections tends to increase exposure

buildup at energies above 10 keV. Kitsos later showed that by including photons from bremsstrahlung and fluorescence, exposure buildup factors increase significantly [30].

These analyses provided the basis upon which many buildup factor studies were performed, including the development of empirical formulas to determine buildup for single-layer [31, 32] and multi-layered shields [33, 34]. A number of authors have explored the relationship between buildup and the angle of incidence in which monoenergetic parallel beams impinge upon infinite slabs, using Monte Carlo methods [19-21, 35]. In general, with increasing angle of incidence relative to normal, buildup factors have been shown to increase for a given shield thickness, thereby identifying a type of angular dependence. From these works it is evident that buildup factors have evolved over time and in parallel with the development of photon cross-section data. Such developments as the inclusion of coherent scattering, the electron binding effect on incoherent scattering, bremsstrahlung, and fluorescence have been demonstrated to greatly increase buildup factors, especially at deep penetrations; the dose may not increase significantly, however, because including these effects reduces the uncollided contribution.

In studies that investigated angular buildup, photons were incident upon slabs of constant normal thickness as the angle of incidence was varied, as shown in Figure 4.1a. For most shielding studies, this information is more than sufficient to allow for designing of effective shields. For codes, however, such as Pandemonium, more detailed information is necessary given the way such tools perform shielding calculations. In particular, it would be helpful to know how the buildup for an oblique photon beam on a slab of given slant-path optical thickness, say for example, b, compares to that for a normal beam on a slab of the same normal optical thickness, b (Figure 4.2). In this case, the uncollided photon contribution remains the same, whereas in the traditional approach, such contribution is inversely related to the cosine of the incident angle (Figure 4.1). To identify what is henceforth termed the 'purely angular buildup' factor, i.e., that for which the uncollided photon contribution remains constant as the angle of incidence is varied, a set of photon transport calculations is presented that (a) uses most recent photon transport cross sections, (b) includes the secondary-photon effects of fluorescence and bremsstrahlung, and (c) identifies the purely-angular effect of incident angle on flux, air exposure, and dose buildup factors. Discrete-

ordinates and Monte Carlo photon transport calculations were performed for comparison, and because each method relies on the quality of cross-section data supplied, consistency was maintained by using the same source of pointwise photon cross sections modified as needed for each type of calculation.

A brief overview of buildup factors is given. The definition of the photon buildup factor is

$$B_x = \frac{\int dE\, R_x(E)\phi(E)}{R_x(E_o)\phi_o(E_o)} \qquad (5.1)$$

where

$R_x(E)$ = response function for quantity desired (flux, dose, exposure, etc.); for flux buildup, $R_x(E) = 1$,

$\phi(E)$ = total flux spectrum, and

$\phi_o(E_o)$ = uncollided flux at initial energy E_o.

The air exposure response function is given by

$$R_{\exp} = C \cdot E \cdot \left(\frac{\mu_{en}(E)}{\rho} \right)_{air} \qquad (5.2)$$

where

$\mu_{en}(E)/\rho$ = mass energy absorption coefficient (cm^2/g)

C = a constant for conversion of units.

5.1 Cross sections

Photoatomic interaction cross sections have been studied for a number of years by different researchers. Hubbell [36] has compiled a number of cross-section libraries, the content of which may take various forms and dimensional units. But regardless of the form, such data

refers to basic physical interactions of photons with matter, or in some cases more explicitly, the atomic electrons within matter. There are numerous physical processes by which photons transfer energy to electrons, four of which are major. Interactions between photons and atomic nuclei (except for pair production) will not be discussed, as they do not significantly contribute to the attenuation of photons through media for the energy range under consideration.

5.1.1 Major photon interactions

For lower energy photons, the photoelectric effect is usually very important. During this process, an energetic photon is completely absorbed while an energetic electron is ejected according to

$$E_e = h\nu - E_b, \tag{5.3}$$

where $h\nu$ is the photon energy and E_b is the electron binding energy. In this process, the ejected photoelectron (usually K-shell) leaves a vacancy in the atomic electron structure, and a cascade of characteristic x-rays is produced as the remaining atomic electrons are rearranged to fill the vacancy. Occasionally such an x-ray may interact with and eject a less tightly bound outer electron (Auger electron) with energy equal to that of the x-ray minus the binding energy of the outer electron.

For medium-Z materials, and intermediate-energy photons above about 100 keV, Compton scattering predominates photon interactions. The interaction between a photon of energy E and an electron, which is usually assumed to be free, results in a transfer of energy T to the electron. The secondary photon, now with energy $E' = E - T$, emerges at angle θ_s while the electron emerges at angle θ_e according to the Compton formula

$$E' = \frac{E}{1 + (E / m_o c^2)(1 - \cos\theta_s)} \tag{5.4}$$

where $m_o c^2$ is the electron rest mass. Although the Klein-Nishina formula describes this process for higher energy photons, correction factors are needed to account for electron binding effects as photon energies approach electron binding energies. Such corrections are often included in photoatomic data libraries.

As was previously mentioned, coherent scattering effects can seriously influence photon transport particularly for low-energy photons interacting with high-Z materials. In this process, a photon interacts with the collective atomic electrons of an atom. Such events result in minimal changes in photon energy and direction and atomic momentum recoil.

The last major photon interaction is pair production. The strong electric field produced near atomic nuclei sometimes induces photons to be absorbed and replaced by an electron-positron pair with kinetic energies T_+ and T_- according to

$$T_+ + T_- = E - 2m_o c^2 . \qquad (5.5)$$

As Equation (5.5) suggests, the photon energy must be in excess of 1.022 MeV (twice the rest energy of an electron) for the interaction to occur. Results of previous authors lead one to conclude that current photon transport calculations must be performed using cross sections that include photoelectric absorption, Compton scattering, including bound electron effects, coherent scattering, and pair production.

5.1.2 Cross-section libraries

The experimental advances in cross-section measurement have been paralleled by the compilation of libraries that contain evaluated data in a number of formats. Berger and Hubbell have maintained the XCOM photoatomic cross-section database for a number of years; however compared to other libraries, the XCOM [Ref. 22] database provides limited information in the form of point-wise tables of macroscopic cross-section values. Other

libraries make use of the Evaluated Nuclear Data File (ENDF) [37] format. Although not suitable for direct use in transport codes, ENDF data can be translated into multigroup and point-wise tables sufficient for both Monte Carlo and discrete-ordinates codes by the cross-section processing code NJOY [38]. The primary photon transport cross sections used in this study are derived from the ENDF/B-VI.8 [39] photoatomic interaction library. Details on the processing of these data are described in the next section.

5.2 Discrete-ordinates calculations

The discrete-ordinates code PARTISN [40] is the most recent version of the DANTSYS family of codes [4]. For a discrete-ordinates calculation (a) energy-group structure, (b) angular-quadrature order, quadratures, and weights, (c) Legendre order of cross-section scattering, (d) multigroup table of cross sections for materials based on (a) and (c), and (e) response functions for air exposure and ambient dose equivalent must all be provided.

5.2.1 Energy group structure and cross sections

The present calculations determine a photon buildup factor that will replace the current buildup calculation approach in Pandemonium. It is appropriate to choose an energy structure that encompasses the range of photon energies within that code: 10 keV to 10 MeV. However, because transport calculations are much more sophisticated than the attenuation calculations done by Pandemonium, more freedom may be exercised developing a multigroup structure to ensure accuracy. Below 100 keV, this energy group structure is based largely upon that of Daskalov [41], who developed a structure ideal for low energy analysis of transport results, particularly those in the vicinity of the K-electron binding energies. In general, groups decrease in width with decreasing energy. Exceptions, however, occur for several groups above 100 keV. To limit the variation between slab thicknesses in the Monte Carlo and discrete-ordinates calculations, both of which are based on the total cross section value at the source energy, group widths at source energies of interest are limited to 1 keV. The 220-group energy structure is shown in Table 5.1. This group

structure forms the basis of the multigroup calculations using discrete-ordinates. Beginning with this, multigroup photon cross sections for primary photon interactions were developed using the GAMINR module of the NJOY cross-section processing code. Based on Kitsos' analysis of Legendre expansions [29], scattering cross sections were calculated with the P_7 approximation and a $1/E$ weight function. As mentioned, previous photon buildup calculations performed using only primary photon interactions ignore the effects due to the secondary effects of bremsstrahlung and florescence. Because NJOY only determines primary photon cross sections from ENDF photoatomic libraries, a method was devised that allows for the inclusion of such secondary effects.

Table 5.1. 220-group energy structure for discrete-ordinates photon buildup calculations including group index number, energy of group upper limit, and group width in keV.

group	*E(keV)*	*⊿E (keV)*	*group*	*E(keV)*	*⊿E (keV)*	*group*	*E(keV)*	*⊿E (keV)*
1	10001	*1*	**37**	2666	*166*	**73**	550	*49*
2	10000	*500*	**38**	2500	*167*	**74**	501	*1*
3	9500	*500*	**39**	2333	*167*	**75**	500	*50*
4	9000	*500*	**40**	2166	*165*	**76**	450	*50*
5	8500	*499*	**41**	2001	*1*	**77**	400	*15*
6	8001	*1*	**42**	2000	*125*	**78**	385	*15*
7	8000	*250*	**43**	1875	*125*	**79**	370	*10*
8	7750	*250*	**44**	1750	*90*	**80**	360	*10*
9	7500	*250*	**45**	1660	*60*	**81**	350	*12.5*
10	7250	*250*	**46**	1600	*100*	**82**	337.5	*12.5*
11	7000	*250*	**47**	1500	*100*	**83**	325	*12.5*
12	6750	*250*	**48**	1400	*65*	**84**	312.5	*12.5*
13	6500	*250*	**49**	1335	*5*	**85**	300	*15*
14	6250	*249*	**50**	1330	*230*	**86**	285	*10*
15	6001	*1*	**51**	1100	*99*	**87**	275	*15*
16	6000	*250*	**52**	1001	*1*	**88**	260	*10*
17	5750	*250*	**53**	1000	*50*	**89**	250	*25*
18	5500	*100*	**54**	950	*50*	**90**	225	*25*
19	5400	*200*	**55**	900	*50*	**91**	200	*5*
20	5200	*199*	**56**	850	*25*	**92**	195	*5*
21	5001	*1*	**57**	825	*25*	**93**	190	*5*
22	5000	*300*	**58**	800	*20*	**94**	185	*5*
23	4700	*200*	**59**	780	*30*	**95**	180	*5*
24	4500	*100*	**60**	750	*15*	**96**	175	*2.5*
25	4400	*200*	**61**	735	*15*	**97**	172.5	*2.5*
26	4200	*199*	**62**	720	*20*	**98**	170	*5*
27	4001	*1*	**63**	700	*10*	**99**	165	*2.5*
28	4000	*100*	**64**	690	*10*	**100**	162.5	*5.5*
29	3900	*100*	**65**	680	*15*	**101**	157	*1*
30	3800	*150*	**66**	665	*30*	**102**	156	*6*
31	3650	*150*	**67**	635	*15*	**103**	150	*5*
32	3500	*167*	**68**	620	*20*	**104**	145	*5*
33	3333	*167*	**69**	600	*2.5*	**105**	140	*2.5*
34	3166	*166*	**70**	597.5	*2.5*	**106**	137.5	*2.5*
35	3000	*167*	**71**	595	*20*	**107**	135	*5*
36	2833	*167*	**72**	575	*25*	**108**	130	*5*

Table 5.1 (continued).

group	*E(keV)*	*⊿E (keV)*	*group*	*E(keV)*	*⊿E (keV)*	*group*	*E(keV)*	*⊿E (keV)*
109	125	*25*	**146**	42.75	*0.25*	**185**	29.75	*0.25*
110	100	*1*	**147**	42.5	*0.25*	**186**	29.5	*0.25*
111	99	*1*	**148**	42.25	*0.25*	**187**	29.25	*0.25*
112	98	*1*	**149**	42	*0.25*	**188**	29	*0.3*
113	97	*1*	**150**	41.75	*0.25*	**189**	28.7	*0.2*
114	96	*1*	**151**	41.5	*0.25*	**190**	28.5	*0.3*
115	95	*1*	**152**	41.25	*0.25*	**191**	28.2	*0.2*
116	94	*1*	**153**	41	*0.5*	**192**	28	*0.4*
117	93	*1*	**154**	40.5	*0.5*	**193**	27.6	*0.35*
118	92	*1*	**155**	40	*0.25*	**194**	27.25	*0.25*
119	91	*1*	**156**	39.75	*0.25*	**195**	27	*0.75*
120	90	*2*	**157**	39.5	*0.25*	**196**	26.25	*0.736*
121	88	*2*	**158**	39.25	*0.25*	**197**	25.514	*1.764*
122	86	*2.8977*	**159**	39	*0.25*	**198**	23.75	*1.25*
123	83.1023	*2.3774*	**160**	38.75	*0.25*	**199**	22.5	*1.25*
124	80.7249	*3.2249*	**161**	38.5	*0.25*	**200**	21.25	*1.25*
125	77.5	*1.389*	**162**	38.25	*0.25*	**201**	20	*1.03*
126	76.111	*6.586*	**163**	38	*0.25*	**202**	18.97	*1.04*
127	69.525	*4.525*	**166**	37.75	*0.25*	**203**	17.93	*1.03*
128	65	*5*	**167**	37.5	*0.75*	**204**	16.9	*1.04*
129	60	*2.5*	**168**	36.75	*0.25*	**205**	15.86	*0.66*
130	57.5	*2.5*	**169**	36.5	*0.25*	**206**	15.2	*0.2*
131	55	*1.5*	**170**	36.25	*0.2654*	**207**	15	*0.1607*
132	53.5	*1*	**171**	35.9846	*0.4346*	**208**	14.8393	*0.4865*
133	52.5	*1.5*	**172**	35.55	*0.55*	**209**	14.3528	*0.4729*
134	51	*1*	**173**	35	*0.25*	**210**	13.8799	*0.4614*
135	50	*1.5*	**174**	34.75	*0.25*	**211**	13.4185	*0.3785*
136	48.5	*1*	**175**	34.5	*0.5*	**212**	13.04	*0.2159*
137	47.5	*1.5*	**176**	34	*0.5*	**213**	12.8241	*0.5402*
138	46	*1*	**177**	33.5	*0.3306*	**214**	12.2839	*0.1841*
139	45	*0.75*	**178**	33.1694	*0.6694*	**215**	12.0998	*0.1898*
140	44.25	*0.25*	**179**	32.5	*0.5*	**216**	11.91	*0.3463*
141	44	*0.3*	**180**	32	*0.5*	**217**	11.5637	*0.3483*
142	43.7	*0.2*	**181**	31.5	*0.5*	**218**	11.2154	*0.4554*
143	43.5	*0.25*	**182**	31	*0.5*	**219**	10.76	*0.3929*
144	43.25	*0.25*	**183**	30.5	*0.5*	**220**	10.3671	*0.3671*
145	43	*0.25*	**184**	30	*0.25*		10	

As detailed by Kitsos [30], the effects of secondary photon processes may be included without altering the discrete-ordinates transport code itself, but by modification to the multigroup cross-section transfer matrices based on separate calculations that determine energy and angular bremsstrahlung photon distributions. Methods of incorporating secondary photon effects into discrete-ordinates calculations were also investigated by Lorence and Morel with the development of their Coupled Electron Photon Cross Section generating code (CEPXS) [42]. In CEPXS, primary photon cross sections are determined based upon empirical formulas that are fit to experimental data as described by Biggs and Lighthill [43, 44]. Electron cross-section models for bremsstrahlung production and fluorescence are formulated after those developed for the Integrated Tiger Series (ITS) Monte Carlo code [45]. The continuous-slowing-down physics approximation used in ITS has also been incorporated into MCNPX. CEPXS, however, goes much farther in general transport cross sections by accounting for interaction processes not only between photons and electrons, but also elastic and inelastic electron-electron collisions, and positron interactions with other positrons, electrons, and photons. The complete range of interactions modeled by CEPXS is described in the following table.

Table 5.2. Table of CEPXS particle interactions and physical phenomena accounted for in coupled cross section tables.

Interaction type	*Physical process*	
$\Sigma_{electron-electron}$	knock-on	radiative scattering
	elastic scattering	inelastic scattering
	Auger production	ionization
$\Sigma_{electron-photon}$	brehmsstrahlung	fluorescence
$\Sigma_{photon-photon}$	incoherent scattering	photoionization
$\Sigma_{photon-electron}$	compton production	photoelectron production
	pair production	Auger production
$\Sigma_{photon-positron}$	pair positron production	
$\Sigma_{positron-positron}$	collisional scattering	radiative scattering
	elastic scattering	
$\Sigma_{positron-photon}$	bremsstrahlung	fluorescence
	annihilation	
$\Sigma_{positron-electron}$	knock-on production	Auger production

Because CEPXS determines cross sections for multiple particle types, some confusion may need to be cleared after reviewing the above Table. Consider an interaction between a photon and an atomic electron. This interaction results in a photon of lower energy and an electron of some other prescribed energy. The photon-photon cross section represents the energy and probability transfer matrix between the initial photon and the scattered photon. Conversely, the photon-electron cross section represents that for the scattered electron. In the Table it should be noted that CEPXS photon-photon interactions only include incoherent scattering and photoionization phenomena; they do not include the electron binding effect on the incoherent scattering cross section as previously discussed. A comparison between CEPXS and ENDF cross sections graphically identifies the discrepancy. Figure 5.1 shows good agreement between total and pair production cross sections, but CEPXS lacks the coherent scattering and bound-electron effects for incoherent scattering (Figure 5.2).

To make use of the secondary photon process cross section capabilities of CEPXS and the latest photon interaction data available from ENDF, a new version of CEPXS was developed allowing for the combination of both sets of data. Source code was added that gives the user the choice of applying the Biggs-Lighthill data, or instead inserting NJOY processed ENDF cross sections for coherent, incoherent, and pair production interactions. A fully coupled cross-section table in CEPXS can contain separate energy group structures for photons and electrons; however, for this study each table maintains the same 220 group structure, resulting in a coupled cross section table length of 440 groups. Further examples of the differences between CEPXS and ENDF cross sections, along with example input for CEPXS, are described in the Appendices.

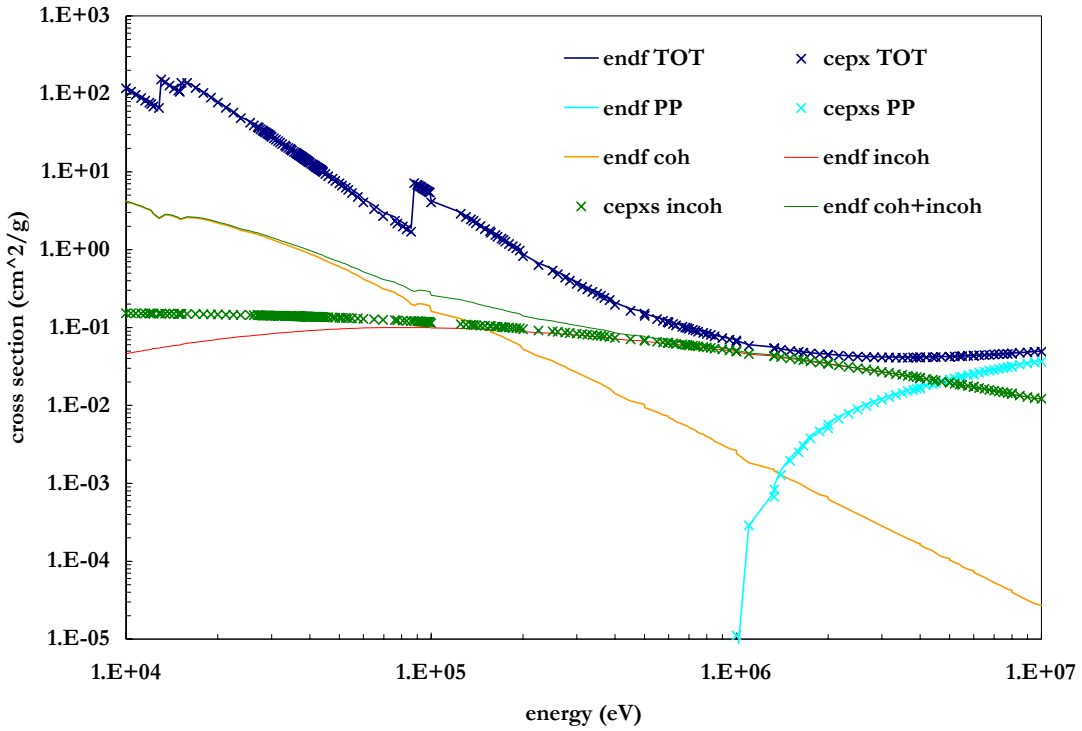

Figure 5.1. Comparison of CEPXS and ENDF/B-VI.8 photon cross sections for lead as a function of energy.

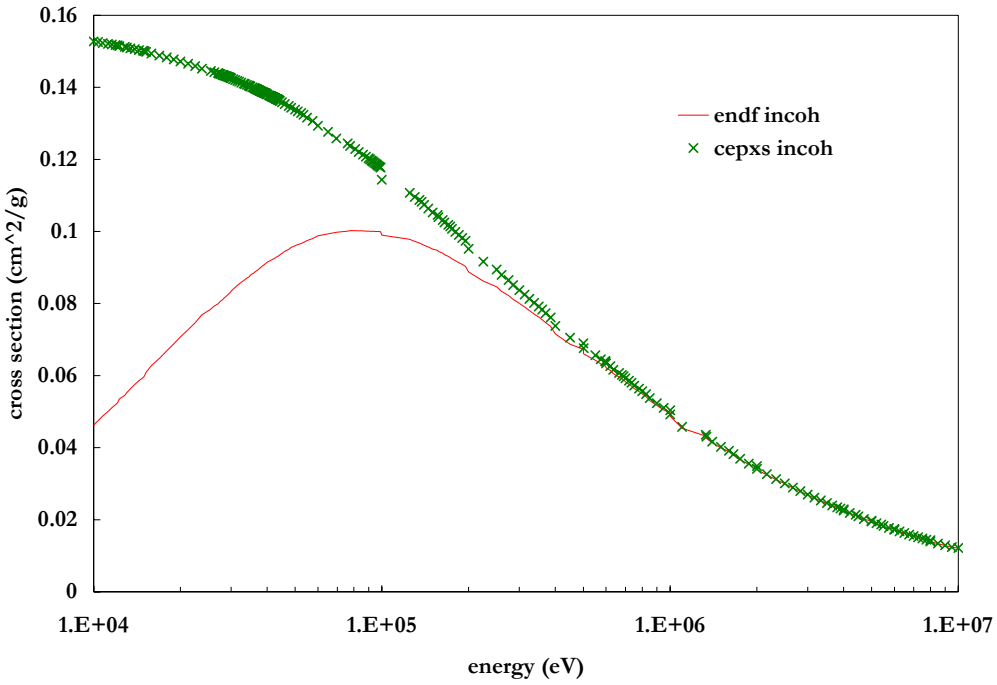

Figure 5.2. Incoherent scattering components of lead cross section magnified on a linear scale. Electron binding (ENDF data) significantly reduces cross section below 0.5 MeV.

5.2.2 Quadrature details

In the theory of discrete-ordinates, the angular variable in the Boltzmann transport equation is represented by a set of user-defined angular quadratures, each with an appropriate weight. In PARTISN the user may choose from a set of built-in quadrature orders or they may input their own. Most quadratures of use in discrete-ordinates calculations (and those built into PARTISN) do not include the normal direction of μ=1.0. Because this study focuses on photon transport through slabs for a variety of incident angles including normal, a Gauss-Lobatto quadrature set of order S_{100} , that specifically includes quadratures at μ=-1.0 and μ=1.0 (shown in Table 5.3), is determined on the closed angular interval [-1,1] and was calculated using Kim's Gauss-Lobatto calculator [46].

5.2.3 Response functions

The purpose of transport techniques and codes that use these techniques to solve the Boltzmann transport equation is to determine the particle flux in the system. As described by Equations (5.1) and (5.2), this flux is modified by an appropriate response function to obtain the quantity of interest. For air exposure, the discrete-ordinates response function is based on the compilation of photon attenuation coefficients of Hubbell and Seltzer [22, 47], whereas the ambient dose equivalent conversion coefficients are those of the International Commission on Radiological Protection (ICRP) Publication 74 [48], both of which are listed in Table 5.4. The set of parameters used in PARTISN are listed in Table 5.5.

As the discrete-ordinates calculations are performed on a 220 energy group structure, the response functions were determined by logarithmically interpolating coefficients at the midpoint of each energy group. The air exposure response was determined by then multiplying each value by that midpoint energy such that $R(E) = E \cdot \mu_{en}(E)/\rho$. A comparison between raw and interpolated response functions is shown in Figure 5.3.

Using the described cross sections, PARTISN was used to calculate photon flux, air exposure, and ambient dose equivalent on the exiting surface of slabs of material, with particles incident along ten angular quadrature directions relative to normal. Slab thicknesses were chosen for each incident angle θ_{inc} according to

$$t_g = \frac{b}{\mu_g} \cos\theta_{inc}, \qquad (5.6)$$

where

t_g = linear slab thickness (cm) for energy group g

b = mean free path optical thickness (unitless), and

μ_g = total linear attenuation coefficient (cm^{-1}) at energy group g.

Table 5.3. First 50 quadratures and weights of the S_{100} set used in PARTISN. The remaining 50 are negative values of those listed.

	quadrature	*weight*		*quadrature*	*weight*
1	1	0.00010101	26	0.69871161	0.011294837
2	0.999258578	0.000622538	27	0.675777444	0.011637424
3	0.997515249	0.00112054	28	0.652169649	0.01196841
4	0.994777307	0.001617163	29	0.627911756	0.012287467
5	0.991047694	0.002112138	30	0.603027948	0.012594275
6	0.986330164	0.002604999	31	0.577543028	0.012888528
7	0.980629431	0.00309526	32	0.5514824	0.013169934
8	0.973951181	0.003582435	33	0.524872043	0.013438212
9	0.966302073	0.004066037	34	0.497738482	0.013693095
10	0.957689734	0.004545587	35	0.470108764	0.013934328
11	0.948122747	0.005020605	36	0.442010432	0.01416167
12	0.937610651	0.005490618	37	0.413471494	0.014374897
13	0.926163923	0.005955158	38	0.384520399	0.014573793
14	0.913793975	0.006413762	39	0.355186006	0.014758163
15	0.900513137	0.006865973	40	0.325497555	0.014927821
16	0.886334648	0.007311339	41	0.295484642	0.015082599
17	0.871272641	0.007749417	42	0.265177182	0.015222342
18	0.85534213	0.00817977	43	0.234605389	0.015346911
19	0.838558996	0.00860197	44	0.203799736	0.015456183
20	0.820939968	0.009015595	45	0.17279093	0.015550047
21	0.802502609	0.009420233	46	0.141609883	0.01562841
22	0.783265298	0.00981548	47	0.110287676	0.015691195
23	0.763247211	0.010200944	48	0.078855532	0.015738338
24	0.742468302	0.010576239	49	0.047344783	0.015769793
25	0.720949285	0.010940991	50	0.01578684	0.015785528

Table 5.4. Mass-energy absorption for air (cm^2/g) and ambient dose equivalent (pSv-cm^2) coefficients used for PARTISN and MCNPX response functions [22, 48].

energy (MeV)	$\mu_{en}(E)/\rho$	*H*(10)*
0.01	4.742	0.061
0.015	1.334	0.83
0.02	0.5389	1.05
0.03	0.1537	0.81
0.04	0.06833	0.64
0.05	0.04098	0.55
0.06	0.03041	0.51
0.08	0.02407	0.53
0.1	0.02325	0.61
0.15	0.02496	0.89
0.2	0.02672	1.2
0.3	0.02872	1.8
0.4	0.02949	2.38
0.5	0.02966	2.93
0.6	0.02953	3.44
0.8	0.02882	4.38
1	0.02789	5.2
1.5	0.02547	6.9
2	0.02345	8.6
3	0.0187	11.1
4	0.0187	13.4
5	0.0174	15.5
6	0.01647	17.6
8	0.01525	21.6
10	0.0145	25.6

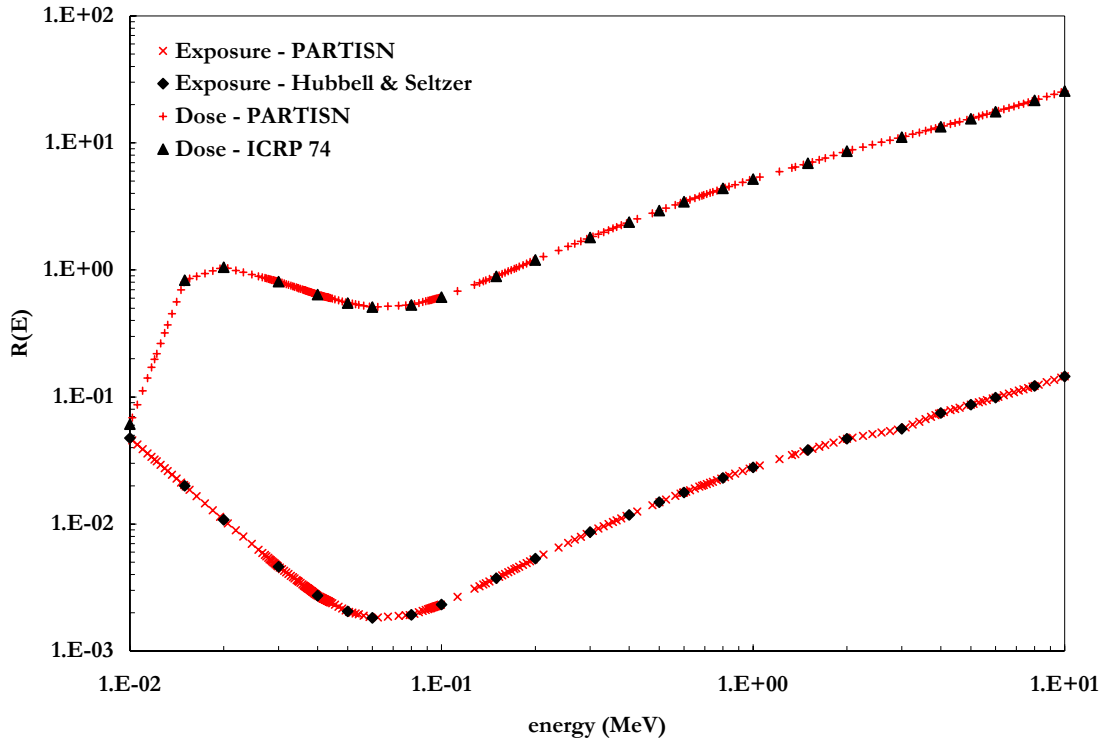

Figure 5.3. Raw and interpolated air exposure response function (units of MeV-cm^2/g) of Hubbell and Seltzer and ICRP ambient dose equivalent conversion coefficients (units of pSv-cm^2).

Table 5.5. Parameters used in discrete-ordinates calculations.

PARTISN property	*value*
convergence criteria	1.E-04
geometry	infinite slab
Legendre scattering order	7
Quadrature order	S_{100}
Number of groups	440 220 photon 220 electron
fine mesh density	100 per mfp

5.3 Monte Carlo calculations

For the purpose of comparison and verification of the discrete-ordinates calculations, numerous calculations were performed using the fundamentally different stochastic techniques of MCNPX. But although the techniques differ, an effort was made to keep the basic particle interaction data, i.e., cross-section data, as consistent as possible.

The ENDF/B-VI.8 primary photon data used for discrete-ordinates calculations has been processed and formatted for Monte Carlo codes in the MCPLIB04 photon library [49]. Several major and minor differences exist between MCPLIB04 and the 220-group discrete-ordinates library. First, Monte Carlo cross-section libraries are continuous energy, meaning that at specific values of energy, the cross section is specified. Should a particle at some point have an energy not specified in the table, the cross section is logarithmically interpolated. This differs from discrete-ordinates multigroup tables in which case particles cannot have specific values of energy, but only values of a group defined between that group's lower and upper limits. For any group, the cross section for that group has been averaged over the group's energy limits. For this reason, Monte Carlo tends to be more accurate than discrete-ordinates[1].

Electron cross sections in MCNPX are derived from the same source as those in CEPXS. Although MCNPX is capable of charged particle transport, such calculations are computationally expensive. This work applies the thick target bremsstrahlung approximation in which electrons produced from photon interactions produce

[1] Although MCNPX does include the capability of performing Monte Carlo calculations with multigroup cross sections, most calculations use continuous-energy cross sections.

bremsstrahlung photons that are later transported, but the electrons themselves are assumed to locally deposit their kinetic energy as they slow to a stop in the material.

In MCNPX it is unnecessary to provide response functions for each bin because the code automatically interpolates these values. The MCNPX "star tally" feature also allows for the multiplication of a particle's energy by its contribution to flux. Again, as each particle's energy is not restricted to the multigroup energy structure, this increases the accuracy of Monte Carlo calculations. Thus, response functions input into MCNPX are the values listed in Table 5.4.

MCNPX calculations are performed using infinite slab geometry, accomplished by using reflective boundary conditions on the slab side-walls. Incident monoenergetic photons are uniformly distributed on the front face of a slab of thickness determined by the MCPLIB04 total cross section at the incident energy and Equation (5.6). Photons are tallied on the slab's back facet. Obliquely incident beams occur at the same angles as those used for PARTISN calculations.

CHAPTER 6 PHOTON BUILDUP FACTORS – RESULTS

The methods and tools described in the previous chapter were used with the discrete-ordinates code PARTISN to determine a set of buildup factors for the materials listed in Table 6.1 for shield thicknesses ranging from 1 to 10 mean free paths. For each mean free path, calculations were performed for 10 incident angles and at 10 source energies as listed in Table 6.2 while adjusting the normal thickness of the shield such that the uncollided photon (slant-path) thickness remained constant.

Comparison calculations in MCNPX were performed for several energies at slant-path thicknesses of 1, 5, and 10 mean free paths. As Monte Carlo calculations are computationally more expensive, the goal was not to repeat each discrete-ordinates calculation, but to perform only enough that a convincing argument may be made regarding the discrete-ordinates method applying coupled electron-photon cross sections and the quality of results compared to a different method.

While the two methods show excellent agreement generally, a number of data points, specifically in the flux comparisons, are observed to differ significantly for low-Z materials and low incident beam energies. Additionally, some angular effects are consistently observed for thin shields of thicknesses below 5 mean free paths for all energies and for all materials. These results for representative cases along with physical interpretations of and reasons for the results are presented in this chapter. Complete results are reserved for the Appendices.

Table 6.1. Materials and physical properties used for discrete-ordinates and Monte-Carlo buildup-factor calculations [18].

element		*density* (g/cm^3)
aluminum		2.6989
iron		7.874
lead		11.35
material & components		*density* (g/cm^3) *weight fraction*
water		1
	hydrogen	0.111
	oxygen	0.889
concrete		2.3
	hydrogen	0.0059
	oxygen	0.4983
	sodium	0.0171
	magnesium	0.0024
	aluminum	0.0456
	silicon	0.3158
	sulfur	0.0012
	potassium	0.0192
	calcium	0.0826
	iron	0.0122

Table 6.2 Incident photon energies and angles for buildup calculations. For each mean-free-path thickness between 1 and 10, calculations are performed at each angle (relative to normal) and each energy listed below.

	$cos(\theta_{inc})$	θ_{inc} degrees	source energy
1	1	0.00	50 keV
2	0.98633	9.48	100 keV
3	0.90051	25.77	500 keV
4	0.74247	42.06	1 MeV
5	0.65217	49.29	2 MeV
6	0.49774	60.15	4 MeV
7	0.35519	69.20	5 MeV
8	0.26518	74.62	6 MeV
9	0.17279	80.05	8 MeV
10	0.07886	85.48	10 MeV

The presentation of results begins with focus on thin slabs of slant-path thicknesses less than 5 mfp of lead, as lead is a primary photon shielding material. Shown in Figure 6.1 are purely-angular flux, exposure, and dose buildup factors for 500-keV photons on 1-mfp slant-path thicknesses. Of particular interest is the noticeable downward trend in buildup with respect to increasing incident beam angles relative to normal. Such trends are observed both using discrete-ordinates techniques and Monte Carlo at all incident energies for all materials for thicknesses less than 5 mfp. For slabs with optical thicknesses greater than 5 mfp, buildup factors tend to increase with increasing angle of incidence.

In Figure 6.2 through Figure 6.6, examples of angular buildup factors for lead (high Z) and water (low Z) with 500-keV incident photons are presented. MCNPX results were obtained with sufficient statistical variations such that the error bars are smaller than the data symbols. For lead, relative standard error varies between 0.09% (5 mfp, normal) and 0.12% (10 mfp, 85 degrees), and for water, relative errors are between 0.03% (1mfp, normal) and 0.08% (5mfp, normal). Figure 6.7 and Figure 6.8 show buildup factors for 10 MeV photons on 1- and 10-mfp thick lead slabs, and the relative differences in dose are between 10% and 30%. Flux differences are, in general, much greater than those for dose or exposure, and a reason for this is discussed later.

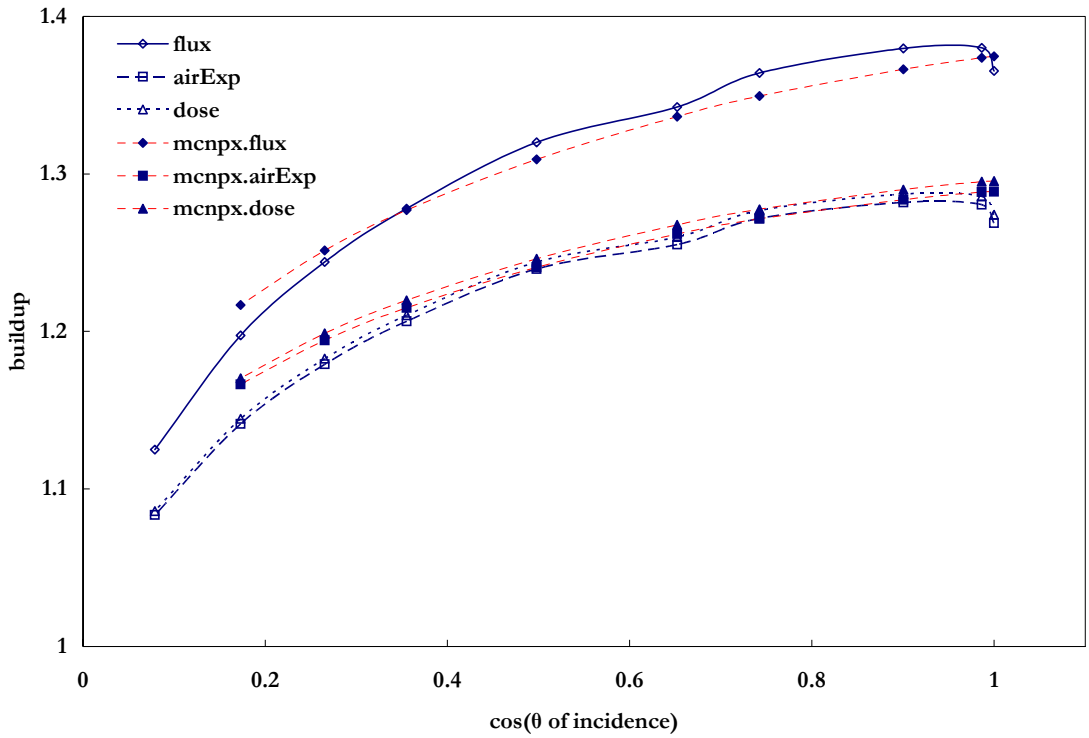

Figure 6.1. Purely-angular photon buildup factors for 500-keV photons incident on 1 mfp of lead. Relative difference between discrete-ordinate and Monte Carlo is ~ 2% at cosine = 0.17.

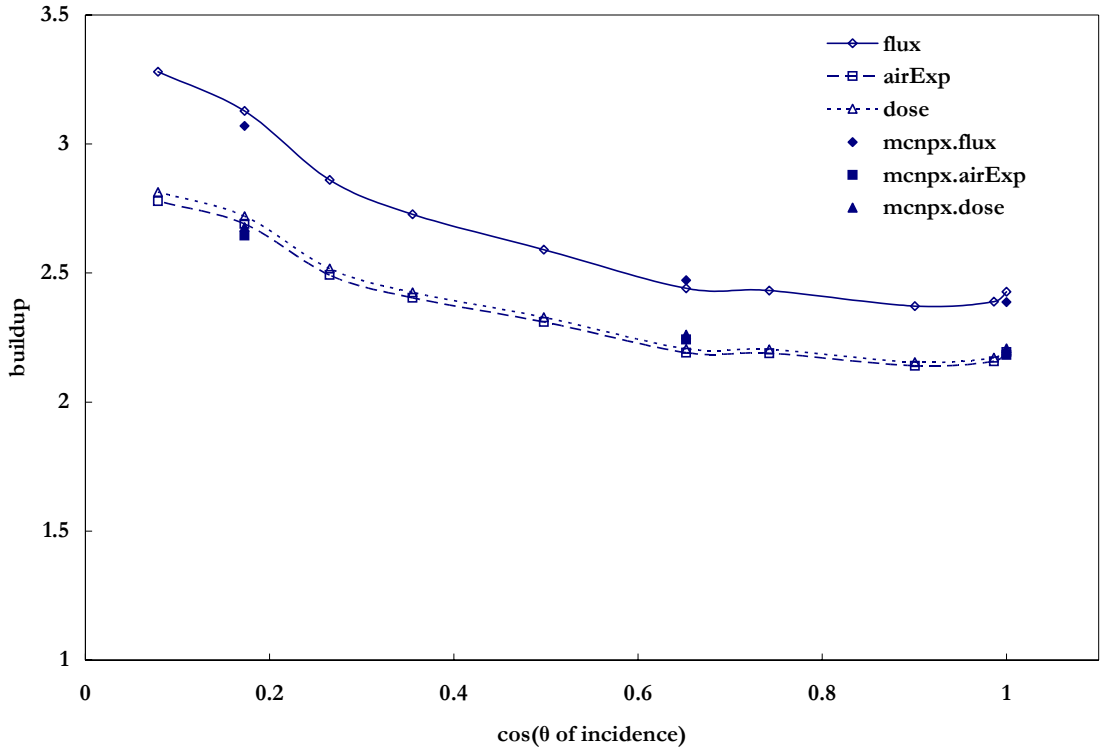

Figure 6.2. Purely-angular photon buildup factors for 500-keV photons incident on 5 mfp of lead. Maximum elative difference ~ 2% at cosine = 0.17.

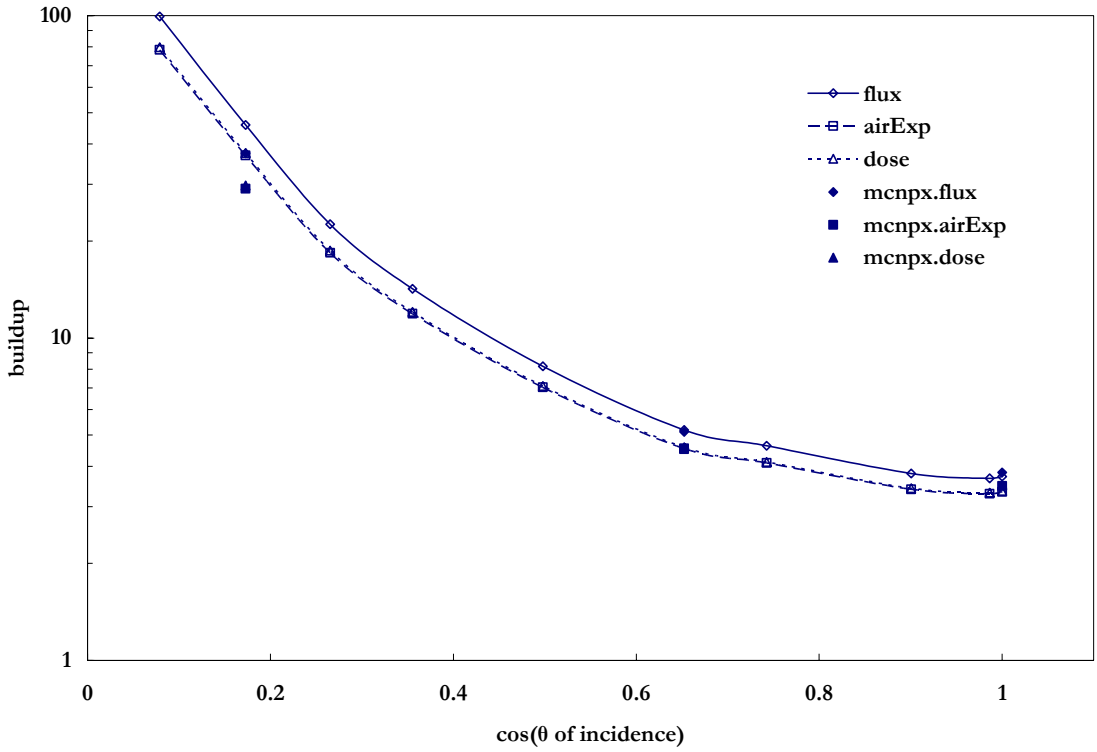

Figure 6.3. Purely-angular photon buildup factors for 500-keV photons incident on 10 mfp of lead. Maximum relative difference ~ 26% at cosine = 0.17.

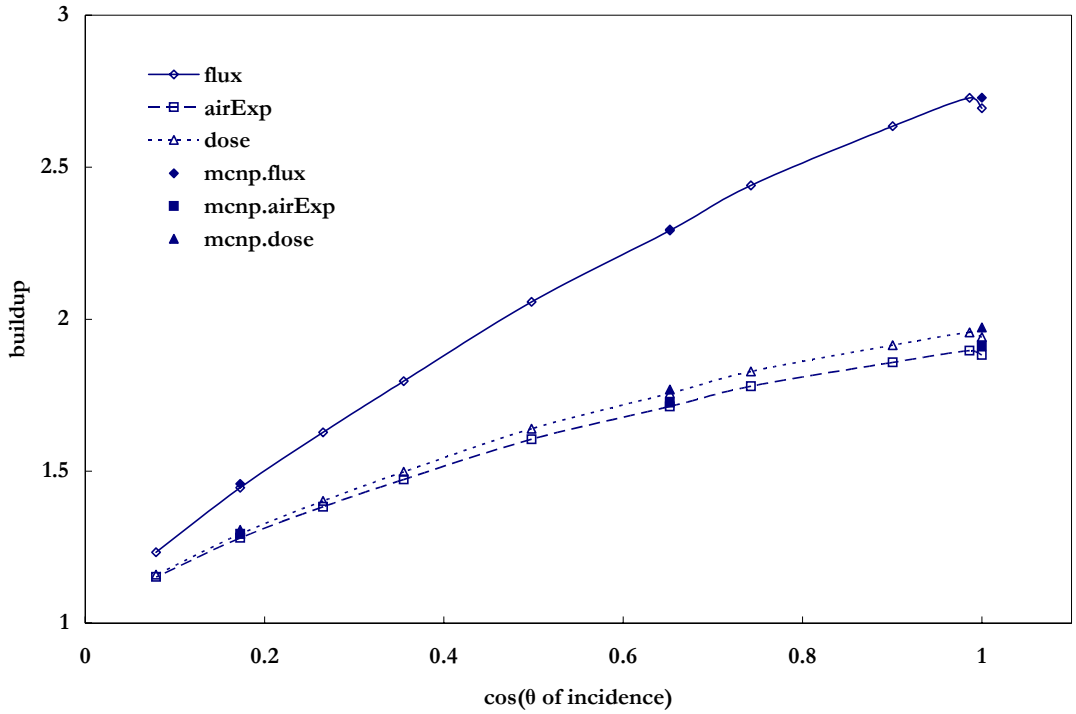

Figure 6.4. Purely-angular photon buildup factors for 500-keV photons incident on 1 mfp of water. Maximum relative difference for exposure ~ 1.5% at cosine = 0.17.

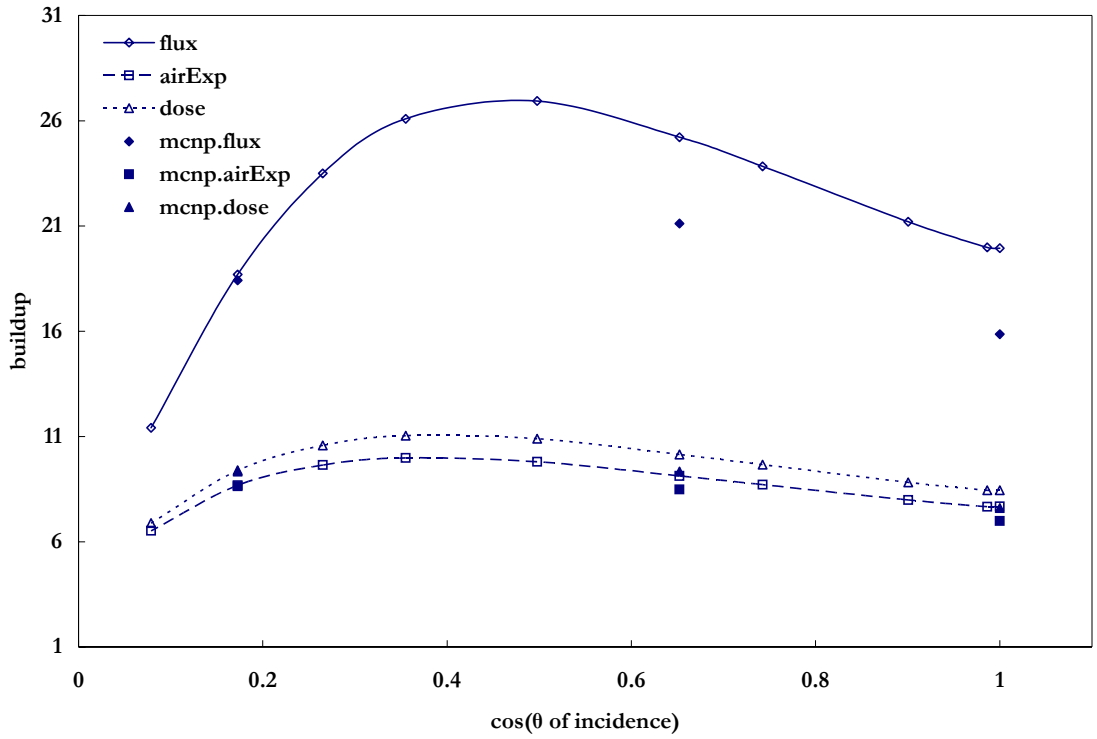

Figure 6.5. Purely-angular photon buildup factors for 500-keV photons incident on 5 mfp of water. Maximum relative difference for exposure ~ 11% at cosine = 1.0.

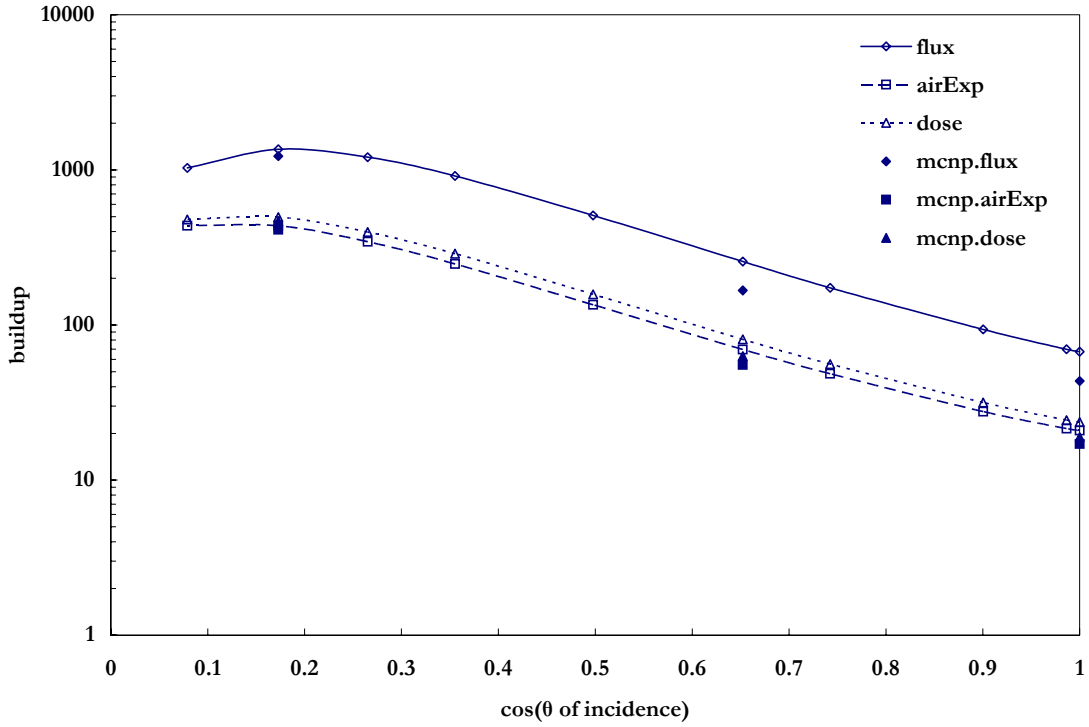

Figure 6.6. Purely-angular photon buildup factors for 500-keV photons incident on 10 mfp of water. Maximum relative difference for exposure ~ 28.4% at cosine = 0.65.

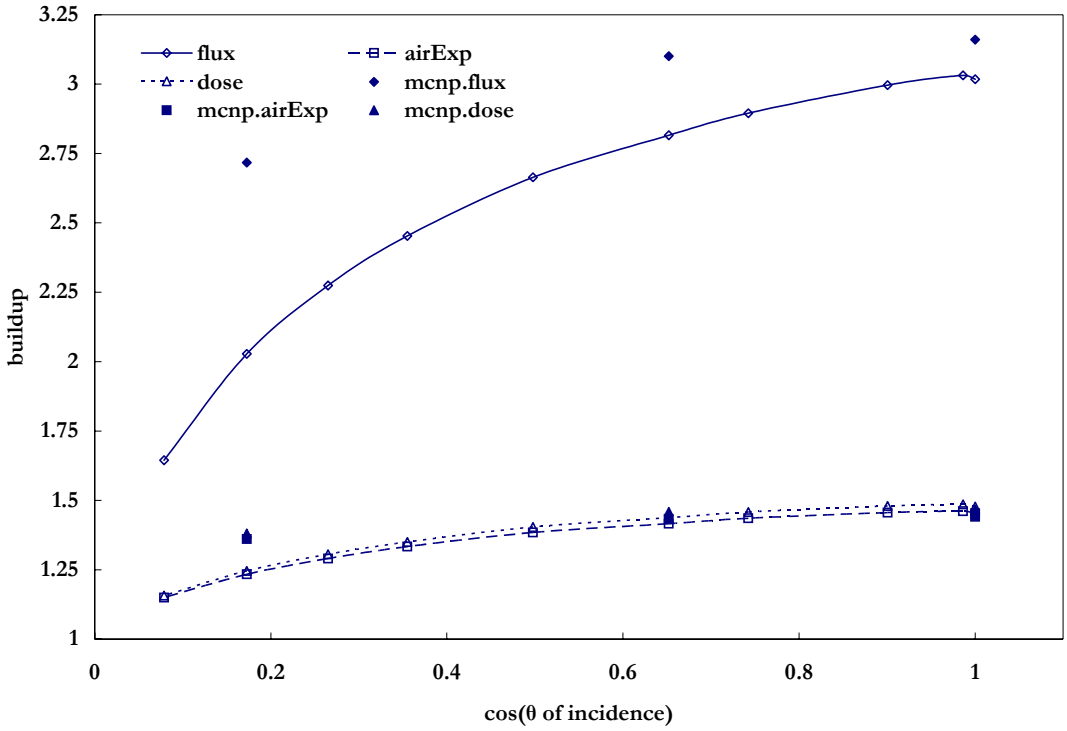

Figure 6.7. Purely-angular photon buildup factors for 10-MeV photons incident on 1 mfp of water. Maximum relative difference for exposure ~ 10.4% at cosine = 0.65.

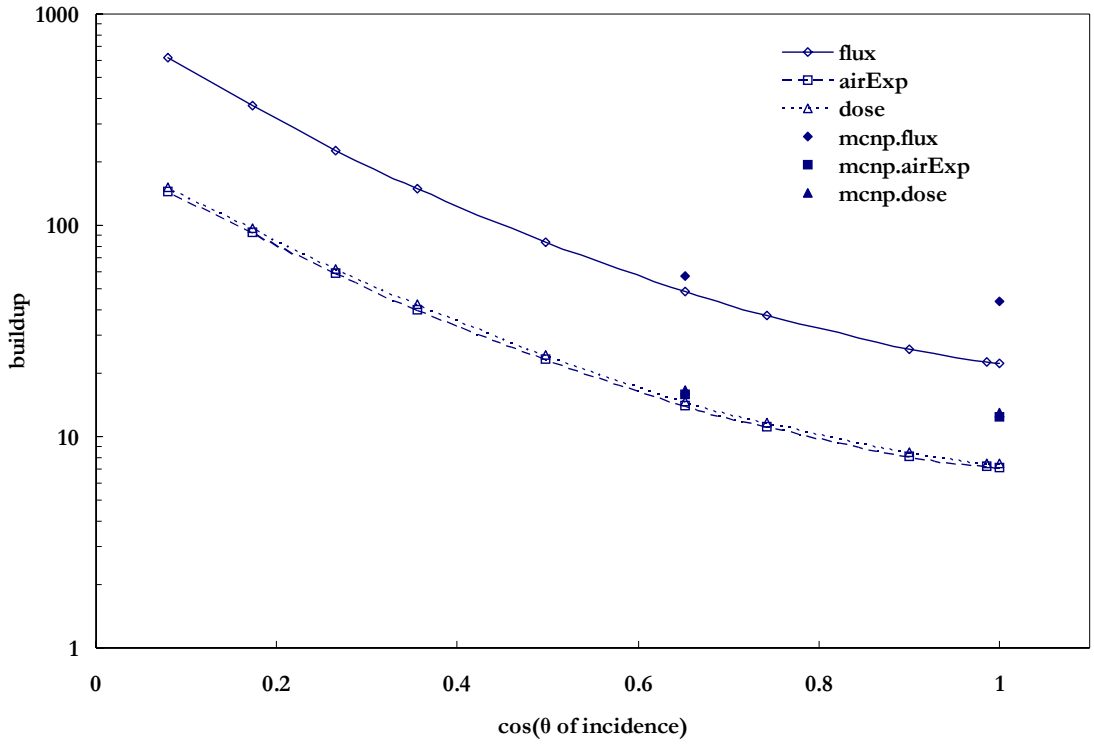

Figure 6.8. Purely-angular photon buildup factors for 500-keV photons incident on 10 mfp of water.

As is indicated by the figures, thin shields of less than 5 mfp show a decreasing buildup with increasing incident angle, while above 5 mfp this trend is reversed, regardless of photon energy. To determine why these trends are observed, a qualitative analysis of thin shields is presented.

The two following Figures provide internal views into a 1-mfp-thick slab with photons incident both normally and obliquely. In Figure 6.9, a photon experiencing an interaction within the shield is subject to scattering into an angle dictated by the Klein-Nishina formula. Since the photon is normally incident upon the slab, the azimuthal component of scattering angle has no influence as to the remaining pathlength that photon must traverse to exit the slab. This implies that all scattered photons exit the slab with equal probability. In the case of Figure 6.10, the azimuthal component of the Klein-Nishina scattering angle has a significant effect on whether that scattered photon will exit the slab. For example, should a photon scatter with an angle such that it follows the 'short' escape path of length optical thickness, b_{short}, the probability it will exit without further scatter is $e^{-b_{short}}$. The same is true for when that photon scatters into the angle that takes it along the 'long' escape path. Hence quantitatively, $e^{-b_{short}} > e^{-b_{long}}$, that is, particles scattered along the short pathlength are more likely to escape the slab. Qualitatively, one can see that the extent by which the short and long escape paths differ depends heavily on depth in the shield at which the collision occurs, and the scattering angle itself. Particles escaping along the short path cross the exit surface with angles far less severe (relative to normal) than those escaping along the long path and thus contribute less to the flux across the slab's exit surface. As the angle of incidence increases, both the normal thickness and b_{short} decrease significantly.

At some oblique angle, b_{long} may even be in the reflected direction, thereby increasing albedo on the incident surface, as shown in Figure 6.11. Such a qualitative prediction is in fact observed by tallying reflected flux across the incident surface in MCNPX. Figure 6.12 clearly indicates that as the incident angle increases, the fraction of reflected photons increases by approximately one order of magnitude.

Another difference between the Monte Carlo and discrete-ordinates calculations is the treatment of the angular variable, which in MCNPX, is also continuous. In discrete-ordinates, the user is forced to choose a set of discrete quadratures. Usually, the denser the quadrature, the better the calculation; however, this discrete treatment of the angular variable can still lead to differences when compared to Monte Carlo results.

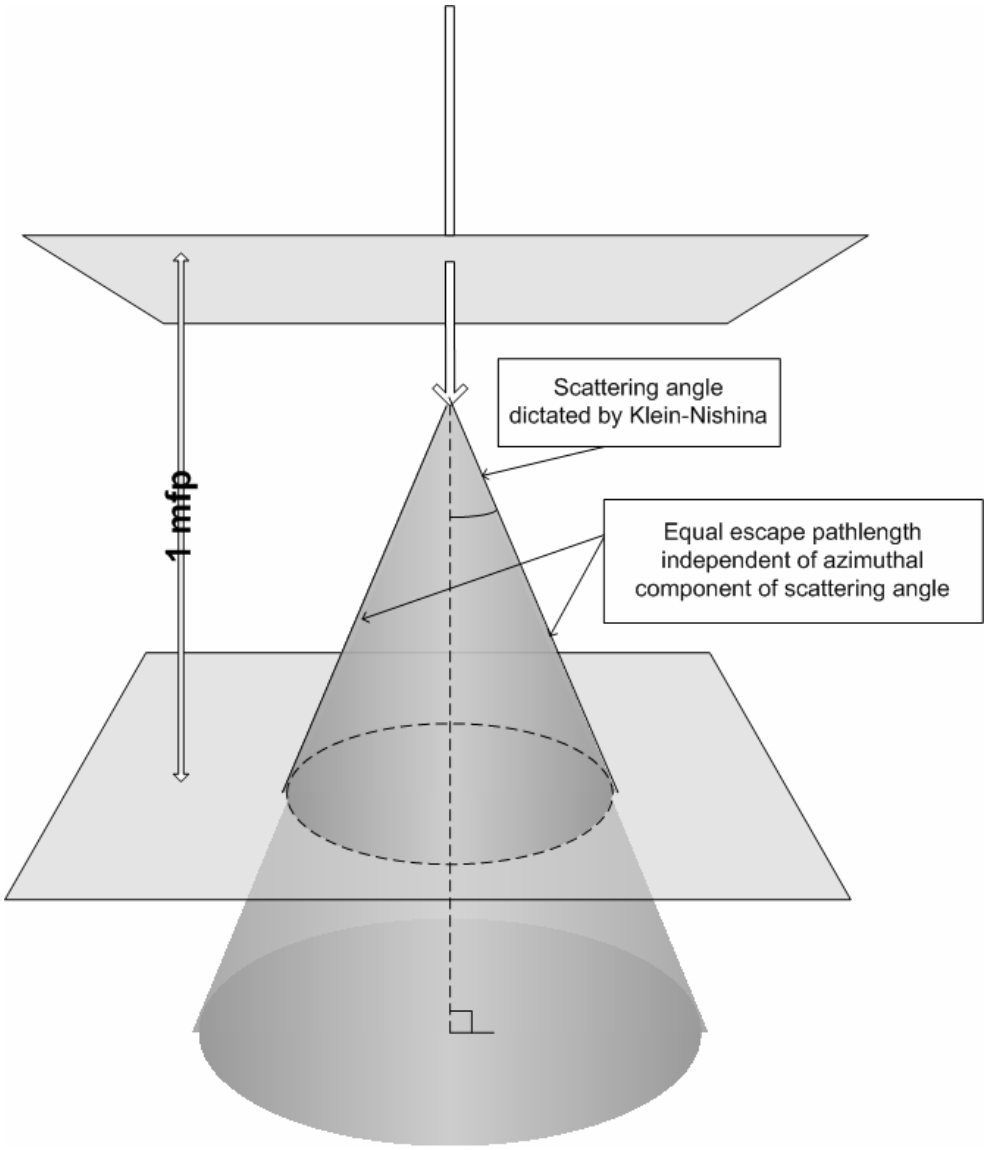

Figure 6.9. Internal view of photons normally incident on 1-mfp thick shield.

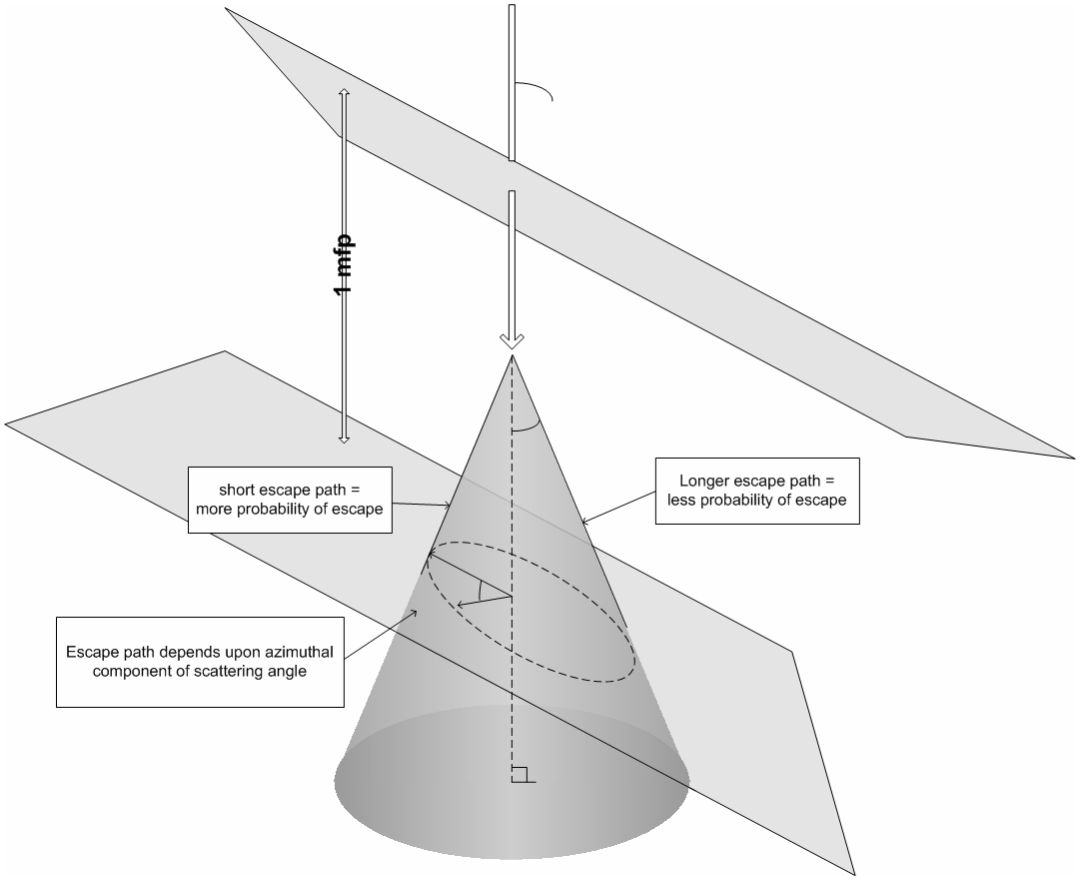

Figure 6.10. Internal view of obliquely-incident photons on 1-mfp (slant-path) thick shield.

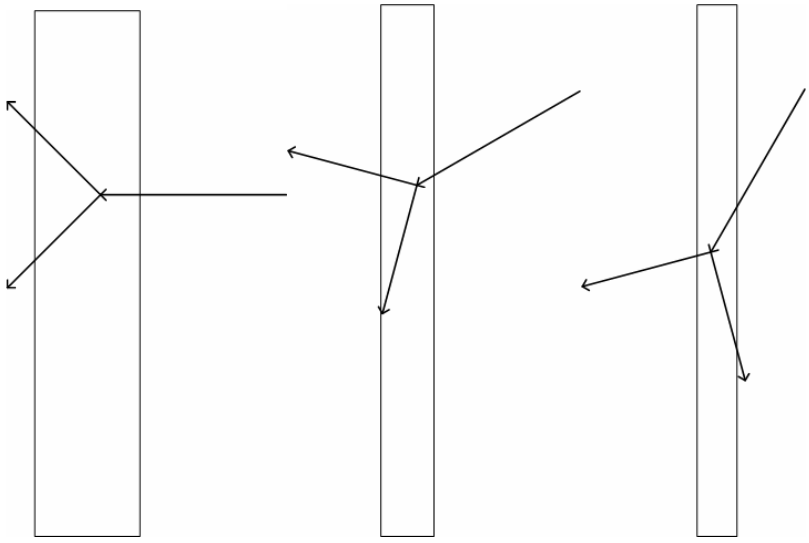

Figure 6.11. Escape path differences for (a) normal, (b) moderate, and (c) extreme incident angles.

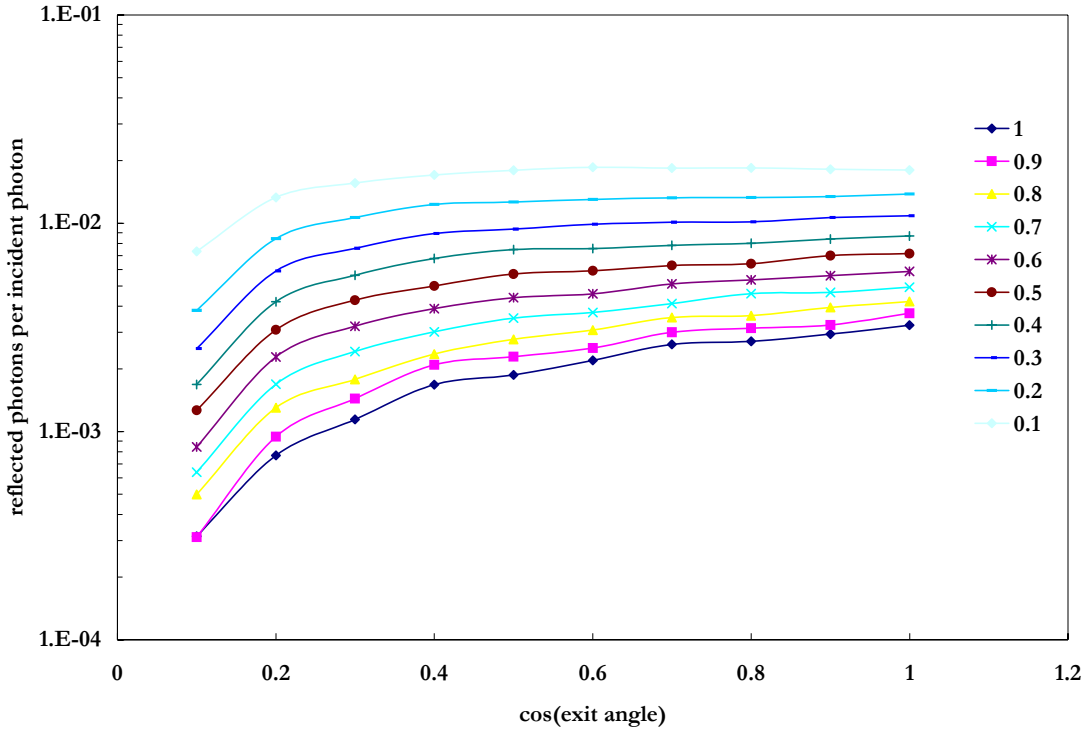

Figure 6.12. Fraction and angular distribution of reflected photons for 500-keV photons on 1 mfp of lead for incident oblique angles in increments of cos(angle)=0.1.

Comparisons between MCNPX and PARTISN are generally encouraging, as both methods indicate similar trends for thin-shield buildup factors as a function of incident angle. However, differences do exist, ranging from ~2% relative difference for 1 mfp to as much as 20% for some 10-mfp shields. Possible explanations for the differences are numerous, and many are explained.

A major difference between Monte Carlo and discrete-ordinates methods lies in the treatment of the energy variable, which in Monte Carlo is continuous. Contrary to the multigroup treatment of energy in discrete-ordinates, photons in Monte Carlo exist at specific energies dictated by the laws of interaction physics. In PARTISN, the fine 220-group energy structure automatically contains features that would yield differences when compared to Monte Carlo methods. One such feature is the arbitrary choice of 1-keV wide groups for the ten source energies of Table 6.2. For source energies above 500 keV, a group width of 1 keV is much less than widths of the adjacent energy groups. The wider the energy group, the more difference exists between the group-averaged cross section and the Monte Carlo pointwise cross section at a similar energy. Thus, source photons scattered into an adjacent energy group below may be subject to much different scattering cross sections than would a photon scattered in the Monte Carlo calculation. Recall, however, that these source groups were chosen to minimize the difference of total cross section between the two methods, thereby preserving a similar slab thickness for each method. These differences in cross section have pronounced effects for thicker shields, where a 1% difference in cross section can lead to ~ 10% variations in flux calculations.

In Figure 6.5 through Figure 6.8, differences in flux between the two methods are more pronounced than those for dose and exposure. This is largely because the flux profile on the exit surface peaks between 70 keV and 125 keV where the dose and exposure coefficients have the smallest values (Figure 5.3). This means that the photons contributing most to flux contribute the least to exposure and dose.

For more extreme oblique angles, photon flux calculations by MCNPX become less reliable, though statistics remain consistently good. In MCNPX a particle's contribution to flux across a surface is determined by dividing that particle's weight by the cosine of its angle

(relative to normal). However, for extreme exit angles of $|\mu| < 0.1$, MCNPX sets the exit angle to $|\mu| = 0.05$. More extreme oblique incident angles result in more photons crossing the exit surface with cosines less than 0.1, and these photons are assigned cosines much smaller than usual, contributing more to exit flux. The result is seen in Figure 6.1 for lower cosines: Monte-Carlo calculations become much less reliable at calculations for which there are more photons exiting at extreme angles. In the calculations for which the incident angle cosine is 0.07, the results are not at all reliable because $|\mu| < 0.1$.

As previously mentioned, past buildup factor calculations have been performed using a variety of methods, geometries, source energies, materials, and cross section data. For this reason, direct comparisons between current and past calculations in which each of the previous variables is identical are not possible. However, current buildup factors with normally-incident photons can be compared to past data in which some (usually not all) variables can be matched. Table 6.3 lists major properties of calculations by previous authors including geometry, method (Monte Carlo, discrete ordinates, or moments.), whether cross sections used included coherent scattering, and if incoherent scattering included the electron binding energy.

The following tables provide comparisons between the buildup factors calculated in this study and those of previous authors. Given the range of properties for which these calculations are performed, there is generally good agreement between the results of this study and those performed within the last few years. For lead, the best comparison is with the results of Chen, for which the only differences are the methods used and cross section origin (although both cross section data include coherent and bound-electron effects). Our results for lead are within 40% at 10 mfp, where cross sections differences significantly accumulate and likely account for the variation. Below 10 mfp, differences are less than 17%. For iron, our results are well within the range of those of other authors, given the major differences between geometries and methods used.

Table 6.3. Properties of buildup-factor calculations by previous authors, including geometries, methods, and cross-section specifics.

Matrix of buildup factor calculation properties

	ANSI	Chen	Kitsos	Hirayama	Chibani	This work
geometry	PI	slab	PI	PI	PI	slab
method	M	MC	S-N	MC	MC	S-N
coherent	no	yes	yes	yes	yes	yes
bound electron	no	yes	yes	yes	yes	yes
brem./fluor.	yes	yes	no	yes	yes	yes
cross sections	Hubbell	Hubbell	ENDF	Hubbell	Hubbell+	ENDF

PI = point isotropic

M = moments

MC = Monte Carlo

S-N = discrete ordinates

\+ = other data included

Table 6.4. Exposure buildup factor comparisons for lead. Data for comparison is extracted from ANSI/ANS [18], Chen[21,50], and Kitsos [29].

Exposure buildup factors comparison - lead				
		100 keV		
	ANSI	Chen	Kitsos	This work
1 mfp	2.04	1.75	1.099	2.03
4 mfp	9.59	4.12	1.343	4.92
10 mfp	29.40	36.90	6.418	50.89
		500 keV		
	ANSI	Chen	Kitsos*	This work
1 mfp	1.24	1.26	1.322	1.27
4 mfp	1.62	1.64	2.096	1.97
10 mfp	2.10	2.05	3.861	3.33
		1 MeV		
	ANSI	Chen	Kitsos	This work
1 mfp	1.38	1.39	1.438	1.37
4 mfp	2.19	2.09	2.575	2.47
10 mfp	3.51	3.16	4.979	4.59
		10 MeV		
	ANSI	Chen	Kitsos	This work
1 mfp	1.51	1.46	1.216	1.45
4 mfp	3.42	2.55	1.758	3.06
10 mfp	15.40	7.91	4.894	7.16

* Kitsos' calculations performed at 511 keV

Table 6.5. Exposure buildup factor comparisons for iron. Data for comparison extracted from ANSI/ANS [18], Hirayama [51], and Chibani [52].

Exposure buildup factors comparison - iron

50 keV

	ANSI	Hirayama	Chibani	This work
1 mfp	1.10	-	1.66	1.13
5 mfp	1.20	-	2.17	1.44
10 mfp	1.26	-	2.81	1.78

100 keV

	ANSI	Hirayama	Chibani	This work
1 mfp	1.40	1.39	1.58	1.33
5 mfp	2.07	2.10	3.18	2.47
10 mfp	2.61	2.66	5.83	4.08

1 MeV

	ANSI	Hirayama	Chibani	This work
1 mfp	1.85	1.86	1.87	1.68
5 mfp	6.74	6.78	6.94	5.31
10 mfp	15.80	16.00	16.9	11.25

10 MeV

	ANSI	Hirayama	Chibani	This work
1 mfp	1.33	1.51	1.53	1.41
5 mfp	2.50	3.27	3.34	2.95
10 mfp	4.69	6.14	6.61	5.34

CHAPTER 7 OVERALL PANDEMONIUM AND MCNPX COMPARISON

To determine the overall performance of Pandemonium and its improvements, an example comparison was performed using versions 1 and 2 of Pandemonium and MCNPX. A description of the model and differences between the two methods is followed by results of the comparison and explanations of observed variations. Finally, several 2-dimensional plots are presented that exemplify the usefulness of Pandemonium as a tool for modeling large complex radiological facilities.

A room containing two gloveboxes of different types (i.e., one with windows and gloveports, and another without), three identical plutonium sources, and five detector positions is considered for this comparison. The glovebox containing two sources is also shielded by a hydrogenous shield. To reproduce this model in MCNPX (which models in 3-D), the MCNPX model was restricted to 22-cm height in the z-direction, beyond which particles were no longer tracked. Gloveport inhomogeneities (windows and gloveports) were modeled in MCNPX as shown in Figure 7.1 through Figure 7.3.

As Pandemonium determines photon and neutron source strengths, these values were used by MCNPX according to the following:

$$S_{MCNPX} = S_{Pandemonium}. \quad (7.1)$$

Several differences exist between the Pandemonium and MCNPX models. First, Pandemonium neutron calculations are performed at 2-MeV and they are based on 1-group cross sections. The MCNPX neutron energy distribution is the Watt fission spectrum of ^{239}Pu at 1-MeV.

Second, as Pandemonium photon calculations are performed at 25 discrete energies listed in Table 4.3, the MCNPX photon source consists of photons at these discrete energies, as opposed to a continuous distribution in energy.

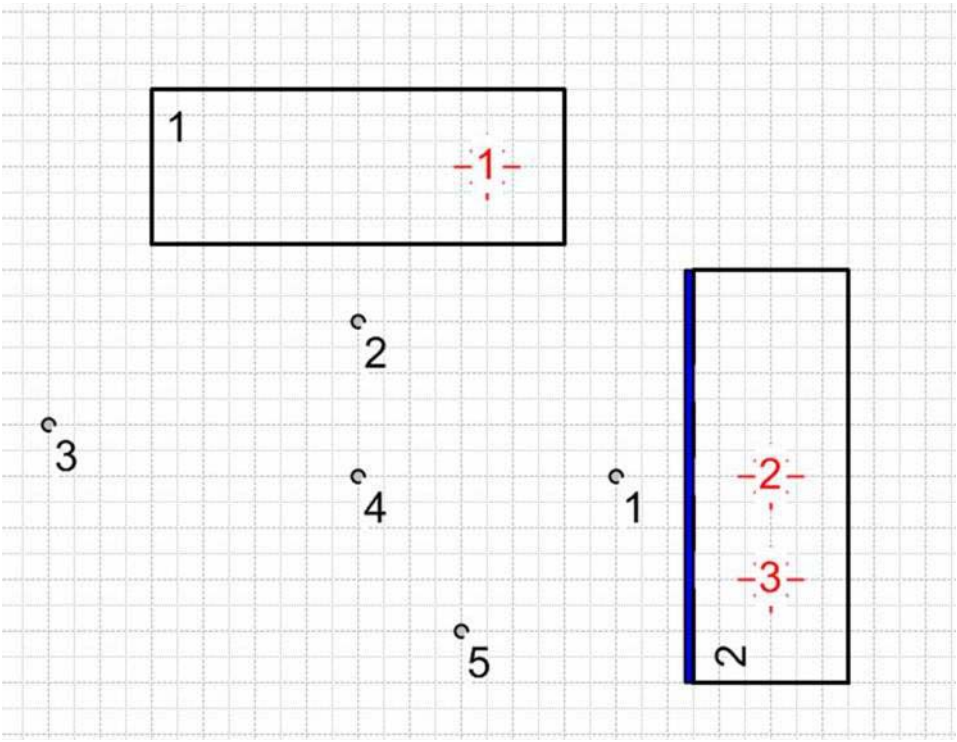

Figure 7.1. Two-dimensional geometry in Pandemonium for comparison with MCNPX. Sources are indicated in red, while the 5 detector positions are shown as small circles. Three sources are housed in two gloveboxes, one containing two sources with a hydrogenous shield and gloveports/windows.

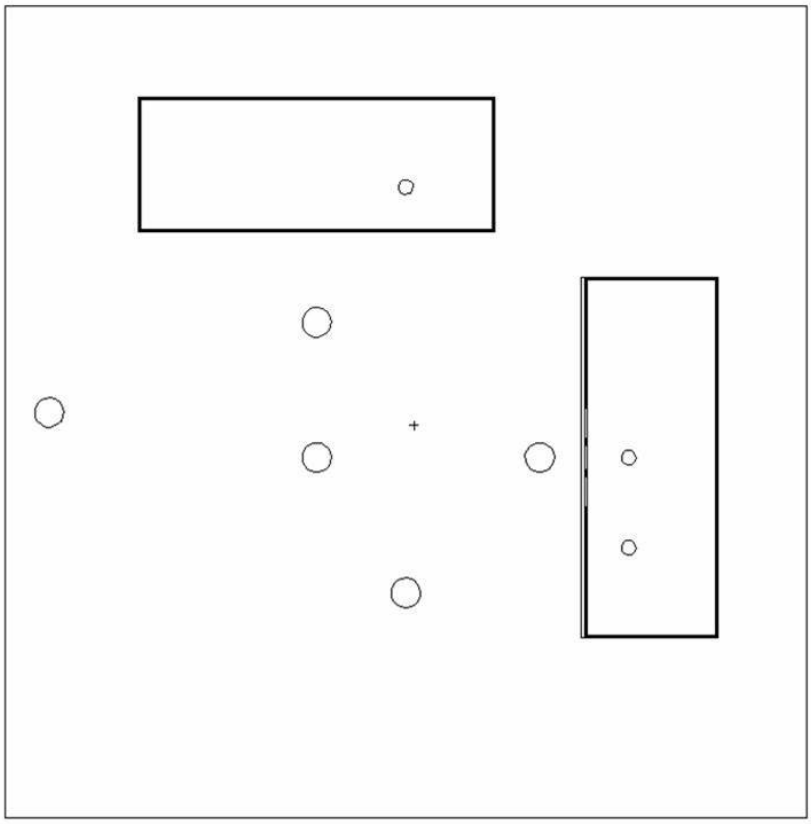

Figure 7.2. MCNPX geometry for Pandemonium comparison. Large circles represent point detector locations and spheres for surface flux tallies.

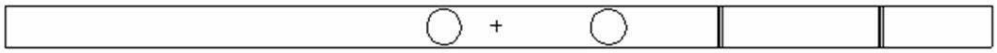

Figure 7.3. MCNPX geometry (x,z) indicating the 22-cm geometry height in the z direction. Particles are not tracked outside of the encompassing surface.

Number densities and physical parameters of the three identical sources are provided in the table below.

Table 7.1. Material and physical properties of plutonium sources used in MCNPX and Pandemonium comparisons.

Plutonium source properties		
composition		
	isotope	*Number Density* $(atoms/cm^3)$
	Pu-238	3.997E+18
	Pu-239	3.73E+22
	Pu-240	2.38E+21
	Pu-241	7.89E+19
	Pu-242	3.93E+18
physical		
	property	*quantity / units*
	density	15.8 g/cm^3
	radius	5 cm
	mass	8.27 kg

For direct comparison between old and new versions of the Pandemonium, the first version of the code was slightly altered to include ICRP 74 dose conversion coefficients, consistent with those used in Pandemonium 2.0 and MCNPX calculations.

Table 7.2. Dose rate comparisons between Pandemonium versions 1 & 2 (P1 & P2), and MCNPX (M). Percent differences are indicated relative to MCNPX results (which are within 2% relative error).

Neutron dose rate (mrem/hr)					
	P1	P2	M	P1 % Diff.	P2 % Diff.
Detector #					
1	2.854	2.850	3.739	-23.67	-23.77
2	2.035	2.040	1.382	47.29	47.64
3	0.398	0.398	0.202	97.36	97.37
4	1.008	1.010	0.691	45.84	46.21
5	0.919	0.919	0.652	40.86	40.90

Photon dose rate (mrem/hr)					
	P1	P2	M	P1 % Diff.	P2 % Diff.
Detector #					
1	0.222	1.150	2.577	-91.37	-55.37
2	0.077	0.141	0.255	-69.64	-44.61
3	0.015	0.039	0.063	-76.42	-38.15
4	0.060	0.133	0.243	-75.31	-45.36
5	0.068	0.175	0.312	-78.38	-44.00

Table 7.2 is designed to compare different features of Pandemonium (identified as P1 and P2). For example, detector 1 is located immediately in front of glovebox 2 and source 2, between which the only shielding materials are air and water. All other detectors are shielded with small amounts of lead and steel. As shown from in the table, both P1 and P2 neutron results compare favorably to those of MCNPX. P1 and P2 results should also be identical, minor differences in the 3rd digit following the decimal likely due to round off errors between the different code languages (FORTRAN and C++).

Except for detector 1, both P1 and P2 conservatively overestimate neutron dose rates by less than a factor of 2. For detector 1, the moderation of the water shield results in reduction in neutron energies that is not accounted for in either Pandemonium code. In MCNPX, the complex neutron slowing-down process is modeled explicitly, for each neutron at its energy. Pandemonium applies an attenuation factor based on neutrons at 2 MeV. This suggests that Pandemonium's determination of moderation affects on neutrons should be revised. For the remaining detectors, this effect is less noticeable as source 1 contributes more to dose as it is not shielded by water.

Lead and steel are transparent in Pandemonium calculations, whereas in MCNPX, neutrons are explicitly followed transported through these materials. In addition, as neutrons collide, their energies are reduced. The result is a combined effect of the removal of neutrons through lead and steel through inelastic (n,γ) collisions and lower energy neutrons which have lower dose coefficients. This explains why the remaining detectors that are shielded by lead and steel overestimate neutron dose – Pandemonium does not account for inelastic neutron collisions nor neutron capture in lead and steel.

To determine the effect of lead and steel in MCNPX calculations, the removal cross sections for these materials were implemented into P2. Defined in terms of neutron attenuation through nonhydrogenous materials immediately next to hydrogenous materials, removal cross sections have been studied [53] and are widely used in shielding applications. Using the tabulated values of Blizard [54] of 3.53 barns/atom for lead and 1.98 barns/atom for steel, macroscopic removal cross sections were calculated for 1-cm thick layers of each material of nominal densities resulting in a combined removal coefficient of 0.28 for detector

5, where the source-to-detector line intersects the glovebox wall close to normal. Thus one expects Pandemonium results for this detector to be reduced by a factor of $e^{-0.28}$ or about 24%. The remaining detectors should receive a reduced dose of greater than 24% as the oblique angles with which they intersect glovebox walls increase the thickness of lead and steel by the inverse cosine of the angle of interception. Indeed, the following table confirms this fact for those detectors shielded by lead and steel (2 through 5); it shows the difference between P2 with no removal and P2 with removal cross sections introduced. Detector 1 experiences a small decrease as well, but not as much, since most of its dose originates from a source shielded only by water. Remaining differences may be attributed to differences between the stochastic transport of MCNPX and the diffusion theory approximations used in Pandemonium.

Table 7.3. The effects of neutron removal cross sections on Pandemonium neutron dose rate calculations.

	Neutron dose rate (mrem/hr)				
	P2	P2*	M	P1 % Diff.	P2 % Diff.
Detector #					
1	2.850	2.690	3.739	-23.77	-28.05
2	2.040	1.490	1.382	47.64	7.84
3	0.398	0.267	0.202	97.37	32.41
4	1.010	0.798	0.691	46.21	15.52
5	0.919	0.756	0.652	40.90	15.91

* with neutron removal

Photon calculations shown in Table 7.2 indicate overall improvement between P1 and P2 relative to MCNPX. Improved geometry, higher energy photons, and new purely-angular buildup factors for 10 of the 25 source energies lead to larger photon doses that are more consistent with MCNPX. The following figures repeat the above Pandemonium calculations with more detectors utilizing the newly-designed "detector grid" feature of P2 to show the neutron and photon dose fields for the example model. Influences of glovebox inhomogeneities and the water shield are easily observed.

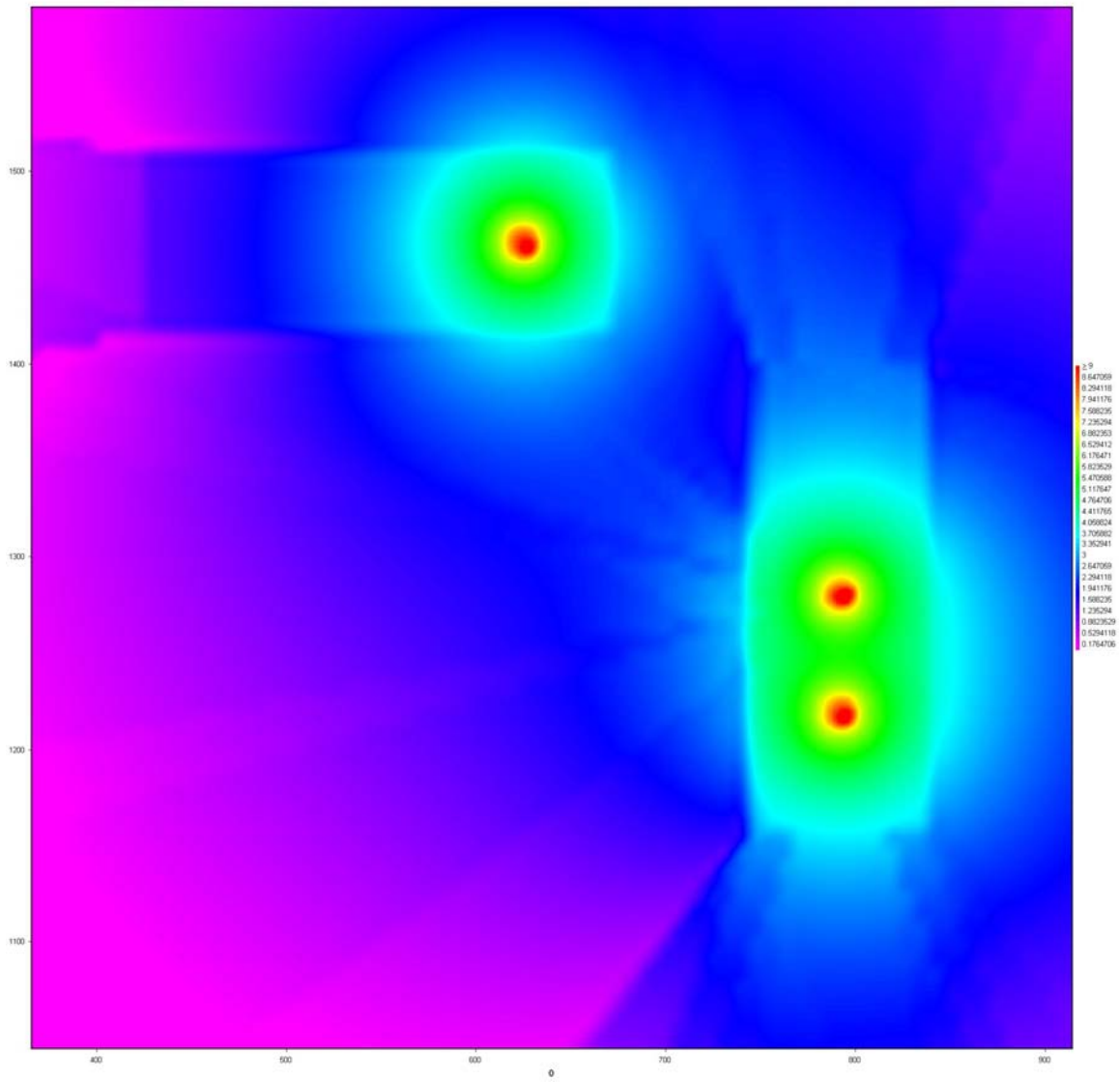

Figure 7.4. Contour plot of neutron dose rates in P2 with 4900 detectors grid across the geometry. The effect of the water shield is clearly visible, as are the influences of gloveports and windows.

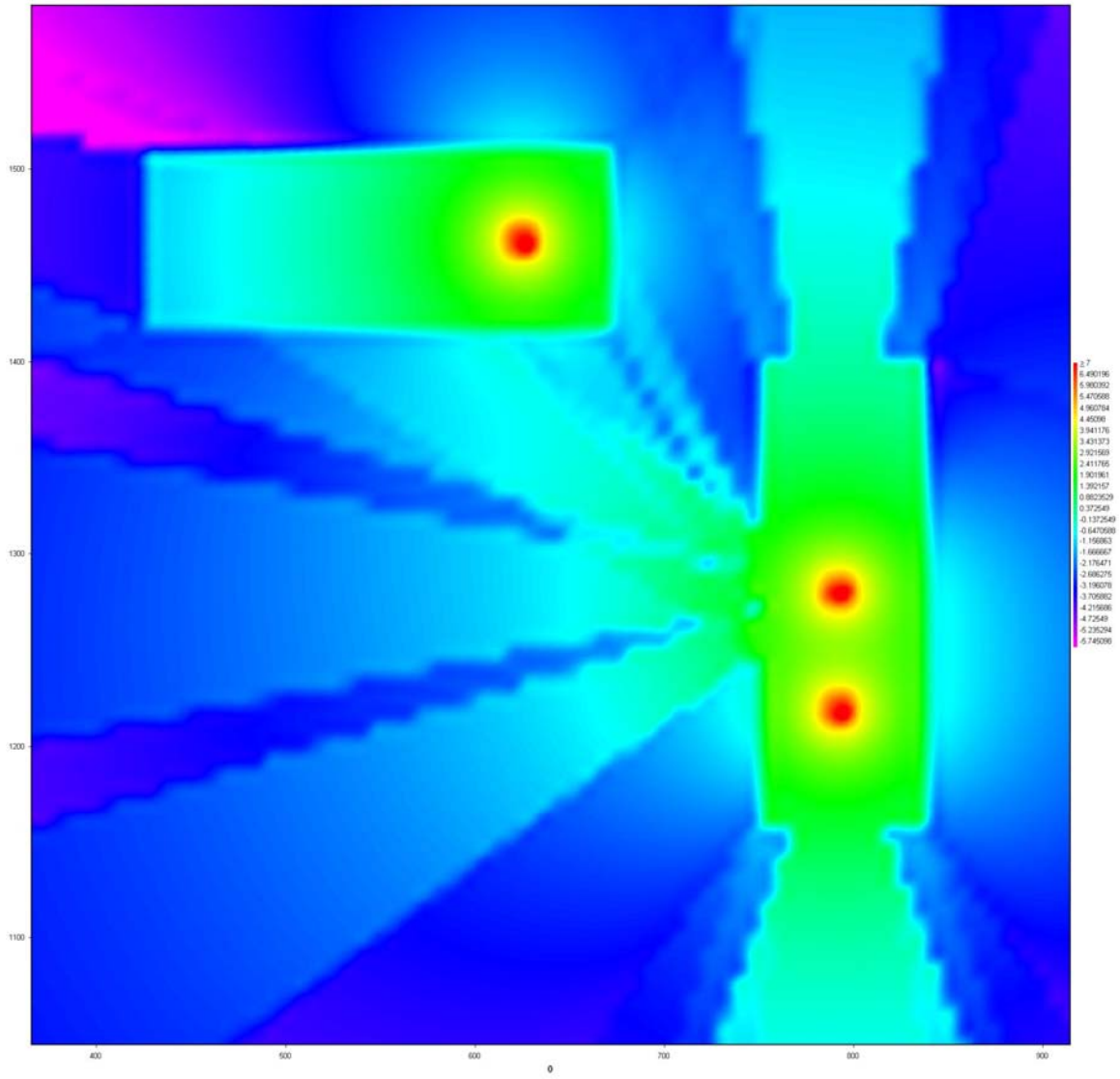

Figure 7.5. Photon contour plot of P2 with 4900 detectors grid across geometry. The dose "shadow" is observed where the glovebox walls absorb photons and decrease dose on the exterior. Also, windows and gloveports allow more photons to escape, contributing to higher dose near those regions.

CHAPTER 8 CONCLUSIONS

Pandemonium has been updated to include an improved photon model based on previously unidentified relationships between buildup factors and incident angle, higher energy photons from fission, and more realistic glovebox geometries. The neutron calculations include a criticality scenario for training purposes and the inclusion of removal cross sections, and the entire code has been made time-dependent. The code serves as a convenient and useful alternative to modeling complex glovebox facilities quickly, while providing reasonable estimates of photon and neutron dose rates, and total doses. A number of improvements are suggested for future work.

This study identifies the importance of new buildup factors that account for the many photon interactions with electrons incorporated into new cross-section libraries. Although buildup factors for 10 incident photon energies are presented in this work, a complete set of buildup factors for all 25 incident photon energies of PANDEMNIUM would greatly enhance the model. Although version 2.0 of the code contains improved glovebox geometries, the windows and gloveports consist of air, whereas in reality, these regions contain leaded glass and leaded rubber. The inclusion of these materials should present an even more realistic representation of the general glovebox.

The effect of the order shielding sequence in Pandemonium should also be addressed. I.e., a study relating the buildup factor for a water-lead layer compared to a lead-water layer should be studied to improve Pandemonium's application of shield layers. The code may also be expanded to include buildup factors for other materials (such as leaded glass and leaded rubber), and thicknesses beyond 10 mfp. The inclusion of inelastic neutron scattering and photons from neutron capture in lead and steel would also enhance the code. Another major effect that may improve Pandemonium is an analysis of the effect of scattered photons from materials not in the source-to-detector line of sight. MCNPX accounts for these scattered photons, but Pandemonium does not. The Pandemonium photon dose rate should significantly increase by the inclusion of these scattered photons.

To represent the shielding effects of other workers on detectors, time-dependent polyshield positions should be introduced. Post-processing of the dose rates determined by the code would add a useful feature. Although the code gives time-integrated dose results, a step-by-step visualization of changing dose rates would certainly provide better insight into the work process. Also, the application of removal cross sections based on thickness of water would improve the neutron calculations.

Lastly, as Pandemonium is to be used by a population not entirely familiar with radiation transport and shielding, a manual of operation for the code remains to be developed, that includes results from simple geometry benchmark experiments.

APPENDIX A BUILDUP FACTOR TABLES

This Appendix contains ambient dose equivalent [H*(10)] and air exposure purely angular photon buildup factors for lead, iron, aluminum, water, and concrete for shields of thicknesses between 1 and 10 mean free paths, and photon energies between 50-keV and 10 MeV.

Table A.1 Ambient dose equivalent photon buildup factors for lead.

50 keV	Angle of Incidence (radians)									
mfp	0.00	0.17	0.45	0.73	0.86	1.05	1.21	1.30	1.40	1.49
1	1.13	1.14	1.13	1.13	1.12	1.11	1.10	1.09	1.08	1.05
2	1.21	1.21	1.21	1.20	1.19	1.18	1.16	1.15	1.13	1.09
3	1.28	1.28	1.28	1.27	1.27	1.26	1.25	1.23	1.21	1.17
4	1.34	1.34	1.35	1.35	1.35	1.36	1.36	1.36	1.35	1.31
5	1.41	1.41	1.42	1.44	1.45	1.49	1.53	1.57	1.61	1.62
6	1.47	1.47	1.49	1.53	1.57	1.66	1.80	1.93	2.10	2.25
7	1.53	1.53	1.56	1.65	1.72	1.91	2.24	2.57	3.04	3.64
8	1.59	1.60	1.64	1.78	1.90	2.28	2.96	3.71	4.92	6.68
9	1.65	1.66	1.72	1.94	2.14	2.81	4.17	5.81	8.70	13.52
10	1.71	1.72	1.81	2.12	2.45	3.60	6.22	9.71	16.38	28.90

100 keV	Angle of Incidence (radians)									
mfp	0.00	0.17	0.45	0.73	0.86	1.05	1.21	1.30	1.40	1.49
1	1.78	1.78	1.75	1.69	1.65	1.57	1.48	1.40	1.31	1.18
2	2.46	2.46	2.44	2.39	2.35	2.25	2.11	1.97	1.78	1.49
3	3.31	3.32	3.35	3.40	3.41	3.36	3.22	3.04	2.72	2.15
4	4.49	4.51	4.68	4.97	5.13	5.33	5.36	5.19	4.74	3.66
5	6.22	6.28	6.70	7.56	8.08	8.98	9.60	9.69	9.20	7.22
6	8.84	8.97	9.91	11.96	13.32	15.92	18.29	19.34	19.24	15.75
7	12.94	13.21	15.14	19.64	22.83	29.43	36.39	40.34	42.22	36.44
8	19.53	20.05	23.88	33.31	40.40	56.16	74.58	86.71	95.46	86.94
9	30.30	31.29	38.70	58.01	73.38	109.71	156.18	190.04	219.66	211.42
10	48.23	50.10	64.29	103.30	136.01	218.14	332.03	422.02	511.92	519.33

Table A.1. Continued.

500 keV	Angle of Incidence (radians)									
mfp	0.00	0.17	0.45	0.73	0.86	1.05	1.21	1.30	1.40	1.49
1	1.27	1.29	1.29	1.28	1.26	1.24	1.21	1.18	1.14	1.09
2	1.53	1.52	1.51	1.50	1.47	1.45	1.40	1.36	1.31	1.21
3	1.76	1.74	1.72	1.72	1.69	1.69	1.64	1.61	1.56	1.44
4	1.99	1.96	1.94	1.95	1.93	1.97	1.97	1.96	1.98	1.90
5	2.21	2.17	2.15	2.20	2.21	2.33	2.43	2.52	2.72	2.81
6	2.43	2.39	2.38	2.49	2.52	2.80	3.10	3.40	4.05	4.73
7	2.66	2.61	2.62	2.81	2.90	3.42	4.12	4.86	6.52	8.82
8	2.88	2.84	2.87	3.19	3.35	4.27	5.69	7.31	11.17	17.67
9	3.12	3.07	3.13	3.62	3.91	5.45	8.15	11.48	20.11	37.04
10	3.36	3.31	3.42	4.13	4.59	7.11	12.06	18.69	37.48	79.86

1 MeV	Angle of Incidence (radians)									
mfp	0.00	0.17	0.45	0.73	0.86	1.05	1.21	1.30	1.40	1.49
1	1.38	1.40	1.40	1.39	1.36	1.34	1.28	1.24	1.18	1.10
2	1.78	1.77	1.75	1.72	1.69	1.65	1.57	1.50	1.42	1.28
3	2.15	2.12	2.08	2.06	2.02	2.01	1.93	1.87	1.79	1.61
4	2.50	2.46	2.41	2.43	2.40	2.45	2.43	2.42	2.43	2.26
5	2.85	2.80	2.76	2.83	2.83	3.02	3.16	3.29	3.57	3.62
6	3.20	3.14	3.11	3.28	3.34	3.77	4.24	4.70	5.66	6.49
7	3.56	3.49	3.48	3.80	3.95	4.79	5.89	7.04	9.57	12.68
8	3.92	3.84	3.88	4.39	4.68	6.17	8.44	10.99	17.03	26.20
9	4.28	4.21	4.29	5.08	5.57	8.10	12.46	17.75	31.44	56.06
10	4.66	4.58	4.74	5.88	6.66	10.82	18.88	29.47	59.63	122.59

2 MeV	Angle of Incidence (radians)									
mfp	0.00	0.17	0.45	0.73	0.86	1.05	1.21	1.30	1.40	1.49
1	1.42	1.44	1.44	1.43	1.40	1.38	1.31	1.27	1.21	1.12
2	1.87	1.86	1.83	1.80	1.77	1.72	1.63	1.56	1.47	1.31
3	2.30	2.27	2.22	2.20	2.16	2.13	2.04	1.97	1.89	1.68
4	2.73	2.68	2.63	2.64	2.61	2.65	2.62	2.60	2.60	2.41
5	3.17	3.11	3.06	3.13	3.14	3.32	3.46	3.59	3.88	3.92
6	3.61	3.54	3.51	3.70	3.78	4.24	4.75	5.24	6.24	7.12
7	4.07	3.99	3.99	4.36	4.55	5.50	6.74	8.00	10.70	14.02
8	4.54	4.46	4.51	5.14	5.52	7.26	9.87	12.74	19.26	29.12
9	5.02	4.94	5.07	6.05	6.71	9.75	14.89	20.97	35.94	62.54
10	5.51	5.43	5.66	7.13	8.21	13.31	23.02	35.44	68.82	137.15

4 MeV	Angle of Incidence (radians)									
mfp	0.00	0.17	0.45	0.73	0.86	1.05	1.21	1.30	1.40	1.49
1	1.37	1.39	1.39	1.39	1.37	1.34	1.29	1.25	1.20	1.12
2	1.75	1.74	1.72	1.70	1.67	1.64	1.57	1.51	1.43	1.30
3	2.13	2.10	2.07	2.05	2.01	1.99	1.92	1.86	1.80	1.63
4	2.53	2.49	2.44	2.45	2.42	2.45	2.43	2.41	2.42	2.27
5	2.95	2.90	2.86	2.92	2.93	3.08	3.19	3.30	3.54	3.60
6	3.40	3.34	3.31	3.48	3.56	3.96	4.39	4.79	5.62	6.41
7	3.88	3.81	3.83	4.17	4.37	5.22	6.31	7.38	9.61	12.48
8	4.39	4.32	4.40	5.02	5.42	7.06	9.45	11.96	17.40	25.75
9	4.93	4.86	5.04	6.06	6.79	9.77	14.65	20.16	32.86	55.19
10	5.51	5.45	5.76	7.36	8.59	13.82	23.39	35.05	63.91	121.11

Table A.1. Continued.

5 MeV	Angle of Incidence (radians)									
mfp	0.00	0.17	0.45	0.73	0.86	1.05	1.21	1.30	1.40	1.49
1	1.37	1.38	1.38	1.38	1.36	1.34	1.29	1.25	1.20	1.12
2	1.71	1.70	1.69	1.67	1.64	1.61	1.55	1.49	1.42	1.29
3	2.07	2.04	2.01	1.99	1.96	1.94	1.88	1.83	1.77	1.61
4	2.44	2.40	2.36	2.37	2.35	2.38	2.36	2.35	2.36	2.23
5	2.85	2.80	2.76	2.83	2.84	2.99	3.10	3.21	3.43	3.50
6	3.29	3.23	3.21	3.38	3.46	3.85	4.27	4.66	5.44	6.20
7	3.77	3.70	3.73	4.07	4.27	5.10	6.17	7.22	9.32	12.03
8	4.29	4.22	4.31	4.94	5.35	6.96	9.32	11.78	16.93	24.81
9	4.85	4.79	4.99	6.03	6.78	9.75	14.63	20.09	32.16	53.22
10	5.46	5.41	5.76	7.41	8.72	14.00	23.69	35.37	63.02	117.00

6 MeV	Angle of Incidence (radians)									
mfp	0.00	0.17	0.45	0.73	0.86	1.05	1.21	1.30	1.40	1.49
1	1.37	1.38	1.38	1.38	1.36	1.34	1.29	1.25	1.20	1.13
2	1.70	1.69	1.67	1.66	1.63	1.60	1.54	1.49	1.42	1.30
3	2.03	2.01	1.98	1.97	1.94	1.93	1.87	1.82	1.76	1.60
4	2.39	2.36	2.33	2.34	2.32	2.35	2.34	2.34	2.35	2.21
5	2.79	2.75	2.72	2.79	2.81	2.95	3.08	3.19	3.41	3.47
6	3.23	3.18	3.17	3.35	3.43	3.82	4.26	4.67	5.42	6.14
7	3.71	3.66	3.69	4.05	4.27	5.11	6.21	7.29	9.33	11.92
8	4.24	4.19	4.30	4.95	5.40	7.04	9.49	12.04	17.09	24.65
9	4.83	4.78	5.01	6.11	6.93	10.01	15.11	20.81	32.73	53.04
10	5.49	5.45	5.85	7.61	9.04	14.59	24.84	37.19	64.72	117.05

8 MeV	Angle of Incidence (radians)									
mfp	0.00	0.17	0.45	0.73	0.86	1.05	1.21	1.30	1.40	1.49
1	1.41	1.42	1.42	1.41	1.39	1.36	1.31	1.27	1.22	1.14
2	1.73	1.73	1.72	1.70	1.67	1.64	1.58	1.52	1.45	1.32
3	2.07	2.06	2.04	2.02	2.00	1.98	1.93	1.88	1.81	1.63
4	2.45	2.42	2.40	2.42	2.41	2.45	2.45	2.44	2.44	2.27
5	2.87	2.83	2.83	2.91	2.95	3.12	3.28	3.41	3.61	3.60
6	3.35	3.31	3.33	3.55	3.68	4.12	4.66	5.12	5.88	6.46
7	3.89	3.85	3.94	4.38	4.68	5.66	7.00	8.25	10.36	12.72
8	4.52	4.48	4.67	5.48	6.08	8.05	11.07	14.09	19.43	26.65
9	5.24	5.21	5.56	6.95	8.06	11.83	18.26	25.18	38.09	58.08
10	6.06	6.06	6.65	8.93	10.90	17.89	31.13	46.51	77.01	129.68

10 MeV	Angle of Incidence (radians)									
mfp	0.00	0.17	0.45	0.73	0.86	1.05	1.21	1.30	1.40	1.49
1	1.48	1.49	1.48	1.46	1.44	1.40	1.35	1.31	1.25	1.16
2	1.83	1.83	1.81	1.79	1.76	1.72	1.65	1.58	1.49	1.35
3	2.22	2.20	2.18	2.17	2.15	2.12	2.05	1.99	1.90	1.69
4	2.65	2.63	2.62	2.64	2.64	2.68	2.68	2.66	2.63	2.40
5	3.15	3.13	3.14	3.25	3.31	3.51	3.70	3.84	4.01	3.88
6	3.74	3.72	3.78	4.06	4.25	4.79	5.45	5.98	6.73	7.11
7	4.44	4.42	4.57	5.16	5.58	6.82	8.50	9.99	12.23	14.28
8	5.27	5.26	5.57	6.67	7.52	10.08	13.95	17.65	23.56	30.41
9	6.26	6.27	6.82	8.76	10.36	15.41	23.85	32.56	47.30	67.20
10	7.45	7.49	8.42	11.68	14.57	24.23	42.06	61.95	97.70	151.93

Table A.2. Ambient dose equivalent photon buildup factors for iron.

50 keV	Angle of Incidence (radians)									
mfp	0.00	0.17	0.45	0.73	0.86	1.05	1.21	1.30	1.40	1.49
1	1.12	1.12	1.12	1.12	1.11	1.11	1.09	1.08	1.07	1.04
2	1.20	1.21	1.21	1.20	1.20	1.19	1.18	1.16	1.14	1.10
3	1.28	1.28	1.29	1.29	1.29	1.28	1.28	1.27	1.25	1.20
4	1.35	1.35	1.36	1.37	1.38	1.40	1.43	1.44	1.44	1.40
5	1.42	1.42	1.44	1.47	1.50	1.56	1.65	1.72	1.80	1.81
6	1.49	1.49	1.52	1.58	1.64	1.78	2.00	2.20	2.47	2.71
7	1.55	1.56	1.60	1.71	1.81	2.08	2.55	3.05	3.79	4.67
8	1.62	1.63	1.69	1.86	2.02	2.51	3.47	4.57	6.40	9.05
9	1.68	1.70	1.78	2.04	2.29	3.14	4.99	7.34	11.67	18.88
10	1.75	1.76	1.87	2.24	2.64	4.07	7.56	12.48	22.40	41.20

100 keV	Angle of Incidence (radians)									
mfp	0.00	0.17	0.45	0.73	0.86	1.05	1.21	1.30	1.40	1.49
1	1.33	1.34	1.34	1.33	1.31	1.29	1.25	1.22	1.17	1.10
2	1.63	1.63	1.62	1.61	1.58	1.56	1.51	1.46	1.39	1.26
3	1.92	1.90	1.90	1.90	1.89	1.90	1.86	1.82	1.75	1.57
4	2.20	2.18	2.19	2.24	2.26	2.34	2.39	2.41	2.40	2.20
5	2.48	2.46	2.51	2.64	2.72	2.95	3.23	3.43	3.65	3.55
6	2.78	2.76	2.85	3.11	3.29	3.83	4.58	5.22	6.07	6.51
7	3.08	3.07	3.22	3.68	4.03	5.11	6.81	8.46	10.91	13.13
8	3.40	3.40	3.64	4.37	4.99	7.00	10.57	14.42	20.73	28.10
9	3.74	3.75	4.10	5.23	6.26	9.82	16.98	25.52	40.90	62.36
10	4.09	4.12	4.61	6.29	7.94	14.11	28.03	46.38	82.73	141.34

500 keV	Angle of Incidence (radians)									
mfp	0.00	0.17	0.45	0.73	0.86	1.05	1.21	1.30	1.40	1.49
1	1.81	1.82	1.79	1.73	1.68	1.59	1.47	1.38	1.28	1.16
2	2.70	2.69	2.62	2.52	2.43	2.29	2.08	1.93	1.73	1.44
3	3.66	3.63	3.57	3.50	3.43	3.30	3.08	2.87	2.56	2.04
4	4.72	4.68	4.68	4.76	4.78	4.84	4.76	4.60	4.24	3.35
5	5.87	5.83	5.97	6.39	6.65	7.24	7.73	7.89	7.70	6.32
6	7.13	7.11	7.48	8.53	9.28	11.04	13.02	14.24	14.99	13.20
7	8.50	8.51	9.24	11.34	12.98	17.11	22.57	26.67	30.55	29.32
8	9.99	10.05	11.30	15.03	18.19	26.85	39.93	51.20	64.08	67.43
9	11.59	11.73	13.68	19.87	25.54	42.53	71.68	99.93	136.86	158.23
10	13.32	13.56	16.45	26.22	35.93	67.85	129.95	197.16	295.66	375.74

1 MeV	Angle of Incidence (radians)									
mfp	0.00	0.17	0.45	0.73	0.86	1.05	1.21	1.30	1.40	1.49
1	1.71	1.74	1.72	1.68	1.62	1.55	1.44	1.36	1.26	1.14
2	2.58	2.56	2.50	2.41	2.33	2.20	2.01	1.86	1.68	1.41
3	3.50	3.45	3.37	3.30	3.22	3.11	2.90	2.71	2.44	1.97
4	4.48	4.41	4.35	4.40	4.39	4.45	4.37	4.22	3.94	3.18
5	5.54	5.45	5.47	5.79	5.96	6.48	6.86	7.01	6.97	5.89
6	6.66	6.57	6.74	7.54	8.07	9.57	11.18	12.26	13.24	12.07
7	7.86	7.77	8.17	9.76	10.92	14.33	18.74	22.24	26.37	26.40
8	9.12	9.06	9.79	12.55	14.77	21.70	32.04	41.43	54.14	59.94
9	10.45	10.42	11.60	16.08	19.99	33.14	55.61	78.51	113.34	139.02
10	11.85	11.87	13.64	20.53	27.05	50.96	97.53	150.53	240.23	326.62

Table A.2. Continued.

2 MeV	Angle of Incidence (radians)									
mfp	0.00	0.17	0.45	0.73	0.86	1.05	1.21	1.30	1.40	1.49
1	1.61	1.63	1.63	1.60	1.56	1.51	1.41	1.34	1.25	1.14
2	2.34	2.33	2.28	2.22	2.16	2.07	1.91	1.79	1.63	1.39
3	3.09	3.04	2.98	2.93	2.87	2.80	2.64	2.49	2.29	1.90
4	3.86	3.80	3.73	3.77	3.75	3.81	3.76	3.68	3.53	2.97
5	4.67	4.58	4.56	4.76	4.85	5.24	5.56	5.75	5.92	5.30
6	5.51	5.41	5.45	5.94	6.23	7.29	8.49	9.44	10.67	10.49
7	6.37	6.27	6.42	7.36	8.00	10.24	13.32	16.10	20.24	22.26
8	7.26	7.16	7.47	9.06	10.25	14.55	21.35	28.25	39.71	49.18
9	8.18	8.09	8.61	11.10	13.13	20.87	34.82	50.58	79.71	111.34
10	9.12	9.04	9.85	13.57	16.83	30.18	57.52	91.86	162.43	255.80

4 MeV	Angle of Incidence (radians)									
mfp	0.00	0.17	0.45	0.73	0.86	1.05	1.21	1.30	1.40	1.49
1	1.51	1.53	1.54	1.52	1.49	1.46	1.38	1.32	1.25	1.14
2	2.09	2.08	2.05	2.02	1.97	1.92	1.80	1.71	1.58	1.37
3	2.67	2.63	2.58	2.56	2.51	2.48	2.37	2.27	2.13	1.82
4	3.26	3.20	3.14	3.17	3.14	3.22	3.20	3.17	3.12	2.74
5	3.88	3.79	3.74	3.87	3.90	4.20	4.45	4.64	4.95	4.70
6	4.51	4.41	4.38	4.68	4.82	5.54	6.38	7.14	8.43	8.98
7	5.15	5.04	5.06	5.63	5.96	7.40	9.41	11.43	15.16	18.41
8	5.82	5.70	5.80	6.74	7.36	10.01	14.24	18.90	28.37	39.53
9	6.50	6.39	6.59	8.05	9.10	13.73	22.02	32.04	54.55	87.22
10	7.20	7.09	7.43	9.61	11.29	19.04	34.70	55.40	106.90	195.72

5 MeV	Angle of Incidence (radians)									
mfp	0.00	0.17	0.45	0.73	0.86	1.05	1.21	1.30	1.40	1.49
1	1.48	1.50	1.51	1.49	1.47	1.44	1.37	1.31	1.24	1.14
2	2.01	2.00	1.97	1.94	1.91	1.86	1.76	1.67	1.55	1.36
3	2.53	2.49	2.45	2.43	2.39	2.37	2.28	2.19	2.07	1.78
4	3.07	3.01	2.95	2.97	2.95	3.03	3.02	3.00	2.97	2.65
5	3.62	3.54	3.49	3.60	3.63	3.89	4.12	4.31	4.63	4.48
6	4.19	4.10	4.06	4.32	4.44	5.07	5.80	6.50	7.75	8.43
7	4.78	4.67	4.68	5.16	5.43	6.68	8.43	10.22	13.72	17.11
8	5.39	5.28	5.34	6.15	6.65	8.95	12.57	16.63	25.32	36.40
9	6.01	5.90	6.05	7.31	8.18	12.15	19.22	27.83	48.12	79.73
10	6.65	6.54	6.81	8.69	10.08	16.73	30.00	47.58	93.39	177.76

6 MeV	Angle of Incidence (radians)									
mfp	0.00	0.17	0.45	0.73	0.86	1.05	1.21	1.30	1.40	1.49
1	1.46	1.48	1.48	1.47	1.44	1.42	1.36	1.31	1.24	1.14
2	1.94	1.93	1.91	1.88	1.85	1.81	1.72	1.64	1.53	1.35
3	2.42	2.38	2.34	2.33	2.29	2.28	2.20	2.12	2.01	1.75
4	2.91	2.85	2.80	2.82	2.80	2.87	2.87	2.86	2.85	2.56
5	3.41	3.34	3.29	3.39	3.41	3.66	3.87	4.05	4.37	4.28
6	3.94	3.85	3.81	4.04	4.14	4.71	5.38	6.02	7.22	7.96
7	4.49	4.39	4.38	4.81	5.04	6.16	7.72	9.34	12.62	16.02
8	5.05	4.94	4.99	5.71	6.15	8.19	11.41	15.04	23.08	33.87
9	5.63	5.52	5.64	6.77	7.53	11.06	17.31	24.96	43.52	73.79
10	6.23	6.13	6.35	8.04	9.26	15.17	26.88	42.38	83.93	163.78

Table A.2. Continued.

8 MeV	Angle of Incidence (radians)									
mfp	0.00	0.17	0.45	0.73	0.86	1.05	1.21	1.30	1.40	1.49
1	1.43	1.45	1.46	1.45	1.42	1.40	1.34	1.30	1.23	1.14
2	1.86	1.85	1.83	1.82	1.79	1.76	1.67	1.60	1.51	1.34
3	2.28	2.25	2.22	2.21	2.18	2.17	2.10	2.04	1.94	1.71
4	2.71	2.67	2.62	2.65	2.63	2.70	2.70	2.70	2.70	2.45
5	3.17	3.10	3.06	3.15	3.16	3.38	3.58	3.75	4.06	4.02
6	3.64	3.56	3.52	3.73	3.81	4.31	4.90	5.48	6.59	7.38
7	4.13	4.04	4.03	4.41	4.61	5.59	6.95	8.39	11.38	14.68
8	4.65	4.55	4.59	5.22	5.60	7.37	10.17	13.36	20.58	30.80
9	5.19	5.09	5.19	6.19	6.84	9.92	15.34	22.00	38.51	66.70
10	5.76	5.66	5.85	7.35	8.41	13.58	23.74	37.18	73.85	147.36

10 MeV	Angle of Incidence (radians)									
mfp	0.00	0.17	0.45	0.73	0.86	1.05	1.21	1.30	1.40	1.49
1	1.43	1.45	1.45	1.44	1.42	1.40	1.34	1.30	1.23	1.14
2	1.83	1.82	1.81	1.79	1.76	1.73	1.66	1.59	1.49	1.33
3	2.22	2.19	2.16	2.16	2.13	2.13	2.06	2.00	1.91	1.68
4	2.62	2.58	2.54	2.57	2.55	2.62	2.62	2.62	2.63	2.40
5	3.04	2.99	2.95	3.04	3.06	3.26	3.45	3.62	3.91	3.88
6	3.49	3.42	3.40	3.59	3.67	4.14	4.70	5.25	6.30	7.06
7	3.96	3.88	3.88	4.24	4.43	5.35	6.63	8.01	10.82	13.97
8	4.46	4.37	4.42	5.02	5.38	7.05	9.70	12.74	19.51	29.22
9	4.99	4.90	5.01	5.96	6.59	9.50	14.65	20.98	36.46	63.15
10	5.54	5.46	5.66	7.10	8.13	13.05	22.73	35.55	69.91	139.36

Table A.3. Ambient dose equivalent photon buildup factors for aluminum.

50 keV	Angle of Incidence (radians)									
mfp	0.00	0.17	0.45	0.73	0.86	1.05	1.21	1.30	1.40	1.49
1	1.48	1.50	1.50	1.47	1.45	1.41	1.36	1.31	1.24	1.14
2	1.92	1.92	1.92	1.89	1.88	1.83	1.76	1.68	1.56	1.37
3	2.33	2.33	2.35	2.38	2.39	2.40	2.36	2.30	2.15	1.82
4	2.75	2.76	2.82	2.95	3.03	3.19	3.33	3.36	3.27	2.80
5	3.20	3.22	3.35	3.65	3.87	4.37	4.95	5.31	5.51	4.97
6	3.68	3.71	3.94	4.53	4.99	6.15	7.72	8.94	10.09	9.88
7	4.19	4.24	4.61	5.63	6.51	8.88	12.56	15.84	19.63	21.19
8	4.74	4.81	5.37	7.04	8.59	13.13	21.13	29.15	39.76	47.49
9	5.32	5.43	6.24	8.85	11.45	19.83	36.48	55.07	82.67	109.21
10	5.96	6.10	7.24	11.18	15.44	30.46	64.16	105.97	174.81	255.04

100 keV	Angle of Incidence (radians)									
mfp	0.00	0.17	0.45	0.73	0.86	1.05	1.21	1.30	1.40	1.49
1	1.93	1.97	1.94	1.87	1.80	1.70	1.56	1.46	1.35	1.19
2	3.03	3.03	2.97	2.89	2.79	2.64	2.39	2.19	1.93	1.55
3	4.23	4.20	4.18	4.21	4.16	4.09	3.82	3.53	3.09	2.33
4	5.58	5.53	5.64	5.98	6.11	6.41	6.39	6.13	5.52	4.10
5	7.11	7.05	7.41	8.38	8.95	10.23	11.13	11.30	10.76	8.23
6	8.83	8.78	9.55	11.65	13.10	16.56	20.00	21.75	22.23	18.02
7	10.78	10.77	12.15	16.14	19.20	27.12	36.73	43.08	47.63	41.51
8	12.98	13.03	15.31	22.29	28.19	44.83	68.46	86.86	104.30	98.38
9	15.45	15.61	19.13	30.73	41.47	74.66	128.88	177.16	231.37	236.87
10	18.22	18.52	23.76	42.32	61.11	125.01	244.34	364.09	517.46	575.79

500 keV	Angle of Incidence (radians)									
mfp	0.00	0.17	0.45	0.73	0.86	1.05	1.21	1.30	1.40	1.49
1	1.91	1.93	1.89	1.81	1.74	1.63	1.50	1.40	1.29	1.16
2	3.01	2.99	2.92	2.78	2.67	2.47	2.21	2.01	1.78	1.46
3	4.26	4.23	4.17	4.08	3.99	3.79	3.45	3.15	2.73	2.09
4	5.68	5.65	5.70	5.84	5.89	5.92	5.71	5.37	4.73	3.52
5	7.30	7.28	7.55	8.24	8.66	9.45	9.91	9.80	9.04	6.83
6	9.11	9.13	9.80	11.51	12.73	15.30	17.77	18.80	18.49	14.67
7	11.14	11.22	12.50	15.96	18.67	25.05	32.62	37.18	39.45	33.43
8	13.38	13.56	15.73	21.99	27.36	41.32	60.74	74.95	86.24	78.75
9	15.84	16.16	19.57	30.15	40.03	68.44	114.09	152.80	191.19	188.99
10	18.53	19.03	24.12	41.13	58.47	113.68	215.43	313.58	427.44	458.50

1 MeV	Angle of Incidence (radians)									
mfp	0.00	0.17	0.45	0.73	0.86	1.05	1.21	1.30	1.40	1.49
1	1.75	1.78	1.76	1.72	1.65	1.57	1.45	1.36	1.26	1.14
2	2.71	2.69	2.63	2.53	2.43	2.29	2.07	1.90	1.70	1.42
3	3.75	3.70	3.62	3.55	3.46	3.33	3.07	2.84	2.52	1.99
4	4.88	4.81	4.77	4.85	4.85	4.93	4.79	4.57	4.17	3.25
5	6.10	6.02	6.09	6.52	6.75	7.39	7.81	7.87	7.59	6.11
6	7.42	7.34	7.60	8.65	9.36	11.24	13.16	14.24	14.84	12.73
7	8.83	8.76	9.33	11.39	12.93	17.29	22.73	26.67	30.37	28.27
8	10.33	10.29	11.29	14.88	17.84	26.79	39.92	51.06	63.91	65.11
9	11.91	11.92	13.51	19.33	24.56	41.77	70.93	99.14	136.75	153.10
10	13.58	13.65	16.01	25.00	33.77	65.39	126.96	194.23	295.67	364.46

Table A.3. Continued.

2 MeV	Angle of Incidence (radians)									
mfp	0.00	0.17	0.45	0.73	0.86	1.05	1.21	1.30	1.40	1.49
1	1.63	1.65	1.65	1.62	1.57	1.52	1.42	1.34	1.26	1.14
2	2.40	2.38	2.33	2.27	2.21	2.11	1.94	1.81	1.64	1.39
3	3.18	3.14	3.07	3.03	2.96	2.89	2.71	2.55	2.32	1.90
4	3.99	3.92	3.87	3.91	3.90	3.99	3.93	3.83	3.62	2.99
5	4.83	4.74	4.73	4.97	5.08	5.53	5.90	6.08	6.18	5.38
6	5.69	5.60	5.66	6.22	6.57	7.75	9.12	10.14	11.31	10.76
7	6.58	6.48	6.67	7.71	8.45	10.97	14.46	17.54	21.75	23.01
8	7.49	7.39	7.75	9.49	10.84	15.65	23.37	31.11	43.20	51.27
9	8.42	8.33	8.92	11.62	13.89	22.49	38.33	56.19	87.60	116.99
10	9.37	9.30	10.17	14.17	17.77	32.54	63.57	102.73	180.01	270.77

4 MeV	Angle of Incidence (radians)									
mfp	0.00	0.17	0.45	0.73	0.86	1.05	1.21	1.30	1.40	1.49
1	1.52	1.55	1.55	1.53	1.50	1.47	1.39	1.33	1.25	1.14
2	2.12	2.11	2.08	2.05	2.00	1.95	1.82	1.72	1.59	1.37
3	2.70	2.66	2.61	2.59	2.55	2.52	2.41	2.30	2.15	1.83
4	3.29	3.22	3.16	3.19	3.17	3.26	3.24	3.21	3.15	2.76
5	3.87	3.78	3.73	3.86	3.90	4.21	4.48	4.68	5.00	4.73
6	4.46	4.35	4.32	4.61	4.75	5.48	6.34	7.13	8.48	9.02
7	5.04	4.93	4.93	5.47	5.77	7.19	9.21	11.27	15.16	18.47
8	5.63	5.51	5.57	6.44	6.99	9.53	13.68	18.35	28.14	39.58
9	6.23	6.10	6.24	7.56	8.46	12.77	20.71	30.56	53.59	87.15
10	6.82	6.70	6.94	8.84	10.25	17.27	31.89	51.83	103.95	195.09

5 MeV	Angle of Incidence (radians)									
mfp	0.00	0.17	0.45	0.73	0.86	1.05	1.21	1.30	1.40	1.49
1	1.49	1.51	1.51	1.50	1.47	1.45	1.38	1.32	1.24	1.14
2	2.03	2.02	1.99	1.97	1.93	1.88	1.78	1.69	1.56	1.36
3	2.55	2.51	2.46	2.45	2.41	2.40	2.30	2.21	2.08	1.79
4	3.07	3.01	2.95	2.98	2.96	3.04	3.03	3.00	2.99	2.66
5	3.59	3.50	3.44	3.55	3.57	3.85	4.08	4.27	4.62	4.48
6	4.10	4.00	3.95	4.20	4.29	4.91	5.63	6.32	7.63	8.39
7	4.62	4.51	4.48	4.92	5.14	6.32	7.98	9.72	13.32	16.93
8	5.13	5.01	5.02	5.73	6.13	8.22	11.57	15.40	24.18	35.80
9	5.64	5.52	5.59	6.66	7.33	10.82	17.14	25.04	45.15	77.89
10	6.16	6.03	6.18	7.71	8.76	14.40	25.90	41.56	86.07	172.48

6 MeV	Angle of Incidence (radians)									
mfp	0.00	0.17	0.45	0.73	0.86	1.05	1.21	1.30	1.40	1.49
1	1.45	1.48	1.48	1.47	1.45	1.42	1.36	1.31	1.24	1.14
2	1.95	1.94	1.92	1.90	1.86	1.83	1.73	1.65	1.54	1.35
3	2.43	2.39	2.34	2.34	2.30	2.29	2.20	2.13	2.02	1.75
4	2.89	2.83	2.77	2.80	2.78	2.86	2.85	2.84	2.84	2.56
5	3.36	3.28	3.21	3.31	3.32	3.57	3.76	3.94	4.30	4.25
6	3.82	3.72	3.67	3.88	3.95	4.49	5.10	5.71	6.96	7.84
7	4.28	4.17	4.13	4.51	4.67	5.69	7.09	8.58	11.90	15.61
8	4.74	4.62	4.61	5.21	5.52	7.30	10.10	13.33	21.23	32.64
9	5.20	5.08	5.10	6.01	6.53	9.49	14.74	21.28	39.05	70.33
10	5.65	5.53	5.62	6.92	7.74	12.50	21.98	34.77	73.47	154.39

Table A.3. Continued.

8 MeV	Angle of Incidence (radians)									
mfp	0.00	0.17	0.45	0.73	0.86	1.05	1.21	1.30	1.40	1.49
1	1.41	1.43	1.44	1.44	1.41	1.40	1.34	1.30	1.23	1.13
2	1.84	1.83	1.82	1.80	1.77	1.75	1.67	1.60	1.50	1.33
3	2.25	2.22	2.18	2.18	2.14	2.15	2.07	2.01	1.92	1.70
4	2.65	2.60	2.54	2.57	2.55	2.62	2.61	2.60	2.63	2.42
5	3.05	2.97	2.91	3.00	2.99	3.20	3.35	3.50	3.86	3.91
6	3.44	3.35	3.29	3.46	3.50	3.94	4.42	4.91	6.05	7.04
7	3.83	3.73	3.68	3.98	4.09	4.91	5.99	7.16	10.05	13.73
8	4.22	4.12	4.08	4.56	4.77	6.19	8.35	10.82	17.48	28.22
9	4.61	4.50	4.49	5.21	5.58	7.92	11.94	16.87	31.48	59.94
10	5.00	4.89	4.92	5.96	6.54	10.30	17.51	27.01	58.23	129.95

10 MeV	Angle of Incidence (radians)									
mfp	0.00	0.17	0.45	0.73	0.86	1.05	1.21	1.30	1.40	1.49
1	1.38	1.40	1.41	1.41	1.39	1.38	1.33	1.28	1.22	1.13
2	1.77	1.76	1.75	1.74	1.71	1.69	1.62	1.56	1.47	1.32
3	2.13	2.10	2.07	2.07	2.04	2.05	1.98	1.92	1.85	1.65
4	2.49	2.44	2.39	2.41	2.39	2.46	2.45	2.44	2.48	2.31
5	2.84	2.77	2.72	2.79	2.78	2.96	3.09	3.22	3.55	3.66
6	3.19	3.11	3.05	3.20	3.22	3.60	4.00	4.42	5.45	6.46
7	3.54	3.44	3.39	3.65	3.73	4.43	5.33	6.31	8.87	12.40
8	3.88	3.78	3.74	4.15	4.31	5.53	7.32	9.36	15.17	25.18
9	4.23	4.13	4.10	4.72	5.01	7.01	10.34	14.37	26.95	52.95
10	4.58	4.47	4.48	5.37	5.83	9.03	15.02	22.72	49.32	113.84

Table A.4. Ambient dose equivalent photon buildup factors for water.

50 keV	Angle of Incidence (radians)									
mfp	0.00	0.17	0.45	0.73	0.86	1.05	1.21	1.30	1.40	1.49
1	2.19	2.22	2.17	2.06	1.98	1.84	1.67	1.55	1.41	1.23
2	3.65	3.66	3.60	3.45	3.33	3.07	2.74	2.46	2.11	1.65
3	5.38	5.39	5.44	5.45	5.40	5.18	4.72	4.26	3.58	2.57
4	7.43	7.47	7.77	8.31	8.57	8.82	8.56	7.96	6.79	4.72
5	9.84	9.95	10.74	12.42	13.46	15.18	16.07	15.73	14.01	9.85
6	12.66	12.88	14.49	18.29	20.98	26.31	30.87	32.21	30.42	22.25
7	15.95	16.32	19.20	26.68	32.56	45.81	60.13	67.32	68.04	52.61
8	19.75	20.35	25.09	38.61	50.34	79.96	118.07	142.39	154.76	127.48
9	24.13	25.04	32.43	55.55	77.57	139.72	232.86	303.14	355.33	313.16
10	29.15	30.47	41.54	79.54	119.23	244.22	460.32	647.74	820.35	775.62

100 keV	Angle of Incidence (radians)									
mfp	0.00	0.17	0.45	0.73	0.86	1.05	1.21	1.30	1.40	1.49
1	2.30	2.35	2.29	2.15	2.03	1.86	1.66	1.53	1.38	1.20
2	4.40	4.40	4.25	3.97	3.73	3.33	2.83	2.49	2.10	1.61
3	7.30	7.27	7.17	6.96	6.69	6.12	5.23	4.52	3.66	2.54
4	11.16	11.11	11.33	11.77	11.77	11.47	10.26	8.99	7.23	4.73
5	16.14	16.13	17.13	19.35	20.36	21.65	20.87	18.96	15.58	10.05
6	22.44	22.55	25.07	31.11	34.70	40.89	43.22	41.33	35.36	23.14
7	30.30	30.62	35.77	49.15	58.39	76.98	90.20	91.61	82.53	55.76
8	39.94	40.65	50.02	76.52	97.15	144.22	188.62	204.55	195.50	137.69
9	51.65	52.95	68.77	117.68	160.08	268.72	394.02	457.93	466.62	344.65
10	65.71	67.89	93.26	179.10	261.53	498.00	821.16	1025.36	1117.86	869.68

500 keV	Angle of Incidence (radians)									
mfp	0.00	0.17	0.45	0.73	0.86	1.05	1.21	1.30	1.40	1.49
1	1.94	1.96	1.91	1.83	1.76	1.64	1.50	1.40	1.29	1.16
2	3.16	3.15	3.06	2.89	2.76	2.52	2.24	2.03	1.78	1.46
3	4.64	4.61	4.54	4.41	4.28	4.00	3.57	3.22	2.75	2.09
4	6.39	6.36	6.43	6.58	6.60	6.53	6.12	5.61	4.83	3.53
5	8.45	8.44	8.81	9.66	10.15	10.90	11.04	10.58	9.39	6.89
6	10.82	10.87	11.78	14.01	15.53	18.45	20.65	21.00	19.62	14.87
7	13.51	13.65	15.43	20.08	23.65	31.48	39.45	42.98	42.81	34.10
8	16.55	16.83	19.87	28.51	35.82	53.89	76.25	89.57	95.76	80.91
9	19.93	20.41	25.24	40.12	53.96	92.28	148.16	188.40	217.26	195.66
10	23.67	24.42	31.69	56.03	80.87	157.78	288.51	398.16	496.90	478.63

1 MeV	Angle of Incidence (radians)									
mfp	0.00	0.17	0.45	0.73	0.86	1.05	1.21	1.30	1.40	1.49
1	1.77	1.80	1.78	1.72	1.66	1.57	1.45	1.36	1.26	1.14
2	2.78	2.77	2.69	2.59	2.48	2.32	2.08	1.91	1.70	1.42
3	3.91	3.86	3.78	3.70	3.60	3.44	3.14	2.87	2.53	1.99
4	5.15	5.08	5.05	5.15	5.15	5.20	5.00	4.71	4.22	3.25
5	6.51	6.43	6.53	7.03	7.31	8.00	8.34	8.27	7.79	6.14
6	7.98	7.90	8.24	9.47	10.31	12.44	14.41	15.31	15.47	12.84
7	9.56	9.50	10.20	12.63	14.47	19.51	25.47	29.32	32.15	28.64
8	11.25	11.22	12.44	16.68	20.23	30.76	45.68	57.31	68.75	66.32
9	13.04	13.06	14.98	21.89	28.19	48.66	82.62	113.40	149.42	156.87
10	14.92	15.03	17.85	28.54	39.14	77.12	150.17	225.94	327.93	375.78

Table A.4. Continued.

2 MeV	Angle of Incidence (radians)									
mfp	0.00	0.17	0.45	0.73	0.86	1.05	1.21	1.30	1.40	1.49
1	1.64	1.66	1.65	1.62	1.58	1.52	1.42	1.34	1.25	1.14
2	2.42	2.41	2.36	2.30	2.23	2.12	1.95	1.81	1.64	1.39
3	3.23	3.19	3.12	3.08	3.02	2.94	2.75	2.57	2.33	1.90
4	4.07	4.00	3.95	4.01	4.00	4.09	4.02	3.89	3.65	2.99
5	4.93	4.85	4.84	5.10	5.23	5.72	6.10	6.26	6.28	5.38
6	5.82	5.72	5.80	6.41	6.79	8.08	9.54	10.56	11.60	10.78
7	6.72	6.62	6.83	7.96	8.76	11.49	15.26	18.47	22.53	23.14
8	7.65	7.55	7.94	9.80	11.26	16.45	24.84	33.08	45.19	51.76
9	8.59	8.51	9.14	12.00	14.44	23.69	40.95	60.21	92.43	118.61
10	9.55	9.49	10.41	14.63	18.47	34.31	68.14	110.77	191.43	275.81

4 MeV	Angle of Incidence (radians)									
mfp	0.00	0.17	0.45	0.73	0.86	1.05	1.21	1.30	1.40	1.49
1	1.52	1.55	1.55	1.54	1.50	1.47	1.39	1.33	1.25	1.14
2	2.13	2.12	2.08	2.05	2.01	1.95	1.83	1.72	1.59	1.37
3	2.71	2.67	2.62	2.60	2.56	2.54	2.41	2.30	2.15	1.82
4	3.28	3.22	3.16	3.20	3.18	3.27	3.25	3.21	3.15	2.75
5	3.85	3.77	3.71	3.85	3.88	4.21	4.48	4.68	4.99	4.71
6	4.41	4.31	4.27	4.57	4.70	5.44	6.31	7.11	8.46	8.95
7	4.97	4.86	4.85	5.37	5.66	7.07	9.09	11.16	15.08	18.30
8	5.52	5.40	5.44	6.28	6.79	9.27	13.36	18.03	27.91	39.17
9	6.07	5.95	6.05	7.30	8.13	12.26	20.00	29.76	52.95	86.19
10	6.61	6.49	6.68	8.45	9.73	16.38	30.44	49.95	102.24	192.84

5 MeV	Angle of Incidence (radians)									
mfp	0.00	0.17	0.45	0.73	0.86	1.05	1.21	1.30	1.40	1.49
1	1.48	1.51	1.51	1.50	1.47	1.45	1.38	1.32	1.25	1.14
2	2.03	2.02	2.00	1.97	1.93	1.89	1.78	1.69	1.57	1.36
3	2.55	2.51	2.47	2.46	2.42	2.41	2.30	2.21	2.08	1.79
4	3.06	2.99	2.93	2.97	2.94	3.03	3.02	3.00	2.98	2.65
5	3.55	3.47	3.40	3.52	3.53	3.81	4.04	4.23	4.58	4.45
6	4.04	3.94	3.88	4.12	4.20	4.81	5.52	6.20	7.53	8.30
7	4.52	4.40	4.36	4.78	4.97	6.11	7.71	9.41	13.03	16.67
8	4.99	4.86	4.85	5.51	5.86	7.83	11.01	14.70	23.44	35.11
9	5.45	5.32	5.35	6.33	6.90	10.14	16.05	23.53	43.38	76.12
10	5.90	5.77	5.86	7.25	8.13	13.28	23.84	38.40	81.91	168.00

6 MeV	Angle of Incidence (radians)									
mfp	0.00	0.17	0.45	0.73	0.86	1.05	1.21	1.30	1.40	1.49
1	1.45	1.47	1.48	1.47	1.45	1.43	1.36	1.31	1.24	1.13
2	1.95	1.94	1.92	1.90	1.87	1.83	1.74	1.65	1.54	1.35
3	2.42	2.38	2.34	2.33	2.30	2.29	2.20	2.12	2.02	1.75
4	2.87	2.81	2.75	2.78	2.76	2.84	2.83	2.81	2.82	2.56
5	3.31	3.23	3.17	3.26	3.27	3.51	3.70	3.87	4.24	4.22
6	3.74	3.65	3.58	3.78	3.83	4.36	4.94	5.52	6.79	7.72
7	4.16	4.05	3.99	4.35	4.48	5.44	6.75	8.15	11.46	15.27
8	4.57	4.46	4.41	4.96	5.21	6.86	9.43	12.41	20.16	31.72
9	4.98	4.85	4.84	5.65	6.07	8.74	13.47	19.40	36.58	67.92
10	5.37	5.24	5.27	6.42	7.06	11.29	19.67	31.01	67.90	148.22

Table A.4. Continued.

8 MeV	Angle of Incidence (radians)									
mfp	0.00	0.17	0.45	0.73	0.86	1.05	1.21	1.30	1.40	1.49
1	1.40	1.42	1.43	1.43	1.41	1.39	1.34	1.29	1.23	1.13
2	1.84	1.83	1.81	1.80	1.77	1.75	1.67	1.60	1.50	1.33
3	2.24	2.20	2.16	2.16	2.13	2.14	2.06	2.00	1.92	1.69
4	2.62	2.56	2.51	2.54	2.51	2.58	2.57	2.56	2.60	2.41
5	2.99	2.91	2.85	2.93	2.91	3.12	3.25	3.39	3.75	3.86
6	3.35	3.26	3.18	3.34	3.36	3.78	4.21	4.64	5.78	6.87
7	3.69	3.59	3.52	3.79	3.86	4.62	5.57	6.59	9.40	13.24
8	4.03	3.92	3.85	4.28	4.42	5.69	7.56	9.67	16.00	26.89
9	4.36	4.24	4.19	4.82	5.07	7.12	10.53	14.63	28.22	56.47
10	4.68	4.56	4.53	5.41	5.82	9.03	15.04	22.74	51.19	121.12

10 MeV	Angle of Incidence (radians)									
mfp	0.00	0.17	0.45	0.73	0.86	1.05	1.21	1.30	1.40	1.49
1	1.36	1.39	1.40	1.40	1.38	1.37	1.32	1.28	1.22	1.13
2	1.75	1.75	1.73	1.72	1.70	1.69	1.62	1.55	1.47	1.31
3	2.11	2.08	2.04	2.04	2.01	2.02	1.96	1.90	1.84	1.65
4	2.44	2.39	2.34	2.36	2.33	2.41	2.39	2.38	2.43	2.29
5	2.76	2.69	2.63	2.70	2.68	2.86	2.96	3.06	3.41	3.58
6	3.07	2.99	2.92	3.05	3.05	3.41	3.74	4.08	5.10	6.22
7	3.37	3.28	3.20	3.43	3.47	4.10	4.85	5.64	8.07	11.75
8	3.66	3.56	3.48	3.84	3.93	4.99	6.47	8.08	13.41	23.45
9	3.95	3.84	3.77	4.29	4.46	6.16	8.86	11.95	23.21	48.55
10	4.22	4.11	4.06	4.79	5.07	7.74	12.49	18.25	41.51	102.82

Table A.5. Ambient dose equivalent photon buildup factors for concrete.

50 keV	Angle of Incidence (radians)									
mfp	0.00	0.17	0.45	0.73	0.86	1.05	1.21	1.30	1.40	1.49
1	1.46	1.48	1.48	1.45	1.43	1.39	1.34	1.29	1.23	1.13
2	1.85	1.86	1.85	1.84	1.82	1.78	1.72	1.65	1.54	1.35
3	2.21	2.21	2.24	2.26	2.28	2.30	2.28	2.22	2.09	1.79
4	2.57	2.58	2.64	2.76	2.85	3.02	3.17	3.23	3.16	2.73
5	2.93	2.95	3.08	3.36	3.58	4.07	4.65	5.04	5.28	4.82
6	3.32	3.35	3.56	4.10	4.54	5.64	7.18	8.41	9.62	9.55
7	3.71	3.76	4.10	5.02	5.83	8.03	11.56	14.78	18.62	20.42
8	4.13	4.19	4.69	6.17	7.57	11.73	19.25	26.99	37.54	45.71
9	4.57	4.66	5.36	7.62	9.93	17.48	32.90	50.64	77.71	104.99
10	5.03	5.15	6.12	9.48	13.18	26.51	57.35	96.77	163.63	244.92

100 keV	Angle of Incidence (radians)									
mfp	0.00	0.17	0.45	0.73	0.86	1.05	1.21	1.30	1.40	1.49
1	1.87	1.91	1.88	1.82	1.75	1.66	1.53	1.44	1.33	1.18
2	2.87	2.86	2.81	2.73	2.65	2.51	2.29	2.11	1.87	1.52
3	3.92	3.89	3.88	3.90	3.86	3.81	3.58	3.33	2.94	2.25
4	5.08	5.03	5.13	5.44	5.57	5.86	5.88	5.68	5.16	3.90
5	6.36	6.31	6.62	7.48	8.01	9.18	10.08	10.31	9.92	7.73
6	7.78	7.74	8.40	10.24	11.52	14.62	17.84	19.59	20.29	16.78
7	9.36	9.36	10.53	13.95	16.63	23.60	32.35	38.38	43.10	38.42
8	11.11	11.16	13.07	18.98	24.06	38.51	59.63	76.65	93.67	90.63
9	13.04	13.18	16.11	25.80	34.90	63.35	111.15	155.01	206.43	217.38
10	15.18	15.44	19.73	35.03	50.77	104.86	208.78	316.09	458.91	526.54

500 keV	Angle of Incidence (radians)									
mfp	0.00	0.17	0.45	0.73	0.86	1.05	1.21	1.30	1.40	1.49
1	1.86	1.87	1.84	1.76	1.70	1.60	1.47	1.38	1.28	1.15
2	2.86	2.85	2.78	2.65	2.55	2.37	2.13	1.95	1.73	1.43
3	3.99	3.96	3.91	3.82	3.74	3.56	3.26	2.99	2.62	2.03
4	5.27	5.24	5.28	5.39	5.43	5.46	5.29	5.00	4.45	3.37
5	6.71	6.69	6.92	7.52	7.89	8.58	9.02	8.98	8.37	6.46
6	8.31	8.32	8.90	10.39	11.45	13.71	15.95	16.97	16.90	13.73
7	10.08	10.16	11.27	14.27	16.63	22.20	28.94	33.18	35.68	31.04
8	12.04	12.20	14.08	19.50	24.15	36.27	53.38	66.27	77.32	72.67
9	14.18	14.46	17.41	26.54	35.07	59.62	99.50	134.06	170.17	173.45
10	16.51	16.94	21.34	35.99	50.90	98.39	186.69	273.36	378.06	418.78

1 MeV	Angle of Incidence (radians)									
mfp	0.00	0.17	0.45	0.73	0.86	1.05	1.21	1.30	1.40	1.49
1	1.71	1.74	1.72	1.68	1.62	1.54	1.43	1.35	1.25	1.13
2	2.60	2.59	2.52	2.43	2.34	2.21	2.00	1.85	1.66	1.40
3	3.56	3.51	3.44	3.37	3.28	3.17	2.93	2.72	2.43	1.94
4	4.60	4.53	4.49	4.55	4.55	4.61	4.49	4.30	3.95	3.13
5	5.72	5.64	5.69	6.06	6.26	6.83	7.21	7.29	7.09	5.81
6	6.92	6.84	7.06	7.99	8.61	10.28	12.00	13.01	13.69	11.98
7	8.20	8.13	8.63	10.44	11.80	15.66	20.52	24.11	27.73	26.40
8	9.56	9.51	10.39	13.57	16.18	24.10	35.75	45.76	57.86	60.42
9	10.99	10.98	12.39	17.55	22.15	37.35	63.10	88.26	123.00	141.32
10	12.49	12.54	14.63	22.60	30.32	58.19	112.37	171.96	264.46	334.88

Table A.5. Continued.

2 MeV	Angle of Incidence (radians)									
mfp	0.00	0.17	0.45	0.73	0.86	1.05	1.21	1.30	1.40	1.49
1	1.61	1.63	1.63	1.60	1.56	1.50	1.41	1.34	1.25	1.14
2	2.34	2.33	2.28	2.23	2.16	2.07	1.91	1.78	1.62	1.38
3	3.09	3.05	2.99	2.94	2.88	2.81	2.64	2.49	2.28	1.88
4	3.87	3.80	3.74	3.78	3.77	3.84	3.78	3.69	3.51	2.93
5	4.67	4.58	4.56	4.78	4.87	5.29	5.62	5.79	5.91	5.22
6	5.49	5.39	5.44	5.95	6.26	7.36	8.61	9.55	10.71	10.35
7	6.33	6.23	6.39	7.35	8.02	10.34	13.54	16.37	20.41	21.99
8	7.19	7.09	7.41	9.02	10.25	14.67	21.74	28.83	40.24	48.70
9	8.07	7.98	8.51	11.01	13.08	21.00	35.47	51.77	81.13	110.57
10	8.96	8.89	9.69	13.39	16.69	30.26	58.57	94.22	165.92	254.81

4 MeV	Angle of Incidence (radians)									
mfp	0.00	0.17	0.45	0.73	0.86	1.05	1.21	1.30	1.40	1.49
1	1.49	1.51	1.51	1.50	1.47	1.44	1.37	1.31	1.23	1.13
2	2.05	2.04	2.01	1.98	1.93	1.88	1.77	1.67	1.55	1.35
3	2.60	2.56	2.51	2.49	2.44	2.42	2.31	2.21	2.07	1.78
4	3.14	3.08	3.02	3.04	3.02	3.10	3.07	3.04	3.00	2.64
5	3.68	3.60	3.54	3.66	3.69	3.98	4.21	4.39	4.69	4.48
6	4.22	4.13	4.09	4.36	4.48	5.14	5.91	6.61	7.87	8.44
7	4.77	4.66	4.65	5.14	5.41	6.71	8.52	10.36	13.93	17.15
8	5.31	5.19	5.24	6.03	6.52	8.84	12.57	16.75	25.68	36.54
9	5.85	5.73	5.85	7.05	7.85	11.77	18.92	27.73	48.67	80.08
10	6.39	6.28	6.48	8.21	9.47	15.85	29.00	46.80	94.03	178.61

5 MeV	Angle of Incidence (radians)									
mfp	0.00	0.17	0.45	0.73	0.86	1.05	1.21	1.30	1.40	1.49
1	1.45	1.48	1.48	1.47	1.45	1.42	1.36	1.30	1.23	1.13
2	1.97	1.96	1.93	1.91	1.87	1.83	1.73	1.65	1.53	1.34
3	2.46	2.43	2.38	2.37	2.33	2.31	2.22	2.13	2.02	1.75
4	2.95	2.89	2.83	2.86	2.83	2.91	2.89	2.86	2.85	2.56
5	3.43	3.35	3.29	3.39	3.41	3.66	3.85	4.02	4.35	4.26
6	3.91	3.82	3.76	3.99	4.07	4.63	5.27	5.88	7.10	7.88
7	4.39	4.28	4.25	4.65	4.84	5.92	7.40	8.95	12.25	15.75
8	4.87	4.75	4.75	5.40	5.75	7.65	10.66	14.06	22.06	33.06
9	5.34	5.22	5.27	6.24	6.83	10.00	15.69	22.70	40.95	71.53
10	5.81	5.69	5.80	7.20	8.12	13.24	23.57	37.45	77.69	157.66

6 MeV	Angle of Incidence (radians)									
mfp	0.00	0.17	0.45	0.73	0.86	1.05	1.21	1.30	1.40	1.49
1	1.43	1.45	1.46	1.45	1.42	1.40	1.35	1.30	1.23	1.13
2	1.90	1.89	1.87	1.85	1.82	1.79	1.69	1.62	1.51	1.33
3	2.35	2.32	2.27	2.26	2.23	2.22	2.14	2.06	1.96	1.72
4	2.79	2.74	2.68	2.70	2.68	2.75	2.73	2.71	2.72	2.48
5	3.23	3.15	3.09	3.18	3.18	3.41	3.58	3.73	4.06	4.05
6	3.66	3.57	3.51	3.70	3.76	4.26	4.80	5.33	6.49	7.39
7	4.09	3.99	3.94	4.29	4.43	5.36	6.61	7.93	10.98	14.56
8	4.52	4.41	4.38	4.93	5.20	6.83	9.35	12.20	19.41	30.20
9	4.94	4.82	4.83	5.66	6.12	8.82	13.54	19.33	35.46	64.67
10	5.36	5.24	5.30	6.49	7.21	11.54	20.05	31.36	66.39	141.25

Table A.5. Continued.

8 MeV	Angle of Incidence (radians)									
mfp	0.00	0.17	0.45	0.73	0.86	1.05	1.21	1.30	1.40	1.49
1	1.38	1.41	1.42	1.41	1.39	1.37	1.33	1.28	1.22	1.13
2	1.80	1.79	1.77	1.76	1.73	1.71	1.63	1.57	1.48	1.32
3	2.19	2.16	2.12	2.11	2.08	2.08	2.01	1.95	1.87	1.66
4	2.57	2.51	2.46	2.48	2.46	2.52	2.51	2.49	2.52	2.34
5	2.94	2.87	2.81	2.88	2.87	3.06	3.19	3.32	3.64	3.73
6	3.31	3.22	3.16	3.32	3.34	3.75	4.17	4.59	5.63	6.62
7	3.67	3.58	3.52	3.79	3.88	4.63	5.60	6.61	9.24	12.76
8	4.04	3.93	3.88	4.32	4.50	5.80	7.72	9.88	15.92	25.99
9	4.39	4.28	4.26	4.92	5.23	7.36	10.95	15.25	28.44	54.80
10	4.75	4.64	4.64	5.59	6.08	9.50	15.94	24.21	52.30	118.11

10 MeV	Angle of Incidence (radians)									
mfp	0.00	0.17	0.45	0.73	0.86	1.05	1.21	1.30	1.40	1.49
1	1.36	1.38	1.39	1.38	1.36	1.35	1.31	1.27	1.21	1.13
2	1.73	1.72	1.71	1.70	1.67	1.66	1.59	1.53	1.45	1.30
3	2.08	2.05	2.01	2.01	1.98	1.99	1.92	1.87	1.80	1.62
4	2.41	2.36	2.31	2.34	2.31	2.37	2.35	2.34	2.38	2.24
5	2.74	2.68	2.62	2.68	2.67	2.84	2.94	3.05	3.36	3.48
6	3.07	2.99	2.93	3.06	3.07	3.43	3.77	4.12	5.07	6.06
7	3.39	3.30	3.24	3.48	3.53	4.18	4.98	5.81	8.14	11.49
8	3.71	3.61	3.56	3.94	4.07	5.18	6.76	8.52	13.76	23.09
9	4.03	3.93	3.89	4.45	4.69	6.50	9.46	12.93	24.23	48.16
10	4.35	4.24	4.23	5.03	5.42	8.32	13.62	20.24	44.06	102.87

Table A.6. Air exposure photon buildup factors for lead.

50 keV	Angle of Incidence (radians)									
mfp	0.00	0.17	0.45	0.73	0.86	1.05	1.21	1.30	1.40	1.49
1	1.47	1.47	1.47	1.45	1.44	1.42	1.40	1.39	1.37	1.31
2	1.57	1.57	1.56	1.54	1.53	1.51	1.49	1.47	1.46	1.46
3	1.66	1.66	1.65	1.64	1.63	1.61	1.59	1.58	1.57	1.63
4	1.74	1.74	1.74	1.74	1.74	1.73	1.74	1.74	1.75	1.88
5	1.83	1.83	1.83	1.85	1.86	1.90	1.96	2.01	2.08	2.34
6	1.91	1.91	1.93	1.97	2.02	2.13	2.30	2.47	2.71	3.20
7	1.99	1.99	2.02	2.12	2.21	2.45	2.85	3.27	3.89	5.05
8	2.06	2.07	2.13	2.29	2.44	2.91	3.77	4.71	6.26	8.97
9	2.13	2.15	2.23	2.49	2.75	3.58	5.30	7.36	11.01	17.69
10	2.21	2.22	2.34	2.73	3.15	4.59	7.89	12.28	20.67	37.17

100 keV	Angle of Incidence (radians)									
mfp	0.00	0.17	0.45	0.73	0.86	1.05	1.21	1.30	1.40	1.49
1	2.03	2.03	2.00	1.93	1.89	1.80	1.69	1.62	1.51	1.38
2	2.76	2.76	2.74	2.68	2.63	2.52	2.36	2.21	2.02	1.75
3	3.67	3.67	3.71	3.74	3.74	3.69	3.53	3.34	3.01	2.46
4	4.92	4.94	5.11	5.41	5.56	5.76	5.77	5.59	5.12	4.07
5	6.74	6.80	7.24	8.13	8.67	9.58	10.21	10.29	9.77	7.80
6	9.51	9.64	10.62	12.76	14.17	16.86	19.29	20.36	20.23	16.71
7	13.83	14.11	16.13	20.82	24.14	30.99	38.18	42.24	44.15	38.27
8	20.76	21.30	25.31	35.16	42.55	58.93	78.00	90.52	99.52	90.82
9	32.08	33.12	40.87	61.05	77.07	114.87	163.05	198.06	228.60	220.22
10	50.89	52.85	67.70	108.47	142.59	228.06	346.22	439.32	532.14	540.05

500 keV	Angle of Incidence (radians)									
mfp	0.00	0.17	0.45	0.73	0.86	1.05	1.21	1.30	1.40	1.49
1	1.27	1.28	1.28	1.27	1.26	1.24	1.21	1.18	1.14	1.08
2	1.52	1.52	1.50	1.49	1.47	1.45	1.40	1.36	1.30	1.21
3	1.75	1.73	1.71	1.71	1.68	1.68	1.63	1.60	1.55	1.44
4	1.97	1.95	1.92	1.94	1.92	1.96	1.95	1.95	1.97	1.88
5	2.19	2.16	2.14	2.19	2.19	2.31	2.40	2.49	2.69	2.78
6	2.41	2.37	2.36	2.47	2.51	2.77	3.07	3.37	4.00	4.66
7	2.64	2.59	2.60	2.79	2.88	3.39	4.07	4.80	6.42	8.67
8	2.87	2.82	2.85	3.16	3.32	4.23	5.62	7.20	10.99	17.35
9	3.10	3.05	3.11	3.59	3.87	5.39	8.05	11.30	19.77	36.34
10	3.33	3.29	3.39	4.09	4.54	7.03	11.90	18.40	36.83	78.33

1 MeV	Angle of Incidence (radians)									
mfp	0.00	0.17	0.45	0.73	0.86	1.05	1.21	1.30	1.40	1.49
1	1.37	1.39	1.39	1.38	1.36	1.33	1.27	1.23	1.18	1.10
2	1.76	1.76	1.73	1.71	1.67	1.63	1.55	1.49	1.41	1.27
3	2.12	2.10	2.06	2.04	2.00	1.98	1.91	1.85	1.78	1.59
4	2.47	2.43	2.38	2.40	2.37	2.42	2.40	2.39	2.40	2.23
5	2.82	2.76	2.72	2.79	2.79	2.98	3.11	3.23	3.51	3.56
6	3.16	3.10	3.07	3.24	3.29	3.71	4.16	4.61	5.54	6.35
7	3.51	3.44	3.43	3.74	3.88	4.70	5.77	6.89	9.35	12.38
8	3.86	3.79	3.82	4.32	4.60	6.06	8.27	10.73	16.61	25.54
9	4.22	4.15	4.23	5.00	5.47	7.95	12.19	17.31	30.63	54.60
10	4.59	4.52	4.66	5.78	6.54	10.61	18.44	28.72	58.06	119.31

Table A.6. Continued.

2 MeV	Angle of Incidence (radians)									
mfp	0.00	0.17	0.45	0.73	0.86	1.05	1.21	1.30	1.40	1.49
1	1.41	1.43	1.43	1.42	1.40	1.37	1.31	1.26	1.20	1.12
2	1.86	1.85	1.82	1.80	1.76	1.72	1.63	1.55	1.46	1.31
3	2.29	2.26	2.21	2.19	2.15	2.12	2.03	1.96	1.88	1.67
4	2.72	2.67	2.61	2.62	2.59	2.63	2.60	2.58	2.58	2.39
5	3.15	3.09	3.04	3.11	3.12	3.30	3.44	3.57	3.85	3.88
6	3.60	3.52	3.49	3.68	3.75	4.21	4.71	5.19	6.18	7.03
7	4.05	3.97	3.97	4.34	4.53	5.46	6.68	7.92	10.58	13.85
8	4.52	4.43	4.49	5.11	5.48	7.20	9.79	12.61	19.04	28.75
9	4.99	4.91	5.04	6.01	6.67	9.67	14.75	20.74	35.52	61.71
10	5.48	5.40	5.63	7.09	8.16	13.20	22.79	35.04	67.98	135.29

4 MeV	Angle of Incidence (radians)									
mfp	0.00	0.17	0.45	0.73	0.86	1.05	1.21	1.30	1.40	1.49
1	1.36	1.37	1.37	1.37	1.35	1.33	1.28	1.24	1.19	1.11
2	1.71	1.71	1.69	1.67	1.64	1.61	1.54	1.48	1.41	1.28
3	2.08	2.05	2.02	2.00	1.97	1.94	1.87	1.82	1.75	1.59
4	2.46	2.42	2.37	2.38	2.36	2.38	2.36	2.34	2.35	2.20
5	2.86	2.81	2.77	2.83	2.84	2.98	3.09	3.19	3.41	3.47
6	3.29	3.23	3.21	3.37	3.44	3.83	4.23	4.62	5.40	6.14
7	3.75	3.68	3.70	4.03	4.22	5.03	6.07	7.10	9.21	11.90
8	4.24	4.17	4.24	4.84	5.22	6.79	9.08	11.48	16.66	24.53
9	4.75	4.69	4.86	5.84	6.54	9.39	14.07	19.34	31.45	52.56
10	5.30	5.25	5.55	7.08	8.26	13.28	22.45	33.61	61.19	115.38

5 MeV	Angle of Incidence (radians)									
mfp	0.00	0.17	0.45	0.73	0.86	1.05	1.21	1.30	1.40	1.49
1	1.35	1.36	1.36	1.36	1.34	1.32	1.28	1.24	1.19	1.12
2	1.68	1.67	1.65	1.64	1.61	1.58	1.52	1.47	1.40	1.28
3	2.02	1.99	1.96	1.95	1.92	1.90	1.84	1.79	1.73	1.58
4	2.38	2.34	2.30	2.31	2.29	2.32	2.30	2.29	2.30	2.16
5	2.77	2.72	2.69	2.75	2.76	2.90	3.01	3.10	3.32	3.38
6	3.19	3.14	3.12	3.28	3.35	3.72	4.12	4.49	5.23	5.94
7	3.65	3.59	3.61	3.94	4.13	4.92	5.94	6.93	8.93	11.48
8	4.15	4.08	4.17	4.77	5.16	6.70	8.96	11.30	16.20	23.63
9	4.68	4.62	4.81	5.81	6.53	9.37	14.03	19.23	30.74	50.66
10	5.27	5.22	5.55	7.13	8.38	13.44	22.70	33.83	60.21	111.36

6 MeV	Angle of Incidence (radians)									
mfp	0.00	0.17	0.45	0.73	0.86	1.05	1.21	1.30	1.40	1.49
1	1.35	1.37	1.37	1.36	1.34	1.32	1.28	1.24	1.19	1.12
2	1.67	1.66	1.64	1.63	1.61	1.58	1.52	1.47	1.40	1.28
3	1.99	1.97	1.94	1.93	1.90	1.89	1.83	1.78	1.73	1.57
4	2.34	2.31	2.27	2.28	2.27	2.30	2.29	2.28	2.28	2.15
5	2.72	2.68	2.65	2.71	2.73	2.88	2.99	3.10	3.30	3.35
6	3.14	3.09	3.08	3.25	3.34	3.71	4.12	4.51	5.22	5.89
7	3.60	3.55	3.58	3.93	4.14	4.94	5.99	7.02	8.96	11.39
8	4.12	4.06	4.17	4.79	5.22	6.79	9.14	11.56	16.37	23.52
9	4.68	4.63	4.85	5.90	6.69	9.63	14.52	19.95	31.33	50.57
10	5.31	5.27	5.65	7.34	8.70	14.02	23.83	35.62	61.91	111.58

Table A.6. Continued.

8 MeV	Angle of Incidence (radians)									
mfp	0.00	0.17	0.45	0.73	0.86	1.05	1.21	1.30	1.40	1.49
1	1.39	1.40	1.40	1.39	1.37	1.34	1.30	1.26	1.21	1.13
2	1.70	1.70	1.68	1.66	1.64	1.61	1.55	1.50	1.42	1.30
3	2.03	2.01	1.99	1.98	1.96	1.94	1.88	1.83	1.77	1.60
4	2.38	2.36	2.34	2.36	2.35	2.38	2.38	2.38	2.37	2.20
5	2.79	2.75	2.75	2.83	2.87	3.03	3.18	3.30	3.48	3.46
6	3.25	3.21	3.23	3.44	3.56	3.99	4.49	4.93	5.63	6.17
7	3.77	3.73	3.81	4.23	4.52	5.45	6.72	7.91	9.90	12.10
8	4.37	4.33	4.51	5.28	5.85	7.73	10.61	13.46	18.52	25.32
9	5.06	5.03	5.36	6.69	7.74	11.34	17.46	24.02	36.28	55.11
10	5.85	5.84	6.40	8.58	10.44	17.11	29.71	44.31	73.31	123.03

10 MeV	Angle of Incidence (radians)									
mfp	0.00	0.17	0.45	0.73	0.86	1.05	1.21	1.30	1.40	1.49
1	1.45	1.46	1.46	1.44	1.42	1.38	1.33	1.29	1.23	1.15
2	1.79	1.79	1.78	1.75	1.73	1.68	1.61	1.55	1.47	1.33
3	2.16	2.15	2.13	2.11	2.09	2.07	2.00	1.94	1.85	1.66
4	2.58	2.56	2.54	2.57	2.57	2.60	2.60	2.58	2.55	2.32
5	3.06	3.03	3.04	3.15	3.21	3.39	3.57	3.70	3.86	3.73
6	3.62	3.60	3.65	3.93	4.10	4.62	5.23	5.73	6.44	6.78
7	4.29	4.27	4.41	4.97	5.37	6.55	8.13	9.54	11.66	13.56
8	5.08	5.07	5.36	6.41	7.21	9.65	13.32	16.82	22.41	28.83
9	6.03	6.04	6.56	8.39	9.91	14.72	22.73	30.98	44.95	63.65
10	7.16	7.20	8.07	11.17	13.92	23.10	40.03	58.89	92.80	143.88

Table A.7. Air exposure photon buildup factors for iron.

50 keV	Angle of Incidence (radians)									
mfp	0.00	0.17	0.45	0.73	0.86	1.05	1.21	1.30	1.40	1.49
1	1.13	1.14	1.14	1.13	1.13	1.12	1.11	1.09	1.08	1.05
2	1.22	1.22	1.23	1.22	1.22	1.21	1.19	1.17	1.15	1.10
3	1.30	1.30	1.31	1.31	1.31	1.30	1.30	1.29	1.26	1.21
4	1.37	1.38	1.38	1.40	1.41	1.43	1.45	1.46	1.46	1.41
5	1.44	1.45	1.46	1.50	1.52	1.59	1.68	1.75	1.83	1.84
6	1.51	1.52	1.54	1.61	1.66	1.81	2.03	2.24	2.53	2.77
7	1.58	1.59	1.63	1.74	1.84	2.12	2.60	3.11	3.88	4.80
8	1.64	1.65	1.72	1.89	2.06	2.56	3.54	4.68	6.58	9.31
9	1.71	1.72	1.81	2.07	2.33	3.20	5.10	7.53	12.00	19.45
10	1.78	1.79	1.91	2.28	2.69	4.15	7.74	12.81	23.07	42.50

100 keV	Angle of Incidence (radians)									
mfp	0.00	0.17	0.45	0.73	0.86	1.05	1.21	1.30	1.40	1.49
1	1.33	1.34	1.34	1.33	1.31	1.29	1.25	1.22	1.17	1.10
2	1.63	1.63	1.62	1.60	1.58	1.56	1.50	1.46	1.38	1.26
3	1.91	1.90	1.90	1.90	1.89	1.89	1.86	1.81	1.74	1.56
4	2.19	2.17	2.19	2.24	2.25	2.33	2.38	2.40	2.39	2.18
5	2.47	2.45	2.50	2.63	2.70	2.94	3.20	3.40	3.61	3.51
6	2.77	2.75	2.84	3.10	3.27	3.80	4.53	5.16	5.99	6.42
7	3.07	3.06	3.21	3.66	4.00	5.06	6.74	8.35	10.75	12.92
8	3.39	3.39	3.62	4.35	4.96	6.93	10.44	14.22	20.40	27.62
9	3.73	3.74	4.08	5.20	6.21	9.73	16.76	25.13	40.21	61.24
10	4.08	4.11	4.59	6.25	7.88	13.96	27.65	45.66	81.29	138.74

500 keV	Angle of Incidence (radians)									
mfp	0.00	0.17	0.45	0.73	0.86	1.05	1.21	1.30	1.40	1.49
1	1.77	1.79	1.76	1.70	1.65	1.56	1.45	1.37	1.27	1.15
2	2.63	2.61	2.55	2.45	2.37	2.23	2.03	1.88	1.70	1.42
3	3.54	3.51	3.45	3.38	3.31	3.18	2.97	2.77	2.49	1.99
4	4.54	4.50	4.50	4.57	4.58	4.63	4.56	4.41	4.07	3.24
5	5.64	5.60	5.73	6.11	6.35	6.89	7.34	7.49	7.32	6.06
6	6.83	6.81	7.15	8.13	8.82	10.45	12.29	13.43	14.16	12.56
7	8.13	8.14	8.82	10.77	12.29	16.13	21.21	25.04	28.72	27.77
8	9.53	9.59	10.75	14.23	17.17	25.23	37.40	47.90	60.04	63.65
9	11.04	11.17	12.99	18.77	24.05	39.86	66.95	93.23	127.89	148.98
10	12.67	12.90	15.59	24.72	33.76	63.45	121.11	183.58	275.70	353.07

1 MeV	Angle of Incidence (radians)									
mfp	0.00	0.17	0.45	0.73	0.86	1.05	1.21	1.30	1.40	1.49
1	1.68	1.70	1.69	1.65	1.60	1.53	1.42	1.34	1.25	1.13
2	2.50	2.49	2.43	2.35	2.26	2.14	1.96	1.82	1.65	1.39
3	3.38	3.33	3.25	3.18	3.11	3.00	2.80	2.62	2.37	1.93
4	4.31	4.24	4.18	4.23	4.21	4.27	4.18	4.04	3.78	3.08
5	5.31	5.23	5.24	5.53	5.68	6.16	6.51	6.65	6.63	5.64
6	6.37	6.28	6.43	7.18	7.66	9.05	10.54	11.54	12.49	11.49
7	7.50	7.42	7.78	9.25	10.32	13.49	17.56	20.82	24.74	24.99
8	8.69	8.63	9.30	11.86	13.91	20.34	29.90	38.60	50.57	56.51
9	9.94	9.91	11.00	15.16	18.77	30.97	51.73	72.91	105.53	130.67
10	11.25	11.27	12.91	19.32	25.35	47.49	90.50	139.44	223.13	306.27

Table A.7. Continued.

2 MeV	Angle of Incidence (radians)									
mfp	0.00	0.17	0.45	0.73	0.86	1.05	1.21	1.30	1.40	1.49
1	1.59	1.62	1.61	1.59	1.55	1.50	1.40	1.33	1.25	1.14
2	2.31	2.29	2.25	2.19	2.13	2.04	1.89	1.77	1.62	1.38
3	3.03	2.99	2.92	2.88	2.82	2.75	2.59	2.45	2.26	1.88
4	3.79	3.72	3.66	3.69	3.66	3.72	3.67	3.59	3.44	2.91
5	4.57	4.49	4.45	4.64	4.72	5.10	5.39	5.57	5.74	5.17
6	5.38	5.28	5.32	5.78	6.06	7.05	8.19	9.09	10.29	10.18
7	6.22	6.12	6.26	7.15	7.75	9.88	12.79	15.42	19.41	21.51
8	7.08	6.98	7.27	8.78	9.91	14.00	20.43	26.95	37.93	47.36
9	7.97	7.88	8.38	10.75	12.68	20.03	33.22	48.11	75.92	106.91
10	8.88	8.81	9.57	13.12	16.22	28.92	54.78	87.16	154.32	245.04

4 MeV	Angle of Incidence (radians)									
mfp	0.00	0.17	0.45	0.73	0.86	1.05	1.21	1.30	1.40	1.49
1	1.48	1.50	1.51	1.49	1.46	1.43	1.36	1.30	1.23	1.13
2	2.03	2.02	1.99	1.96	1.92	1.86	1.75	1.66	1.54	1.35
3	2.58	2.54	2.49	2.47	2.42	2.40	2.29	2.19	2.06	1.77
4	3.14	3.08	3.02	3.04	3.02	3.09	3.06	3.03	2.99	2.64
5	3.72	3.64	3.58	3.70	3.73	4.01	4.24	4.41	4.70	4.48
6	4.31	4.22	4.19	4.47	4.60	5.27	6.04	6.75	7.95	8.47
7	4.92	4.82	4.84	5.37	5.67	7.02	8.89	10.75	14.23	17.30
8	5.55	5.44	5.53	6.42	6.99	9.49	13.42	17.74	26.56	37.02
9	6.20	6.09	6.28	7.66	8.64	12.98	20.73	30.03	50.98	81.54
10	6.86	6.75	7.07	9.12	10.70	17.99	32.63	51.87	99.84	182.77

5 MeV	Angle of Incidence (radians)									
mfp	0.00	0.17	0.45	0.73	0.86	1.05	1.21	1.30	1.40	1.49
1	1.45	1.47	1.48	1.47	1.44	1.41	1.35	1.30	1.23	1.13
2	1.95	1.94	1.92	1.89	1.86	1.81	1.72	1.63	1.52	1.34
3	2.45	2.41	2.37	2.35	2.32	2.30	2.20	2.12	2.01	1.74
4	2.96	2.90	2.85	2.87	2.85	2.91	2.90	2.88	2.85	2.55
5	3.49	3.41	3.36	3.46	3.48	3.73	3.94	4.11	4.40	4.27
6	4.03	3.94	3.90	4.14	4.25	4.84	5.52	6.15	7.31	7.97
7	4.59	4.49	4.48	4.94	5.19	6.36	7.98	9.63	12.88	16.09
8	5.17	5.06	5.11	5.87	6.35	8.50	11.88	15.62	23.70	34.11
9	5.76	5.65	5.78	6.98	7.78	11.52	18.12	26.09	44.96	74.53
10	6.37	6.26	6.51	8.28	9.58	15.84	28.25	44.55	87.17	165.89

6 MeV	Angle of Incidence (radians)									
mfp	0.00	0.17	0.45	0.73	0.86	1.05	1.21	1.30	1.40	1.49
1	1.43	1.45	1.46	1.45	1.42	1.40	1.34	1.29	1.22	1.13
2	1.89	1.88	1.86	1.84	1.81	1.77	1.68	1.61	1.51	1.33
3	2.35	2.32	2.27	2.26	2.23	2.22	2.13	2.06	1.96	1.71
4	2.82	2.76	2.71	2.74	2.72	2.78	2.77	2.75	2.74	2.48
5	3.30	3.23	3.18	3.27	3.29	3.52	3.71	3.87	4.17	4.09
6	3.81	3.72	3.68	3.90	3.99	4.52	5.13	5.72	6.83	7.55
7	4.33	4.23	4.22	4.63	4.84	5.90	7.34	8.84	11.90	15.11
8	4.87	4.76	4.80	5.48	5.89	7.82	10.82	14.18	21.67	31.81
9	5.42	5.32	5.42	6.49	7.20	10.54	16.39	23.48	40.78	69.13
10	6.00	5.89	6.10	7.69	8.84	14.43	25.41	39.82	78.56	153.16

Table A.7. Continued.

8 MeV	Angle of Incidence (radians)									
mfp	0.00	0.17	0.45	0.73	0.86	1.05	1.21	1.30	1.40	1.49
1	1.41	1.43	1.43	1.42	1.40	1.38	1.33	1.28	1.22	1.13
2	1.82	1.81	1.79	1.77	1.75	1.72	1.64	1.57	1.48	1.32
3	2.22	2.19	2.16	2.15	2.12	2.11	2.04	1.98	1.89	1.67
4	2.63	2.59	2.54	2.57	2.55	2.61	2.61	2.60	2.60	2.37
5	3.07	3.00	2.96	3.04	3.06	3.26	3.43	3.58	3.88	3.84
6	3.52	3.44	3.41	3.60	3.67	4.14	4.68	5.20	6.24	6.98
7	3.99	3.90	3.89	4.25	4.43	5.35	6.61	7.93	10.70	13.80
8	4.49	4.39	4.42	5.02	5.37	7.04	9.65	12.59	19.29	28.83
9	5.01	4.91	5.00	5.94	6.55	9.45	14.52	20.67	36.01	62.27
10	5.54	5.45	5.63	7.04	8.04	12.92	22.44	34.89	68.98	137.31

10 MeV	Angle of Incidence (radians)									
mfp	0.00	0.17	0.45	0.73	0.86	1.05	1.21	1.30	1.40	1.49
1	1.41	1.42	1.43	1.42	1.40	1.38	1.33	1.28	1.22	1.14
2	1.78	1.78	1.76	1.75	1.72	1.69	1.62	1.56	1.47	1.31
3	2.16	2.13	2.11	2.10	2.07	2.07	2.00	1.94	1.86	1.65
4	2.55	2.50	2.47	2.49	2.48	2.53	2.53	2.53	2.53	2.32
5	2.95	2.89	2.86	2.94	2.95	3.15	3.31	3.46	3.73	3.71
6	3.38	3.31	3.28	3.47	3.54	3.97	4.49	4.99	5.96	6.67
7	3.83	3.75	3.75	4.09	4.26	5.12	6.31	7.57	10.17	13.12
8	4.31	4.22	4.26	4.83	5.17	6.74	9.21	12.00	18.27	27.31
9	4.81	4.72	4.82	5.73	6.31	9.06	13.87	19.72	34.07	58.88
10	5.34	5.26	5.45	6.81	7.78	12.42	21.48	33.36	65.26	129.68

Table A.8. Air exposure photon buildup factors for aluminum.

50 keV	Angle of Incidence (radians)									
mfp	0.00	0.17	0.45	0.73	0.86	1.05	1.21	1.30	1.40	1.49
1	1.50	1.52	1.52	1.49	1.47	1.43	1.37	1.32	1.25	1.15
2	1.95	1.95	1.95	1.93	1.91	1.87	1.79	1.71	1.59	1.38
3	2.37	2.38	2.40	2.43	2.44	2.46	2.42	2.36	2.20	1.86
4	2.81	2.82	2.89	3.02	3.11	3.29	3.44	3.48	3.38	2.89
5	3.27	3.29	3.43	3.75	3.99	4.52	5.14	5.52	5.74	5.16
6	3.76	3.79	4.04	4.65	5.15	6.38	8.05	9.35	10.57	10.33
7	4.29	4.33	4.73	5.80	6.73	9.23	13.14	16.63	20.65	22.24
8	4.85	4.92	5.51	7.26	8.89	13.68	22.15	30.67	41.93	49.98
9	5.45	5.56	6.41	9.13	11.87	20.68	38.28	58.01	87.29	115.12
10	6.10	6.25	7.44	11.55	16.01	31.79	67.38	111.71	184.76	269.17

100 keV	Angle of Incidence (radians)									
mfp	0.00	0.17	0.45	0.73	0.86	1.05	1.21	1.30	1.40	1.49
1	1.91	1.95	1.92	1.85	1.78	1.69	1.55	1.45	1.34	1.19
2	2.98	2.98	2.93	2.84	2.74	2.59	2.35	2.16	1.90	1.54
3	4.16	4.12	4.10	4.12	4.07	4.00	3.74	3.46	3.03	2.30
4	5.47	5.41	5.52	5.84	5.97	6.26	6.23	5.97	5.39	4.02
5	6.95	6.89	7.24	8.17	8.72	9.95	10.82	10.98	10.46	8.02
6	8.63	8.58	9.32	11.35	12.74	16.08	19.40	21.09	21.56	17.52
7	10.52	10.51	11.84	15.69	18.64	26.29	35.57	41.69	46.12	40.28
8	12.65	12.70	14.90	21.65	27.34	43.42	66.21	83.98	100.88	95.35
9	15.05	15.20	18.61	29.82	40.19	72.24	124.56	171.16	223.63	229.39
10	17.74	18.03	23.09	41.03	59.17	120.87	236.01	351.55	499.86	557.26

500 keV	Angle of Incidence (radians)									
mfp	0.00	0.17	0.45	0.73	0.86	1.05	1.21	1.30	1.40	1.49
1	1.86	1.87	1.84	1.77	1.70	1.60	1.47	1.38	1.28	1.15
2	2.88	2.86	2.79	2.66	2.56	2.38	2.14	1.96	1.73	1.44
3	4.02	3.99	3.94	3.85	3.76	3.58	3.28	3.00	2.62	2.04
4	5.32	5.29	5.33	5.45	5.48	5.51	5.33	5.03	4.47	3.38
5	6.79	6.77	7.01	7.61	7.98	8.68	9.11	9.05	8.42	6.48
6	8.43	8.44	9.03	10.54	11.62	13.91	16.16	17.15	17.03	13.78
7	10.25	10.32	11.46	14.52	16.92	22.58	29.39	33.61	36.00	31.18
8	12.26	12.42	14.34	19.89	24.64	36.99	54.33	67.25	78.14	73.04
9	14.47	14.75	17.77	27.13	35.86	60.96	101.48	136.32	172.24	174.45
10	16.87	17.31	21.82	36.86	52.15	100.80	190.77	278.46	383.24	421.47

1 MeV	Angle of Incidence (radians)									
mfp	0.00	0.17	0.45	0.73	0.86	1.05	1.21	1.30	1.40	1.49
1	1.71	1.74	1.72	1.68	1.62	1.54	1.43	1.35	1.25	1.14
2	2.61	2.59	2.53	2.44	2.35	2.21	2.01	1.85	1.66	1.40
3	3.57	3.53	3.45	3.38	3.30	3.18	2.93	2.72	2.43	1.94
4	4.62	4.55	4.50	4.57	4.57	4.63	4.51	4.31	3.96	3.13
5	5.75	5.67	5.72	6.10	6.30	6.87	7.25	7.32	7.12	5.82
6	6.96	6.88	7.11	8.04	8.66	10.35	12.08	13.09	13.75	12.01
7	8.25	8.18	8.68	10.52	11.90	15.79	20.68	24.27	27.87	26.47
8	9.62	9.58	10.47	13.68	16.32	24.33	36.07	46.14	58.22	60.60
9	11.07	11.07	12.49	17.71	22.37	37.74	63.74	89.08	123.86	141.79
10	12.59	12.65	14.76	22.82	30.63	58.84	113.61	173.71	266.52	336.13

Table A.8. Continued.

2 MeV	Angle of Incidence (radians)									
mfp	0.00	0.17	0.45	0.73	0.86	1.05	1.21	1.30	1.40	1.49
1	1.61	1.63	1.63	1.60	1.56	1.50	1.41	1.34	1.25	1.14
2	2.35	2.33	2.29	2.23	2.16	2.07	1.91	1.78	1.62	1.38
3	3.10	3.06	2.99	2.95	2.89	2.82	2.65	2.49	2.28	1.88
4	3.88	3.81	3.75	3.80	3.78	3.85	3.80	3.70	3.52	2.93
5	4.68	4.60	4.58	4.80	4.89	5.31	5.64	5.82	5.94	5.23
6	5.51	5.42	5.47	5.98	6.30	7.40	8.66	9.61	10.76	10.38
7	6.36	6.26	6.43	7.40	8.07	10.41	13.63	16.49	20.53	22.06
8	7.23	7.13	7.46	9.08	10.32	14.79	21.92	29.07	40.52	48.89
9	8.12	8.03	8.57	11.10	13.19	21.18	35.80	52.25	81.75	111.06
10	9.02	8.95	9.76	13.51	16.84	30.57	59.17	95.17	167.32	256.06

4 MeV	Angle of Incidence (radians)									
mfp	0.00	0.17	0.45	0.73	0.86	1.05	1.21	1.30	1.40	1.49
1	1.49	1.51	1.52	1.50	1.47	1.44	1.37	1.31	1.24	1.13
2	2.05	2.04	2.01	1.98	1.94	1.89	1.77	1.68	1.55	1.35
3	2.60	2.56	2.51	2.49	2.45	2.43	2.31	2.21	2.08	1.78
4	3.15	3.09	3.03	3.06	3.03	3.11	3.09	3.06	3.01	2.65
5	3.70	3.62	3.56	3.68	3.71	4.00	4.24	4.42	4.72	4.49
6	4.25	4.15	4.12	4.39	4.51	5.19	5.97	6.69	7.94	8.49
7	4.80	4.70	4.69	5.19	5.47	6.79	8.63	10.51	14.11	17.28
8	5.36	5.24	5.29	6.11	6.61	8.97	12.78	17.04	26.07	36.87
9	5.92	5.80	5.92	7.15	7.98	11.99	19.30	28.32	49.53	80.94
10	6.47	6.36	6.58	8.35	9.66	16.20	29.69	47.94	95.91	180.78

5 MeV	Angle of Incidence (radians)									
mfp	0.00	0.17	0.45	0.73	0.86	1.05	1.21	1.30	1.40	1.49
1	1.46	1.48	1.48	1.47	1.45	1.42	1.36	1.30	1.23	1.13
2	1.97	1.96	1.94	1.91	1.87	1.84	1.73	1.65	1.53	1.34
3	2.47	2.43	2.38	2.37	2.33	2.32	2.22	2.14	2.02	1.75
4	2.96	2.90	2.84	2.87	2.84	2.92	2.90	2.88	2.86	2.57
5	3.45	3.37	3.31	3.41	3.43	3.68	3.88	4.05	4.38	4.28
6	3.94	3.84	3.79	4.02	4.11	4.68	5.33	5.96	7.18	7.93
7	4.43	4.32	4.29	4.70	4.90	6.00	7.52	9.10	12.44	15.89
8	4.92	4.80	4.81	5.47	5.84	7.79	10.87	14.37	22.48	33.44
9	5.40	5.28	5.34	6.34	6.96	10.22	16.08	23.31	41.86	72.49
10	5.89	5.77	5.90	7.34	8.31	13.59	24.25	38.61	79.67	160.11

6 MeV	Angle of Incidence (radians)									
mfp	0.00	0.17	0.45	0.73	0.86	1.05	1.21	1.30	1.40	1.49
1	1.43	1.45	1.46	1.45	1.42	1.40	1.35	1.30	1.23	1.13
2	1.91	1.89	1.87	1.85	1.82	1.79	1.70	1.62	1.51	1.33
3	2.36	2.32	2.28	2.27	2.23	2.23	2.14	2.07	1.97	1.72
4	2.80	2.75	2.69	2.72	2.69	2.76	2.75	2.73	2.73	2.49
5	3.25	3.17	3.11	3.20	3.21	3.44	3.61	3.76	4.10	4.07
6	3.69	3.60	3.54	3.74	3.80	4.30	4.86	5.41	6.58	7.44
7	4.13	4.03	3.98	4.34	4.49	5.44	6.74	8.09	11.18	14.72
8	4.57	4.46	4.44	5.01	5.30	6.97	9.57	12.53	19.85	30.62
9	5.01	4.89	4.91	5.77	6.25	9.04	13.93	19.95	36.42	65.73
10	5.45	5.33	5.40	6.63	7.40	11.88	20.74	32.54	68.44	143.93

Table A.8. Continued.

8 MeV	Angle of Incidence (radians)									
mfp	0.00	0.17	0.45	0.73	0.86	1.05	1.21	1.30	1.40	1.49
1	1.39	1.41	1.42	1.41	1.39	1.38	1.33	1.28	1.22	1.13
2	1.80	1.79	1.78	1.76	1.74	1.71	1.64	1.57	1.48	1.32
3	2.20	2.16	2.12	2.12	2.09	2.09	2.02	1.95	1.88	1.66
4	2.58	2.53	2.47	2.50	2.47	2.54	2.53	2.51	2.54	2.35
5	2.96	2.89	2.83	2.91	2.90	3.09	3.23	3.36	3.68	3.75
6	3.34	3.25	3.19	3.35	3.39	3.80	4.24	4.68	5.73	6.68
7	3.71	3.62	3.56	3.85	3.94	4.72	5.72	6.79	9.47	12.94
8	4.09	3.99	3.94	4.40	4.60	5.94	7.95	10.22	16.40	26.47
9	4.47	4.35	4.34	5.03	5.37	7.59	11.35	15.90	29.47	56.02
10	4.84	4.72	4.75	5.74	6.28	9.84	16.62	25.41	54.45	121.16

10 MeV	Angle of Incidence (radians)									
mfp	0.00	0.17	0.45	0.73	0.86	1.05	1.21	1.30	1.40	1.49
1	1.36	1.38	1.39	1.39	1.37	1.36	1.31	1.27	1.21	1.13
2	1.74	1.73	1.71	1.70	1.68	1.66	1.59	1.53	1.45	1.30
3	2.09	2.06	2.02	2.02	1.99	2.00	1.93	1.88	1.81	1.62
4	2.43	2.38	2.33	2.35	2.33	2.39	2.38	2.37	2.40	2.25
5	2.76	2.70	2.65	2.71	2.70	2.87	2.99	3.10	3.41	3.51
6	3.10	3.02	2.96	3.10	3.12	3.49	3.85	4.22	5.18	6.14
7	3.44	3.35	3.29	3.54	3.61	4.28	5.12	6.01	8.39	11.70
8	3.77	3.68	3.63	4.02	4.17	5.33	7.00	8.88	14.28	23.64
9	4.11	4.01	3.98	4.57	4.84	6.74	9.87	13.60	25.33	49.56
10	4.44	4.34	4.34	5.19	5.63	8.67	14.32	21.48	46.31	106.30

Table A.9. Air exposure photon buildup factors for water.

50 keV	Angle of Incidence (radians)									
mfp	0.00	0.17	0.45	0.73	0.86	1.05	1.21	1.30	1.40	1.49
1	2.29	2.32	2.27	2.15	2.06	1.90	1.72	1.59	1.43	1.24
2	3.96	3.97	3.90	3.73	3.59	3.28	2.89	2.58	2.19	1.68
3	5.98	5.99	6.04	6.04	5.97	5.69	5.13	4.58	3.80	2.68
4	8.39	8.44	8.79	9.41	9.69	9.93	9.54	8.77	7.37	5.00
5	11.25	11.38	12.32	14.29	15.49	17.42	18.26	17.67	15.46	10.57
6	14.62	14.87	16.80	21.31	24.48	30.63	35.61	36.73	34.02	24.13
7	18.55	19.00	22.45	31.39	38.38	53.94	70.19	77.67	76.93	57.51
8	23.13	23.85	29.55	45.79	59.83	94.97	139.09	165.81	176.53	140.24
9	28.41	29.51	38.43	66.31	92.81	167.10	276.33	355.71	408.37	346.42
10	34.48	36.08	49.47	95.44	143.40	293.68	549.53	764.90	948.95	862.35

100 keV	Angle of Incidence (radians)									
mfp	0.00	0.17	0.45	0.73	0.86	1.05	1.21	1.30	1.40	1.49
1	2.28	2.32	2.26	2.12	2.01	1.84	1.64	1.51	1.37	1.20
2	4.38	4.37	4.22	3.92	3.68	3.27	2.79	2.45	2.06	1.60
3	7.32	7.28	7.17	6.94	6.65	6.05	5.14	4.43	3.58	2.50
4	11.28	11.23	11.44	11.83	11.80	11.41	10.12	8.81	7.05	4.62
5	16.43	16.42	17.43	19.61	20.58	21.71	20.70	18.65	15.19	9.77
6	23.00	23.10	25.68	31.78	35.35	41.33	43.16	40.86	34.55	22.45
7	31.21	31.55	36.86	50.54	59.89	78.36	90.68	91.07	80.91	54.07
8	41.34	42.08	51.80	79.14	100.25	147.73	190.82	204.49	192.39	133.55
9	53.67	55.04	71.54	122.32	166.05	276.80	400.87	460.25	461.02	334.52
10	68.54	70.84	97.39	186.95	272.50	515.44	839.70	1035.65	1108.85	845.01

500 keV	Angle of Incidence (radians)									
mfp	0.00	0.17	0.45	0.73	0.86	1.05	1.21	1.30	1.40	1.49
1	1.88	1.90	1.86	1.78	1.71	1.61	1.47	1.38	1.28	1.15
2	2.99	2.98	2.90	2.75	2.63	2.42	2.16	1.96	1.74	1.43
3	4.32	4.29	4.22	4.10	3.99	3.74	3.37	3.05	2.64	2.04
4	5.87	5.84	5.89	6.02	6.04	5.97	5.64	5.22	4.54	3.39
5	7.68	7.67	7.98	8.71	9.13	9.80	9.98	9.65	8.69	6.52
6	9.74	9.78	10.56	12.48	13.79	16.35	18.38	18.84	17.89	13.93
7	12.08	12.20	13.72	17.72	20.78	27.57	34.67	38.08	38.57	31.68
8	14.71	14.95	17.56	24.95	31.22	46.77	66.36	78.55	85.44	74.66
9	17.63	18.04	22.18	34.89	46.71	79.52	127.96	163.90	192.29	179.50
10	20.84	21.48	27.70	48.47	69.63	135.19	247.66	344.10	436.77	436.77

1 MeV	Angle of Incidence (radians)									
mfp	0.00	0.17	0.45	0.73	0.86	1.05	1.21	1.30	1.40	1.49
1	1.72	1.75	1.73	1.68	1.62	1.55	1.43	1.35	1.25	1.14
2	2.66	2.64	2.58	2.48	2.38	2.23	2.02	1.86	1.66	1.40
3	3.69	3.64	3.56	3.49	3.40	3.25	2.98	2.75	2.44	1.94
4	4.81	4.75	4.71	4.79	4.79	4.83	4.66	4.41	4.00	3.14
5	6.04	5.96	6.04	6.47	6.71	7.31	7.64	7.61	7.26	5.84
6	7.37	7.29	7.57	8.64	9.36	11.23	13.00	13.87	14.20	12.08
7	8.78	8.72	9.32	11.43	13.03	17.43	22.70	26.22	29.17	26.73
8	10.29	10.26	11.31	15.01	18.08	27.25	40.31	50.73	61.75	61.47
9	11.89	11.90	13.56	19.58	25.03	42.81	72.35	99.56	133.13	144.52
10	13.56	13.65	16.10	25.41	34.58	67.48	130.72	197.06	290.17	344.33

Table A.9. Continued.

2 MeV	Angle of Incidence (radians)									
mfp	0.00	0.17	0.45	0.73	0.86	1.05	1.21	1.30	1.40	1.49
1	1.61	1.64	1.63	1.60	1.56	1.50	1.41	1.34	1.25	1.13
2	2.37	2.35	2.31	2.25	2.18	2.08	1.91	1.78	1.62	1.38
3	3.14	3.09	3.03	2.99	2.92	2.85	2.67	2.50	2.28	1.88
4	3.93	3.87	3.81	3.86	3.85	3.92	3.86	3.74	3.53	2.93
5	4.75	4.67	4.65	4.89	5.00	5.44	5.78	5.94	6.00	5.23
6	5.59	5.49	5.56	6.11	6.45	7.62	8.94	9.90	10.95	10.38
7	6.45	6.35	6.53	7.56	8.28	10.76	14.18	17.13	21.05	22.12
8	7.32	7.23	7.58	9.28	10.60	15.33	22.92	30.42	41.87	49.17
9	8.22	8.13	8.70	11.33	13.54	21.98	37.58	55.01	85.05	112.05
10	9.12	9.05	9.89	13.77	17.27	31.72	62.26	100.68	175.14	259.23

4 MeV	Angle of Incidence (radians)									
mfp	0.00	0.17	0.45	0.73	0.86	1.05	1.21	1.30	1.40	1.49
1	1.49	1.51	1.52	1.50	1.47	1.44	1.37	1.31	1.24	1.13
2	2.06	2.05	2.02	1.99	1.94	1.89	1.78	1.68	1.55	1.35
3	2.61	2.57	2.52	2.50	2.46	2.43	2.32	2.22	2.08	1.78
4	3.14	3.08	3.02	3.05	3.03	3.11	3.09	3.05	3.00	2.64
5	3.68	3.59	3.54	3.66	3.69	3.98	4.22	4.40	4.70	4.47
6	4.20	4.11	4.06	4.34	4.45	5.13	5.91	6.63	7.89	8.42
7	4.73	4.62	4.60	5.09	5.34	6.64	8.47	10.34	13.96	17.11
8	5.24	5.13	5.16	5.93	6.39	8.68	12.41	16.62	25.69	36.43
9	5.76	5.64	5.73	6.88	7.64	11.46	18.52	27.34	48.55	79.83
10	6.26	6.15	6.32	7.97	9.13	15.28	28.13	45.79	93.51	178.04

5 MeV	Angle of Incidence (radians)									
mfp	0.00	0.17	0.45	0.73	0.86	1.05	1.21	1.30	1.40	1.49
1	1.45	1.48	1.48	1.48	1.45	1.42	1.36	1.31	1.23	1.13
2	1.98	1.97	1.94	1.92	1.88	1.84	1.74	1.65	1.54	1.35
3	2.47	2.43	2.38	2.37	2.34	2.32	2.23	2.14	2.02	1.75
4	2.95	2.89	2.83	2.86	2.83	2.91	2.89	2.87	2.85	2.56
5	3.42	3.34	3.27	3.38	3.39	3.64	3.84	4.01	4.34	4.25
6	3.88	3.78	3.72	3.94	4.02	4.58	5.22	5.83	7.06	7.85
7	4.33	4.22	4.18	4.57	4.74	5.80	7.26	8.79	12.13	15.66
8	4.77	4.66	4.64	5.26	5.57	7.41	10.32	13.66	21.71	32.79
9	5.21	5.09	5.11	6.03	6.55	9.57	15.00	21.79	40.03	70.77
10	5.64	5.52	5.60	6.89	7.70	12.51	22.25	35.50	75.41	155.67

6 MeV	Angle of Incidence (radians)									
mfp	0.00	0.17	0.45	0.73	0.86	1.05	1.21	1.30	1.40	1.49
1	1.43	1.45	1.46	1.45	1.42	1.41	1.35	1.30	1.23	1.13
2	1.91	1.90	1.87	1.86	1.82	1.79	1.70	1.62	1.52	1.34
3	2.36	2.32	2.28	2.27	2.23	2.23	2.14	2.07	1.97	1.72
4	2.79	2.73	2.67	2.70	2.67	2.75	2.73	2.71	2.72	2.48
5	3.21	3.13	3.07	3.16	3.16	3.38	3.55	3.70	4.04	4.05
6	3.62	3.53	3.46	3.65	3.69	4.18	4.71	5.24	6.42	7.35
7	4.02	3.92	3.86	4.19	4.30	5.21	6.41	7.69	10.76	14.43
8	4.42	4.30	4.26	4.78	5.00	6.55	8.93	11.65	18.84	29.80
9	4.80	4.68	4.66	5.43	5.81	8.33	12.73	18.16	34.06	63.53
10	5.18	5.06	5.08	6.16	6.76	10.74	18.56	28.97	63.11	138.18

Table A.9. Continued.

8 MeV	Angle of Incidence (radians)									
mfp	0.00	0.17	0.45	0.73	0.86	1.05	1.21	1.30	1.40	1.49
1	1.38	1.40	1.41	1.41	1.39	1.38	1.33	1.28	1.22	1.13
2	1.80	1.79	1.77	1.76	1.73	1.72	1.64	1.57	1.48	1.32
3	2.19	2.15	2.11	2.11	2.08	2.09	2.01	1.95	1.87	1.67
4	2.56	2.50	2.45	2.47	2.44	2.51	2.49	2.48	2.51	2.34
5	2.91	2.84	2.77	2.85	2.83	3.02	3.14	3.26	3.60	3.72
6	3.25	3.17	3.09	3.25	3.26	3.65	4.05	4.44	5.50	6.55
7	3.59	3.49	3.42	3.68	3.74	4.45	5.34	6.27	8.89	12.54
8	3.92	3.81	3.74	4.15	4.28	5.48	7.23	9.17	15.06	25.33
9	4.23	4.12	4.06	4.66	4.89	6.84	10.05	13.84	26.50	52.99
10	4.54	4.43	4.39	5.23	5.61	8.67	14.34	21.48	48.03	113.34

10 MeV	Angle of Incidence (radians)									
mfp	0.00	0.17	0.45	0.73	0.86	1.05	1.21	1.30	1.40	1.49
1	1.35	1.37	1.38	1.38	1.36	1.35	1.31	1.27	1.21	1.12
2	1.72	1.72	1.70	1.69	1.67	1.66	1.59	1.53	1.45	1.30
3	2.07	2.03	2.00	2.00	1.97	1.98	1.92	1.86	1.80	1.62
4	2.39	2.34	2.29	2.31	2.28	2.35	2.33	2.31	2.36	2.23
5	2.70	2.63	2.57	2.64	2.61	2.78	2.87	2.96	3.29	3.45
6	3.00	2.92	2.85	2.98	2.97	3.31	3.62	3.93	4.88	5.95
7	3.29	3.20	3.12	3.34	3.37	3.98	4.69	5.41	7.68	11.16
8	3.58	3.47	3.40	3.74	3.82	4.84	6.23	7.72	12.72	22.18
9	3.85	3.74	3.67	4.17	4.33	5.96	8.52	11.40	21.98	45.75
10	4.12	4.01	3.95	4.65	4.92	7.48	12.00	17.38	39.29	96.68

Table A.10. Air exposure photon buildup factors for concrete.

50 keV	Angle of Incidence (radians)									
mfp	0.00	0.17	0.45	0.73	0.86	1.05	1.21	1.30	1.40	1.49
1	1.46	1.48	1.48	1.45	1.43	1.39	1.34	1.29	1.23	1.13
2	1.85	1.86	1.85	1.84	1.82	1.78	1.72	1.65	1.54	1.35
3	2.21	2.21	2.24	2.26	2.28	2.30	2.28	2.22	2.09	1.79
4	2.57	2.58	2.64	2.76	2.85	3.02	3.17	3.23	3.16	2.73
5	2.93	2.95	3.08	3.36	3.58	4.07	4.65	5.04	5.28	4.82
6	3.32	3.35	3.56	4.10	4.54	5.64	7.18	8.41	9.62	9.55
7	3.71	3.76	4.10	5.02	5.83	8.03	11.56	14.78	18.62	20.42
8	4.13	4.19	4.69	6.17	7.57	11.73	19.25	26.99	37.54	45.71
9	4.57	4.66	5.36	7.62	9.93	17.48	32.90	50.64	77.71	104.99
10	5.03	5.15	6.12	9.48	13.18	26.51	57.35	96.77	163.63	244.92

100 keV	Angle of Incidence (radians)									
mfp	0.00	0.17	0.45	0.73	0.86	1.05	1.21	1.30	1.40	1.49
1	1.87	1.91	1.88	1.82	1.75	1.66	1.53	1.44	1.33	1.18
2	2.87	2.86	2.81	2.73	2.65	2.51	2.29	2.11	1.87	1.52
3	3.92	3.89	3.88	3.90	3.86	3.81	3.58	3.33	2.94	2.25
4	5.08	5.03	5.13	5.44	5.57	5.86	5.88	5.68	5.16	3.90
5	6.36	6.31	6.62	7.48	8.01	9.18	10.08	10.31	9.92	7.73
6	7.78	7.74	8.40	10.24	11.52	14.62	17.84	19.59	20.29	16.78
7	9.36	9.36	10.53	13.95	16.63	23.60	32.35	38.38	43.10	38.42
8	11.11	11.16	13.07	18.98	24.06	38.51	59.63	76.65	93.67	90.63
9	13.04	13.18	16.11	25.80	34.90	63.35	111.15	155.01	206.43	217.38
10	15.18	15.44	19.73	35.03	50.77	104.86	208.78	316.09	458.91	526.54

500 keV	Angle of Incidence (radians)									
mfp	0.00	0.17	0.45	0.73	0.86	1.05	1.21	1.30	1.40	1.49
1	1.86	1.87	1.84	1.76	1.70	1.60	1.47	1.38	1.28	1.15
2	2.86	2.85	2.78	2.65	2.55	2.37	2.13	1.95	1.73	1.43
3	3.99	3.96	3.91	3.82	3.74	3.56	3.26	2.99	2.62	2.03
4	5.27	5.24	5.28	5.39	5.43	5.46	5.29	5.00	4.45	3.37
5	6.71	6.69	6.92	7.52	7.89	8.58	9.02	8.98	8.37	6.46
6	8.31	8.32	8.90	10.39	11.45	13.71	15.95	16.97	16.90	13.73
7	10.08	10.16	11.27	14.27	16.63	22.20	28.94	33.18	35.68	31.04
8	12.04	12.20	14.08	19.50	24.15	36.27	53.38	66.27	77.32	72.67
9	14.18	14.46	17.41	26.54	35.07	59.62	99.50	134.06	170.17	173.45
10	16.51	16.94	21.34	35.99	50.90	98.39	186.69	273.36	378.06	418.78

1 MeV	Angle of Incidence (radians)									
mfp	0.00	0.17	0.45	0.73	0.86	1.05	1.21	1.30	1.40	1.49
1	1.71	1.74	1.72	1.68	1.62	1.54	1.43	1.35	1.25	1.13
2	2.60	2.59	2.52	2.43	2.34	2.21	2.00	1.85	1.66	1.40
3	3.56	3.51	3.44	3.37	3.28	3.17	2.93	2.72	2.43	1.94
4	4.60	4.53	4.49	4.55	4.55	4.61	4.49	4.30	3.95	3.13
5	5.72	5.64	5.69	6.06	6.26	6.83	7.21	7.29	7.09	5.81
6	6.92	6.84	7.06	7.99	8.61	10.28	12.00	13.01	13.69	11.98
7	8.20	8.13	8.63	10.44	11.80	15.66	20.52	24.11	27.73	26.40
8	9.56	9.51	10.39	13.57	16.18	24.10	35.75	45.76	57.86	60.42
9	10.99	10.98	12.39	17.55	22.15	37.35	63.10	88.26	123.00	141.32
10	12.49	12.54	14.63	22.60	30.32	58.19	112.37	171.96	264.46	334.88

Table A.10. Continued.

2 MeV	Angle of Incidence (radians)									
mfp	0.00	0.17	0.45	0.73	0.86	1.05	1.21	1.30	1.40	1.49
1	1.61	1.63	1.63	1.60	1.56	1.50	1.41	1.34	1.25	1.14
2	2.34	2.33	2.28	2.23	2.16	2.07	1.91	1.78	1.62	1.38
3	3.09	3.05	2.99	2.94	2.88	2.81	2.64	2.49	2.28	1.88
4	3.87	3.80	3.74	3.78	3.77	3.84	3.78	3.69	3.51	2.93
5	4.67	4.58	4.56	4.78	4.87	5.29	5.62	5.79	5.91	5.22
6	5.49	5.39	5.44	5.95	6.26	7.36	8.61	9.55	10.71	10.35
7	6.33	6.23	6.39	7.35	8.02	10.34	13.54	16.37	20.41	21.99
8	7.19	7.09	7.41	9.02	10.25	14.67	21.74	28.83	40.24	48.70
9	8.07	7.98	8.51	11.01	13.08	21.00	35.47	51.77	81.13	110.57
10	8.96	8.89	9.69	13.39	16.69	30.26	58.57	94.22	165.92	254.81

4 MeV	Angle of Incidence (radians)									
mfp	0.00	0.17	0.45	0.73	0.86	1.05	1.21	1.30	1.40	1.49
1	1.49	1.51	1.51	1.50	1.47	1.44	1.37	1.31	1.23	1.13
2	2.05	2.04	2.01	1.98	1.93	1.88	1.77	1.67	1.55	1.35
3	2.60	2.56	2.51	2.49	2.44	2.42	2.31	2.21	2.07	1.78
4	3.14	3.08	3.02	3.04	3.02	3.10	3.07	3.04	3.00	2.64
5	3.68	3.60	3.54	3.66	3.69	3.98	4.21	4.39	4.69	4.48
6	4.22	4.13	4.09	4.36	4.48	5.14	5.91	6.61	7.87	8.44
7	4.77	4.66	4.65	5.14	5.41	6.71	8.52	10.36	13.93	17.15
8	5.31	5.19	5.24	6.03	6.52	8.84	12.57	16.75	25.68	36.54
9	5.85	5.73	5.85	7.05	7.85	11.77	18.92	27.73	48.67	80.08
10	6.39	6.28	6.48	8.21	9.47	15.85	29.00	46.80	94.03	178.61

5 MeV	Angle of Incidence (radians)									
mfp	0.00	0.17	0.45	0.73	0.86	1.05	1.21	1.30	1.40	1.49
1	1.45	1.48	1.48	1.47	1.45	1.42	1.36	1.30	1.23	1.13
2	1.97	1.96	1.93	1.91	1.87	1.83	1.73	1.65	1.53	1.34
3	2.46	2.43	2.38	2.37	2.33	2.31	2.22	2.13	2.02	1.75
4	2.95	2.89	2.83	2.86	2.83	2.91	2.89	2.86	2.85	2.56
5	3.43	3.35	3.29	3.39	3.41	3.66	3.85	4.02	4.35	4.26
6	3.91	3.82	3.76	3.99	4.07	4.63	5.27	5.88	7.10	7.88
7	4.39	4.28	4.25	4.65	4.84	5.92	7.40	8.95	12.25	15.75
8	4.87	4.75	4.75	5.40	5.75	7.65	10.66	14.06	22.06	33.06
9	5.34	5.22	5.27	6.24	6.83	10.00	15.69	22.70	40.95	71.53
10	5.81	5.69	5.80	7.20	8.12	13.24	23.57	37.45	77.69	157.66

6 MeV	Angle of Incidence (radians)									
mfp	0.00	0.17	0.45	0.73	0.86	1.05	1.21	1.30	1.40	1.49
1	1.43	1.45	1.46	1.45	1.42	1.40	1.35	1.30	1.23	1.13
2	1.90	1.89	1.87	1.85	1.82	1.79	1.69	1.62	1.51	1.33
3	2.35	2.32	2.27	2.26	2.23	2.22	2.14	2.06	1.96	1.72
4	2.79	2.74	2.68	2.70	2.68	2.75	2.73	2.71	2.72	2.48
5	3.23	3.15	3.09	3.18	3.18	3.41	3.58	3.73	4.06	4.05
6	3.66	3.57	3.51	3.70	3.76	4.26	4.80	5.33	6.49	7.39
7	4.09	3.99	3.94	4.29	4.43	5.36	6.61	7.93	10.98	14.56
8	4.52	4.41	4.38	4.93	5.20	6.83	9.35	12.20	19.41	30.20
9	4.94	4.82	4.83	5.66	6.12	8.82	13.54	19.33	35.46	64.67
10	5.36	5.24	5.30	6.49	7.21	11.54	20.05	31.36	66.39	141.25

Table A.10. Continued.

8 MeV	Angle of Incidence (radians)									
mfp	0.00	0.17	0.45	0.73	0.86	1.05	1.21	1.30	1.40	1.49
1	1.38	1.41	1.42	1.41	1.39	1.37	1.33	1.28	1.22	1.13
2	1.80	1.79	1.77	1.76	1.73	1.71	1.63	1.57	1.48	1.32
3	2.19	2.16	2.12	2.11	2.08	2.08	2.01	1.95	1.87	1.66
4	2.57	2.51	2.46	2.48	2.46	2.52	2.51	2.49	2.52	2.34
5	2.94	2.87	2.81	2.88	2.87	3.06	3.19	3.32	3.64	3.73
6	3.31	3.22	3.16	3.32	3.34	3.75	4.17	4.59	5.63	6.62
7	3.67	3.58	3.52	3.79	3.88	4.63	5.60	6.61	9.24	12.76
8	4.04	3.93	3.88	4.32	4.50	5.80	7.72	9.88	15.92	25.99
9	4.39	4.28	4.26	4.92	5.23	7.36	10.95	15.25	28.44	54.80
10	4.75	4.64	4.64	5.59	6.08	9.50	15.94	24.21	52.30	118.11

10 MeV	Angle of Incidence (radians)									
mfp	0.00	0.17	0.45	0.73	0.86	1.05	1.21	1.30	1.40	1.49
1	1.36	1.38	1.39	1.38	1.36	1.35	1.31	1.27	1.21	1.13
2	1.73	1.72	1.71	1.70	1.67	1.66	1.59	1.53	1.45	1.30
3	2.08	2.05	2.01	2.01	1.98	1.99	1.92	1.87	1.80	1.62
4	2.41	2.36	2.31	2.34	2.31	2.37	2.35	2.34	2.38	2.24
5	2.74	2.68	2.62	2.68	2.67	2.84	2.94	3.05	3.36	3.48
6	3.07	2.99	2.93	3.06	3.07	3.43	3.77	4.12	5.07	6.06
7	3.39	3.30	3.24	3.48	3.53	4.18	4.98	5.81	8.14	11.49
8	3.71	3.61	3.56	3.94	4.07	5.18	6.76	8.52	13.76	23.09
9	4.03	3.93	3.89	4.45	4.69	6.50	9.46	12.93	24.23	48.16
10	4.35	4.24	4.23	5.03	5.42	8.32	13.62	20.24	44.06	102.87

APPENDIX B ENDF AND CEPXS PHOTON CROSS SECTIONS

Further differences between photon cross sections from ENDF and the CEPXS cross section codes are presented for iron, aluminum, and oxygen. No significant differences were observed for hydrogen. The cross sections for lead are shown in Figure 5.1 and Figure 5.2.

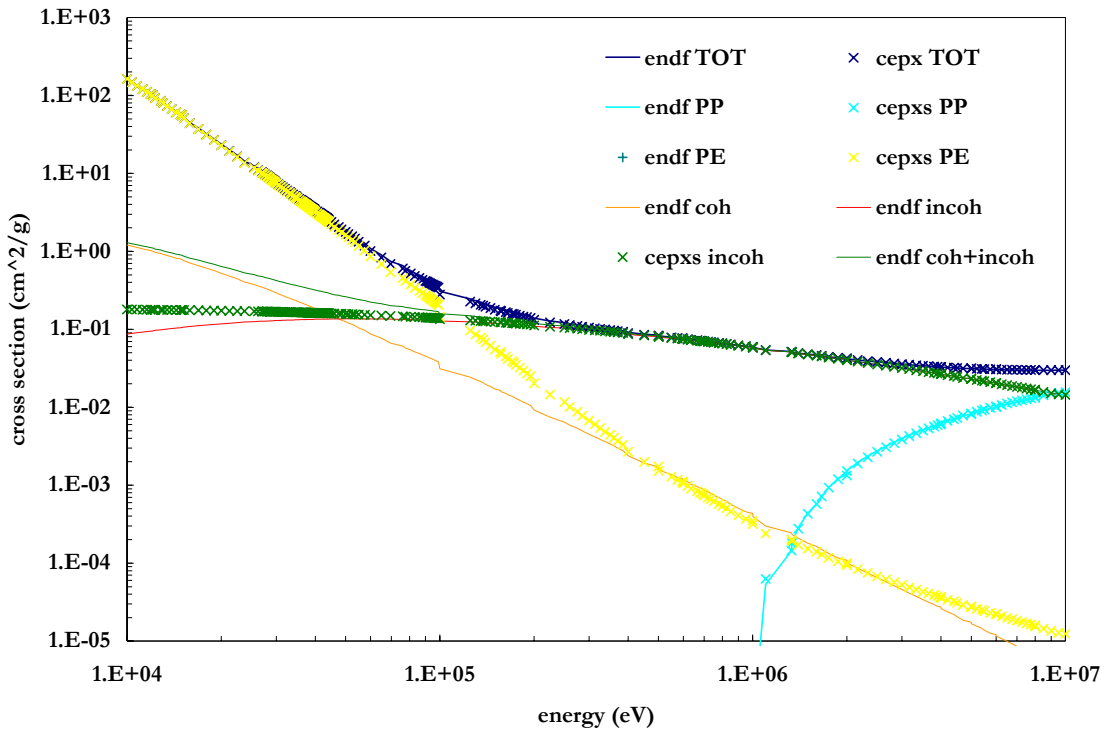

Figure B.1. CEPXS (crosses) and ENDF/B-VI.8 (curves) photon cross sections for iron as a function of energy.

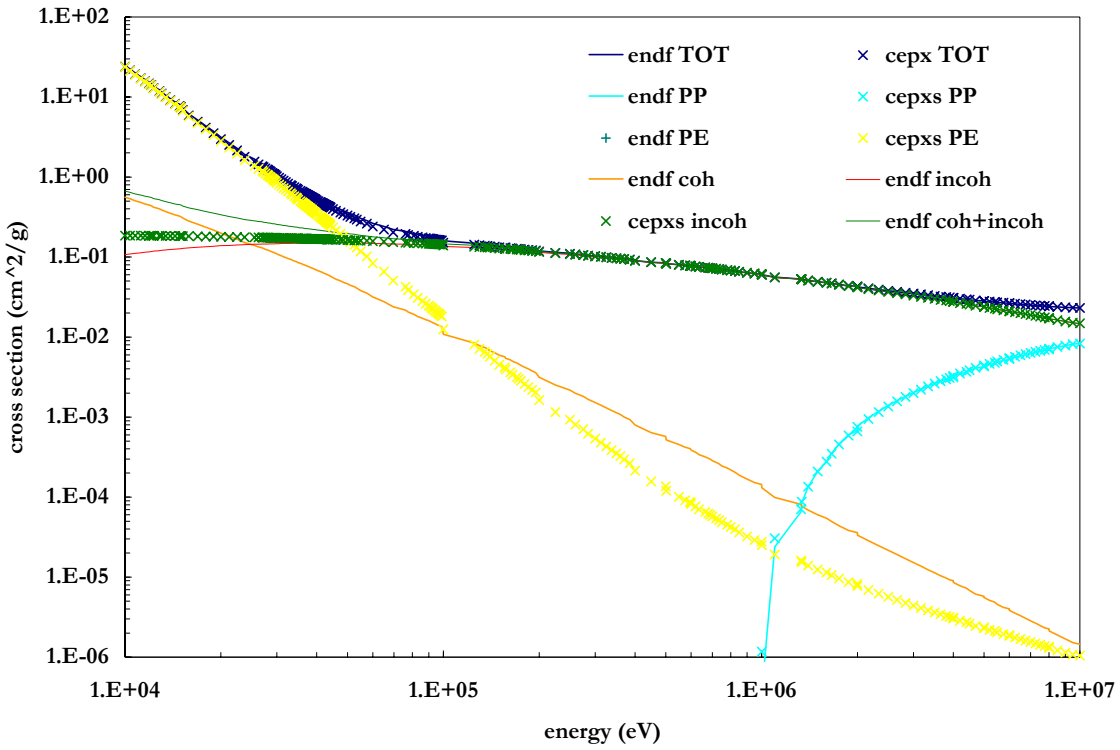

Figure B.2. CEPXS (crosses) and ENDF/B-VI.8 (curves) photon cross sections for aluminum as a function of energy.

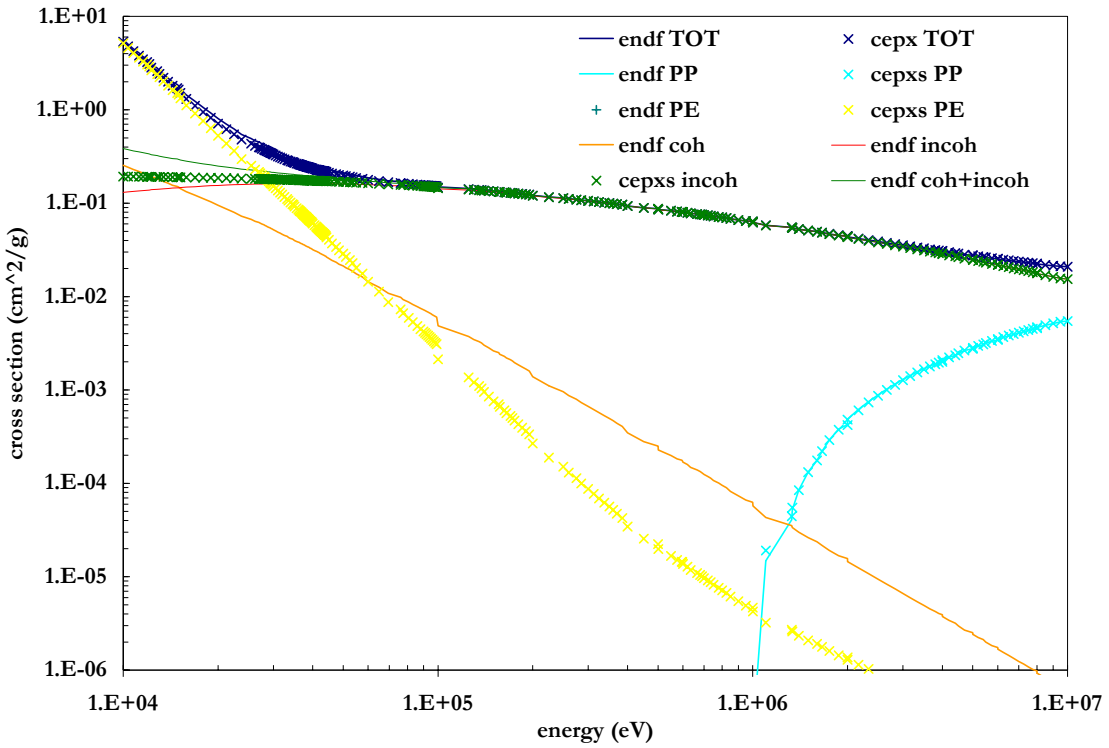

Figure B.3. CEPXS (crosses) and ENDF/B-VI.8 (curves) photon cross sections for oxygen as a function of energy.

APPENDIX C SAMPLE INPUT FILES FOR CODES

The Appendix includes sample input files for each of the major codes used in this research. For PARTISN and MCNPX, the input files describe 500 keV photons normally incident on a 1-mfp thick slab. The NJOY input file details the compilation of the 220 group photon cross sections for lead, and the CEPXS input file creates the coupled electron-photon cross sections in 440 groups. The Pandemonium input file, describes the test problem in Chapter 7 with five detectors. To create input files with different parameters, such as energy, incident angle, or material, one should refer to the original manuals of the codes of interest.

C.1 PARTISN sample input file

```
    6     0      0
E       =   500 keV
mat     =   lead
mu      =   1
mfp     =   1/100
Sn      =   s100
P       =   p7
/**************  BLOCK 1  **************
igeom=1 ngroup=440 isn=  50 niso= 1 mt= 1 nzone=  1
im=1 it= 100 idimen=1 maxlcm=3000000 maxscm=  4000000
iquad= 3 nn=1
t
/**************  BLOCK 2  **************
xmesh=0.0 0.55326
xints=  100
zones=1
t
/**************  BLOCK 3  **************
lib=bxslib maxord= 7 ihm=885 iht= 6 ihs= 446 ifido=0 ititl=1 i2lp1=0
edname=char secp ener
ebound=
 10.001000 10.000000  9.500000  9.000000  8.500000  8.001000  8.000000
  7.750000  7.500000  7.250000  7.000000  6.750000  6.500000  6.250000
  6.001000  6.000000  5.750000  5.500000  5.400000  5.200000  5.001000
  5.000000  4.700000  4.500000  4.400000  4.200000  4.001000  4.000000
  3.900000  3.800000  3.650000  3.500000  3.333000  3.166000  3.000000
  2.833000  2.666000  2.500000  2.333000  2.166000  2.001000  2.000000
  1.875000  1.750000  1.660000  1.600000  1.500000  1.400000  1.335000
  1.330000  1.100000  1.001000  1.000000  0.950000  0.900000  0.850000
  0.825000  0.800000  0.780000  0.750000  0.735000  0.720000  0.700000
  0.690000  0.680000  0.665000  0.635000  0.620000  0.600000  0.597500
  0.595000  0.575000  0.550000  0.501000  0.500000  0.450000  0.400000
  0.385000  0.370000  0.360000  0.350000  0.337500  0.325000  0.312500
  0.300000  0.285000  0.275000  0.260000  0.250000  0.225000  0.200000
  0.195000  0.190000  0.185000  0.180000  0.175000  0.172500  0.170000
  0.165000  0.162500  0.157000  0.156000  0.150000  0.145000  0.140000
  0.137500  0.135000  0.130000  0.125000  0.100000  0.099000  0.098000
  0.097000  0.096000  0.095000  0.094000  0.093000  0.092000  0.091000
  0.090000  0.088000  0.086000  0.083102  0.080725  0.077500  0.076111
  0.069525  0.065000  0.060000  0.057500  0.055000  0.053500  0.052500
  0.051000  0.050000  0.048500  0.047500  0.046000  0.045000  0.044250
  0.044000  0.043700  0.043500  0.043250  0.043000  0.042750  0.042500
  0.042250  0.042000  0.041750  0.041500  0.041250  0.041000  0.040500
  0.040000  0.039750  0.039500  0.039250  0.039000  0.038750  0.038500
  0.038250  0.038000  0.037750  0.037500  0.037250  0.037000  0.036750
  0.036500  0.036250  0.035985  0.035550  0.035000  0.034750  0.034500
  0.034000  0.033500  0.033169  0.032500  0.032000  0.031500  0.031000
  0.030500  0.030000  0.029750  0.029500  0.029250  0.029000  0.028700
  0.028500  0.028200  0.028000  0.027600  0.027250  0.027000  0.026250
  0.025514  0.023750  0.022500  0.021250  0.020000  0.018970  0.017930
  0.016900  0.015860  0.015200  0.015000  0.014839  0.014353  0.013880
  0.013418  0.013040  0.012824  0.012284  0.012100  0.011910  0.011564
  0.011215  0.010760  0.010367  0.010000 10.000000  9.500000  9.000000
  8.500000  8.001000  8.000000  7.750000  7.500000  7.250000  7.000000
  6.750000  6.500000  6.250000  6.001000  6.000000  5.750000  5.500000
  5.400000  5.200000  5.001000  5.000000  4.700000  4.500000  4.400000
  4.200000  4.001000  4.000000  3.900000  3.800000  3.650000  3.500000
  3.333000  3.166000  3.000000  2.833000  2.666000  2.500000  2.333000
  2.166000  2.001000  2.000000  1.875000  1.750000  1.660000  1.600000
  1.500000  1.400000  1.335000  1.330000  1.100000  1.001000  1.000000
  0.950000  0.900000  0.850000  0.825000  0.800000  0.780000  0.750000
  0.735000  0.720000  0.700000  0.690000  0.680000  0.665000  0.635000
  0.620000  0.600000  0.597500  0.595000  0.575000  0.550000  0.501000
  0.500000  0.450000  0.400000  0.385000  0.370000  0.360000  0.350000
  0.337500  0.325000  0.312500  0.300000  0.285000  0.275000  0.260000
  0.250000  0.225000  0.200000  0.195000  0.190000  0.185000  0.180000
  0.175000  0.172500  0.170000  0.165000  0.162500  0.157000  0.156000
  0.150000  0.145000  0.140000  0.137500  0.135000  0.130000  0.125000
  0.100000  0.099000  0.098000  0.097000  0.096000  0.095000  0.094000
  0.093000  0.092000  0.091000  0.090000  0.088000  0.086000  0.083102
  0.080725  0.077500  0.076111  0.069525  0.065000  0.060000  0.057500
  0.055000  0.053500  0.052500  0.051000  0.050000  0.048500  0.047500
  0.046000  0.045000  0.044250  0.044000  0.043700  0.043500  0.043250
  0.043000  0.042750  0.042500  0.042250  0.042000  0.041750  0.041500
  0.041250  0.041000  0.040500  0.040000  0.039750  0.039500  0.039250
  0.039000  0.038750  0.038500  0.038250  0.038000  0.037750  0.037500
  0.037250  0.037000  0.036750  0.036500  0.036250  0.035985  0.035550
  0.035000  0.034750  0.034500  0.034000  0.033500  0.033169  0.032500
  0.032000  0.031500  0.031000  0.030500  0.030000  0.029750  0.029500
  0.029250  0.029000  0.028700  0.028500  0.028200  0.028000  0.027600
  0.027250  0.027000  0.026250  0.025514  0.023750  0.022500  0.021250
  0.020000  0.018970  0.017930  0.016900  0.015860  0.015200  0.015000
  0.014839  0.014353  0.013880  0.013418  0.013040  0.012824  0.012284
  0.012100  0.011910  0.011564  0.011215  0.010760  0.010367  0.010000
t
/**************  BLOCK 4  **************
matls=isos assign=
 1  1 1.0;
t
/**************  BLOCK 5  **************
 mu=1.00000000000  0.99925857797  0.99751524904
    0.99477730719  0.99104769371  0.98633016382
    0.98062943072  0.97395118101  0.96630207344
    0.95768973368  0.94812274716  0.93761065074
    0.92616392325  0.91379397517  0.90051313718
    0.88633464797  0.87127264099  0.85534213042
    0.83855899613  0.82093996795  0.80250260891
    0.78326529779  0.76324721074  0.74246830226
    0.72094928520  0.69871161020  0.67577744426
    0.65216964865  0.62791175614  0.60302794752
    0.57754302752  0.55148240007  0.52487204296
    0.49773848198  0.47010876445  0.44201043227
    0.41347149448  0.38452039931  0.35518600584
    0.32549755523  0.29548464157  0.26517718240
    0.23460538884  0.20379973553  0.17279093021
    0.14160988313  0.11028767624  0.07885553219
    0.04734478323  0.01578683997 ;
 wgt=0.00010101010  0.00062253833  0.00112053988
     0.00161716296  0.00211213817  0.00260499904
     0.00309526016  0.00358243461  0.00406603742
     0.00454558681  0.00502060489  0.00549061821
     0.00595515830  0.00641376212  0.00686597253
     0.00731133877  0.00774941690  0.00817977022
     0.00860196977  0.00901559468  0.00942023264
```

```
     0.00981548031  0.01020094369  0.01057623855
     0.01094099078  0.01129483679  0.01163742386
     0.01196841049  0.01228746675  0.01259427460
     0.01288852819  0.01316993423  0.01343821218
     0.01369309463  0.01393432751  0.01416167035
     0.01437489652  0.01457379349  0.01475816298
     0.01492782121  0.01508259907  0.01522234226
     0.01534691149  0.01545618259  0.01555004662
     0.01562841004  0.01569119471  0.01573833806
     0.01576979309  0.01578552845;
 /
ievt= 0 isct= 7 ith=0 ibl=0 ibr=0 epsi=1.e-4 iitl=100 nll=50
saleft=
50r0; 72y1;
1,49r0;
50r0; 365y1;
norm=1 sourcp=3 xsectp=1
t
/**************  BLOCK 6  **************
pted=1 icoll= 220,220
rsfnam= flux, airExp, Dose
/ normalized flux
rsfe=440r1.0;
/ air exposure
  1.4496E-01  1.4219E-01  1.3651E-01  1.3076E-01
  1.2495E-01  1.2201E-01  1.2060E-01  1.1778E-01
  1.1494E-01  1.1208E-01  1.0918E-01  1.0626E-01
  1.0331E-01  1.0033E-01  9.8826E-02  9.7377E-02
  9.4463E-02  9.2399E-02  9.0615E-02  8.8218E-02
  8.7006E-02  8.5224E-02  8.2224E-02  8.0399E-02
  7.8554E-02  7.6068E-02  7.4806E-02  7.3865E-02
  7.1995E-02  6.9657E-02  6.6853E-02  6.3889E-02
  6.0766E-02  5.7652E-02  5.5405E-02  5.3980E-02
  5.2511E-02  5.0988E-02  4.9400E-02  4.7755E-02
  4.6905E-02  4.5851E-02  4.3722E-02  4.1858E-02
  4.0537E-02  3.9108E-02  3.7213E-02  3.5559E-02
  3.4851E-02  3.2441E-02  2.8977E-02  2.7901E-02
  2.7294E-02  2.6096E-02  2.4888E-02  2.3975E-02
  2.3363E-02  2.2792E-02  2.2131E-02  2.1534E-02
  2.1136E-02  2.0670E-02  2.0270E-02  2.0003E-02
  1.9668E-02  1.9065E-02  1.8460E-02  1.7988E-02
  1.7682E-02  1.7610E-02  1.7286E-02  1.6637E-02
  1.5568E-02  1.4845E-02  1.4070E-02  1.2553E-02
  1.1555E-02  1.1073E-02  1.0674E-02  1.0355E-02
  9.9969E-03  9.6006E-03  9.2057E-03  8.8122E-03
  8.3628E-03  7.9434E-03  7.5274E-03  7.1148E-03
  6.5432E-03  5.7396E-03  5.2615E-03  5.0972E-03
  4.9340E-03  4.7718E-03  4.6106E-03  4.4904E-03
  4.4107E-03  4.2915E-03  4.1730E-03  4.0473E-03
  3.9457E-03  3.8368E-03  3.6708E-03  3.5250E-03
  3.4163E-03  3.3440E-03  3.2362E-03  3.0931E-03
  2.6701E-03  2.3152E-03  2.2955E-03  2.2758E-03
  2.2561E-03  2.2363E-03  2.2165E-03  2.1967E-03
  2.1768E-03  2.1569E-03  2.1370E-03  2.1071E-03
  2.0670E-03  2.0177E-03  1.9644E-03  1.9216E-03
  1.9110E-03  1.8920E-03  1.8641E-03  1.8386E-03
  1.8492E-03  1.9011E-03  1.9454E-03  1.9744E-03
  2.0046E-03  2.0361E-03  2.0894E-03  2.1599E-03
  2.2348E-03  2.3143E-03  2.3731E-03  2.4079E-03
  2.4274E-03  2.4454E-03  2.4618E-03  2.4802E-03
  2.4989E-03  2.5178E-03  2.5370E-03  2.5565E-03
  2.5762E-03  2.5962E-03  2.6165E-03  2.6371E-03
  2.6684E-03  2.7113E-03  2.7488E-03  2.7804E-03
  2.8126E-03  2.8453E-03  2.8787E-03  2.9126E-03
  2.9472E-03  2.9825E-03  3.0183E-03  3.0549E-03
  3.0921E-03  3.1301E-03  3.1688E-03  3.2082E-03
  3.2484E-03  3.2907E-03  3.3494E-03  3.4349E-03
  3.5069E-03  3.5530E-03  3.6241E-03  3.7222E-03
  3.8070E-03  3.9130E-03  4.0430E-03  4.1594E-03
  4.2812E-03  4.4086E-03  4.5419E-03  4.6515E-03
  4.7341E-03  4.8188E-03  4.9058E-03  5.0043E-03
  5.0963E-03  5.1909E-03  5.2881E-03  5.4083E-03
  5.5643E-03  5.6939E-03  5.9201E-03  6.2816E-03
  6.9677E-03  7.9525E-03  8.9339E-03  1.0105E-02
  1.1400E-02  1.2820E-02  1.4515E-02  1.6559E-02
  1.8570E-02  1.9726E-02  2.0240E-02  2.1207E-02
  2.2770E-02  2.4460E-02  2.6142E-02  2.7437E-02
  2.9225E-02  3.1103E-02  3.2143E-02  3.3725E-02
  3.5951E-02  3.8807E-02  4.2198E-02  4.5619E-02
/ repeat 220 groups for electrons/positrons
  1.4496E-01  1.4219E-01  1.3651E-01  1.3076E-01
  1.2495E-01  1.2201E-01  1.2060E-01  1.1778E-01
  1.1494E-01  1.1208E-01  1.0918E-01  1.0626E-01
  1.0331E-01  1.0033E-01  9.8826E-02  9.7377E-02
  9.4463E-02  9.2399E-02  9.0615E-02  8.8218E-02
  8.7006E-02  8.5224E-02  8.2224E-02  8.0399E-02
  7.8554E-02  7.6068E-02  7.4806E-02  7.3865E-02
  7.1995E-02  6.9657E-02  6.6853E-02  6.3889E-02
  6.0766E-02  5.7652E-02  5.5405E-02  5.3980E-02
  5.2511E-02  5.0988E-02  4.9400E-02  4.7755E-02
  4.6905E-02  4.5851E-02  4.3722E-02  4.1858E-02
  4.0537E-02  3.9108E-02  3.7213E-02  3.5559E-02
  3.4851E-02  3.2441E-02  2.8977E-02  2.7901E-02
  2.7294E-02  2.6096E-02  2.4888E-02  2.3975E-02
  2.3363E-02  2.2792E-02  2.2131E-02  2.1534E-02
  2.1136E-02  2.0670E-02  2.0270E-02  2.0003E-02
  1.9668E-02  1.9065E-02  1.8460E-02  1.7988E-02
  1.7682E-02  1.7610E-02  1.7286E-02  1.6637E-02
  1.5568E-02  1.4845E-02  1.4070E-02  1.2553E-02
  1.1555E-02  1.1073E-02  1.0674E-02  1.0355E-02
  9.9969E-03  9.6006E-03  9.2057E-03  8.8122E-03
  8.3628E-03  7.9434E-03  7.5274E-03  7.1148E-03
  6.5432E-03  5.7396E-03  5.2615E-03  5.0972E-03
  4.9340E-03  4.7718E-03  4.6106E-03  4.4904E-03
  4.4107E-03  4.2915E-03  4.1730E-03  4.0473E-03
  3.9457E-03  3.8368E-03  3.6708E-03  3.5250E-03
  3.4163E-03  3.3440E-03  3.2362E-03  3.0931E-03
  2.6701E-03  2.3152E-03  2.2955E-03  2.2758E-03
  2.2561E-03  2.2363E-03  2.2165E-03  2.1967E-03
  2.1768E-03  2.1569E-03  2.1370E-03  2.1071E-03
  2.0670E-03  2.0177E-03  1.9644E-03  1.9216E-03
  1.9110E-03  1.8920E-03  1.8641E-03  1.8386E-03
  1.8492E-03  1.9011E-03  1.9454E-03  1.9744E-03
  2.0046E-03  2.0361E-03  2.0894E-03  2.1599E-03
  2.2348E-03  2.3143E-03  2.3731E-03  2.4079E-03
  2.4274E-03  2.4454E-03  2.4618E-03  2.4802E-03
  2.4989E-03  2.5178E-03  2.5370E-03  2.5565E-03
  2.5762E-03  2.5962E-03  2.6165E-03  2.6371E-03
  2.6684E-03  2.7113E-03  2.7488E-03  2.7804E-03
  2.8126E-03  2.8453E-03  2.8787E-03  2.9126E-03
  2.9472E-03  2.9825E-03  3.0183E-03  3.0549E-03
  3.0921E-03  3.1301E-03  3.1688E-03  3.2082E-03
  3.2484E-03  3.2907E-03  3.3494E-03  3.4349E-03
  3.5069E-03  3.5530E-03  3.6241E-03  3.7222E-03
  3.8070E-03  3.9130E-03  4.0430E-03  4.1594E-03
  4.2812E-03  4.4086E-03  4.5419E-03  4.6515E-03
```

```
  4.7341E-03  4.8188E-03  4.9058E-03  5.0043E-03
  5.0963E-03  5.1909E-03  5.2881E-03  5.4083E-03
  5.5643E-03  5.6939E-03  5.9201E-03  6.2816E-03
  6.9677E-03  7.9525E-03  8.9339E-03  1.0105E-02
  1.1400E-02  1.2820E-02  1.4515E-02  1.6559E-02
  1.8570E-02  1.9726E-02  2.0240E-02  2.1207E-02
  2.2770E-02  2.4460E-02  2.6142E-02  2.7437E-02
  2.9225E-02  3.1103E-02  3.2143E-02  3.3725E-02
  3.5951E-02  3.8807E-02  4.2198E-02  4.5619E-02;
/ H*(10) flux response
  2.5605E+01  2.5111E+01  2.4125E+01  2.3125E+01
  2.2113E+01  2.1601E+01  2.1359E+01  2.0874E+01
  2.0385E+01  1.9890E+01  1.9391E+01  1.8886E+01
  1.8376E+01  1.7861E+01  1.7601E+01  1.7344E+01
  1.6826E+01  1.6459E+01  1.6142E+01  1.5717E+01
  1.5501E+01  1.5195E+01  1.4679E+01  1.4365E+01
  1.4047E+01  1.3619E+01  1.3401E+01  1.3290E+01
  1.3069E+01  1.2790E+01  1.2450E+01  1.2086E+01
  1.1696E+01  1.1300E+01  1.0905E+01  1.0507E+01
  1.0102E+01  9.6873E+00  9.2604E+00  8.8243E+00
  8.6013E+00  8.3935E+00  7.9757E+00  7.6110E+00
  7.3533E+00  7.0754E+00  6.7387E+00  6.4689E+00
  6.3529E+00  5.9567E+00  5.3818E+00  5.2018E+00
  5.0997E+00  4.8974E+00  4.6925E+00  4.5371E+00
  4.4325E+00  4.3340E+00  4.2185E+00  4.1141E+00
  4.0442E+00  3.9623E+00  3.8919E+00  3.8448E+00
  3.7858E+00  3.6792E+00  3.5719E+00  3.4881E+00
  3.4337E+00  3.4211E+00  3.3642E+00  3.2500E+00
  3.0611E+00  2.9326E+00  2.7933E+00  2.5183E+00
  2.3367E+00  2.2499E+00  2.1775E+00  2.1196E+00
  2.0543E+00  1.9818E+00  1.9091E+00  1.8364E+00
  1.7550E+00  1.6800E+00  1.6050E+00  1.5300E+00
  1.4250E+00  1.2750E+00  1.1844E+00  1.1533E+00
  1.1222E+00  1.0911E+00  1.0601E+00  1.0368E+00
  1.0213E+00  9.9810E-01  9.7490E-01  9.5017E-01
  9.3010E-01  9.0850E-01  8.7617E-01  8.4847E-01
  8.2765E-01  8.1375E-01  7.9286E-01  7.6495E-01
  6.8075E-01  6.0808E-01  6.0422E-01  6.0035E-01
  5.9646E-01  5.9256E-01  5.8864E-01  5.8471E-01
  5.8076E-01  5.7680E-01  5.7282E-01  5.6682E-01
  5.5876E-01  5.4880E-01  5.3795E-01  5.2921E-01
  5.2712E-01  5.2338E-01  5.1785E-01  5.1279E-01
  5.1447E-01  5.2381E-01  5.3173E-01  5.3689E-01
  5.4222E-01  5.4774E-01  5.5568E-01  5.6546E-01
  5.7569E-01  5.8638E-01  5.9417E-01  5.9873E-01
  6.0128E-01  6.0362E-01  6.0574E-01  6.0812E-01
  6.1053E-01  6.1296E-01  6.1541E-01  6.1789E-01
  6.2040E-01  6.2292E-01  6.2548E-01  6.2806E-01
  6.3198E-01  6.3730E-01  6.4164E-01  6.4495E-01
  6.4831E-01  6.5170E-01  6.5513E-01  6.5860E-01
  6.6211E-01  6.6566E-01  6.6926E-01  6.7290E-01
  6.7658E-01  6.8031E-01  6.8408E-01  6.8790E-01
  6.9177E-01  6.9581E-01  7.0138E-01  7.0939E-01
  7.1604E-01  7.2027E-01  7.2672E-01  7.3553E-01
  7.4302E-01  7.5227E-01  7.6342E-01  7.7326E-01
  7.8337E-01  7.9379E-01  8.0451E-01  8.1217E-01
  8.1655E-01  8.2099E-01  8.2549E-01  8.3052E-01
  8.3516E-01  8.3987E-01  8.4464E-01  8.5046E-01
  8.5789E-01  8.6395E-01  8.7430E-01  8.9028E-01
  9.1894E-01  9.5683E-01  9.9147E-01  1.0295E+00
  1.0279E+00  9.8301E-01  9.3770E-01  8.9190E-01
  8.5389E-01  8.3452E-01  8.0181E-01  6.9623E-01
  5.6146E-01  4.5207E-01  3.6969E-01  3.1938E-01
  2.6383E-01  2.1852E-01  1.9782E-01  1.7106E-01
  1.4098E-01  1.1187E-01  8.6824E-02  6.8581E-02
/ repeat 220 groups for electrons/positrons
  2.5605E+01  2.5111E+01  2.4125E+01  2.3125E+01
  2.2113E+01  2.1601E+01  2.1359E+01  2.0874E+01
  2.0385E+01  1.9890E+01  1.9391E+01  1.8886E+01
  1.8376E+01  1.7861E+01  1.7601E+01  1.7344E+01
  1.6826E+01  1.6459E+01  1.6142E+01  1.5717E+01
  1.5501E+01  1.5195E+01  1.4679E+01  1.4365E+01
  1.4047E+01  1.3619E+01  1.3401E+01  1.3290E+01
  1.3069E+01  1.2790E+01  1.2450E+01  1.2086E+01
  1.1696E+01  1.1300E+01  1.0905E+01  1.0507E+01
  1.0102E+01  9.6873E+00  9.2604E+00  8.8243E+00
  8.6013E+00  8.3935E+00  7.9757E+00  7.6110E+00
  7.3533E+00  7.0754E+00  6.7387E+00  6.4689E+00
  6.3529E+00  5.9567E+00  5.3818E+00  5.2018E+00
  5.0997E+00  4.8974E+00  4.6925E+00  4.5371E+00
  4.4325E+00  4.3340E+00  4.2185E+00  4.1141E+00
  4.0442E+00  3.9623E+00  3.8919E+00  3.8448E+00
  3.7858E+00  3.6792E+00  3.5719E+00  3.4881E+00
  3.4337E+00  3.4211E+00  3.3642E+00  3.2500E+00
  3.0611E+00  2.9326E+00  2.7933E+00  2.5183E+00
  2.3367E+00  2.2499E+00  2.1775E+00  2.1196E+00
  2.0543E+00  1.9818E+00  1.9091E+00  1.8364E+00
  1.7550E+00  1.6800E+00  1.6050E+00  1.5300E+00
  1.4250E+00  1.2750E+00  1.1844E+00  1.1533E+00
  1.1222E+00  1.0911E+00  1.0601E+00  1.0368E+00
  1.0213E+00  9.9810E-01  9.7490E-01  9.5017E-01
  9.3010E-01  9.0850E-01  8.7617E-01  8.4847E-01
  8.2765E-01  8.1375E-01  7.9286E-01  7.6495E-01
  6.8075E-01  6.0808E-01  6.0422E-01  6.0035E-01
  5.9646E-01  5.9256E-01  5.8864E-01  5.8471E-01
  5.8076E-01  5.7680E-01  5.7282E-01  5.6682E-01
  5.5876E-01  5.4880E-01  5.3795E-01  5.2921E-01
  5.2712E-01  5.2338E-01  5.1785E-01  5.1279E-01
  5.1447E-01  5.2381E-01  5.3173E-01  5.3689E-01
  5.4222E-01  5.4774E-01  5.5568E-01  5.6546E-01
  5.7569E-01  5.8638E-01  5.9417E-01  5.9873E-01
  6.0128E-01  6.0362E-01  6.0574E-01  6.0812E-01
  6.1053E-01  6.1296E-01  6.1541E-01  6.1789E-01
  6.2040E-01  6.2292E-01  6.2548E-01  6.2806E-01
  6.3198E-01  6.3730E-01  6.4164E-01  6.4495E-01
  6.4831E-01  6.5170E-01  6.5513E-01  6.5860E-01
  6.6211E-01  6.6566E-01  6.6926E-01  6.7290E-01
  6.7658E-01  6.8031E-01  6.8408E-01  6.8790E-01
  6.9177E-01  6.9581E-01  7.0138E-01  7.0939E-01
  7.1604E-01  7.2027E-01  7.2672E-01  7.3553E-01
  7.4302E-01  7.5227E-01  7.6342E-01  7.7326E-01
  7.8337E-01  7.9379E-01  8.0451E-01  8.1217E-01
  8.1655E-01  8.2099E-01  8.2549E-01  8.3052E-01
  8.3516E-01  8.3987E-01  8.4464E-01  8.5046E-01
  8.5789E-01  8.6395E-01  8.7430E-01  8.9028E-01
  9.1894E-01  9.5683E-01  9.9147E-01  1.0295E+00
  1.0279E+00  9.8301E-01  9.3770E-01  8.9190E-01
  8.5389E-01  8.3452E-01  8.0181E-01  6.9623E-01
  5.6146E-01  4.5207E-01  3.6969E-01  3.1938E-01
  2.6383E-01  2.1852E-01  1.9782E-01  1.7106E-01
  1.4098E-01  1.1187E-01  8.6824E-02  6.8581E-02;
/
points=1,100
t
```

C.2 MCNPX input file

```
0.501 MeV 1 mfp slab of material 1 at normal
c
c
c  1mfp lead slab, normal photon beam at 0.5 MeV
c  flux tally  for comparison with SN method
c  energy bin structure mirrors 220 groups of the SN calculation
c  mcplib04 is used, consistent with the xsects used for SN
c
c  CELL
 1  1 -11.35          -1  2 -3  4 -5  6    imp:p=1 $ in slab
 2  0          #1                   imp:p=0 $ outside slab

c  SURFACE
*1  px  1.0   $ x max -refl
*2  px -1.0   $ x min -refl
*3  py  1.0   $ y max -refl
*4  py -1.0   $ y min -refl
 5  pz  0.54962  $ z max - 1 mfp @ normal
 6  pz  0.0   $ z min

c  DATA
nps 20000000
cut:p 1 .01   $ time cutoff = 1shake, low E cutoff at 10keV
print
mode p
m1  82000 -1.0  plib=04p
ext:p s 0  $ exponential transform in slab pg. 3-37 MCNP4C manual
c
c  SOURCE
sdef  x=d1 y=d2 z=0.0   vec=0 0 1.0
     dir=1   erg=0.501
si1 -1.0   1.0
sp1   0     1
si2 -1.0   1.0
sp2   0     1
c
c  TALLIES
e0 1.03671e-002 1.07600e-002 1.12154e-002 1.15637e-002  &
   1.19100e-002 1.20998e-002 1.22839e-002 1.28241e-002  &
   1.30400e-002 1.34185e-002 1.38799e-002 1.43528e-002  &
   1.48393e-002 1.50000e-002 1.52000e-002 1.58600e-002  &
   1.69000e-002 1.79300e-002 1.89700e-002 2.00000e-002  &
   2.12500e-002 2.25000e-002 2.37500e-002 2.55140e-002  &
   2.62500e-002 2.70000e-002 2.72500e-002 2.76000e-002  &
   2.80000e-002 2.82000e-002 2.85000e-002 2.87000e-002  &
   2.90000e-002 2.92500e-002 2.95000e-002 2.97500e-002  &
   3.00000e-002 3.05000e-002 3.10000e-002 3.15000e-002  &
   3.20000e-002 3.25000e-002 3.31694e-002 3.35000e-002  &
   3.40000e-002 3.45000e-002 3.47500e-002 3.50000e-002  &
   3.55500e-002 3.59846e-002 3.62500e-002 3.65000e-002  &
   3.67500e-002 3.70000e-002 3.72500e-002 3.75000e-002  &
   3.77500e-002 3.80000e-002 3.82500e-002 3.85000e-002  &
   3.87500e-002 3.90000e-002 3.92500e-002 3.95000e-002  &
   3.97500e-002 4.00000e-002 4.05000e-002 4.10000e-002  &
   4.12500e-002 4.15000e-002 4.17500e-002 4.20000e-002  &
   4.22500e-002 4.25000e-002 4.27500e-002 4.30000e-002  &
   4.32500e-002 4.35000e-002 4.37000e-002 4.40000e-002  &
   4.42500e-002 4.50000e-002 4.60000e-002 4.75000e-002  &
   4.85000e-002 5.00000e-002 5.10000e-002 5.25000e-002  &
   5.35000e-002 5.50000e-002 5.75000e-002 6.00000e-002  &



6.50000e-002 6.95250e-002 7.61110e-002 7.75000e-002  &
   8.07249e-002 8.31023e-002 8.60000e-002 8.80000e-002  &
   9.00000e-002 9.10000e-002 9.20000e-002 9.30000e-002  &
   9.40000e-002 9.50000e-002 9.60000e-002 9.70000e-002  &
   9.80000e-002 9.90000e-002 1.00000e-001 1.25000e-001  &
   1.30000e-001 1.35000e-001 1.37500e-001 1.40000e-001  &
   1.45000e-001 1.50000e-001 1.56000e-001 1.57000e-001  &
   1.62500e-001 1.65000e-001 1.70000e-001 1.72500e-001  &
   1.75000e-001 1.80000e-001 1.85000e-001 1.90000e-001  &
   1.95000e-001 2.00000e-001 2.25000e-001 2.50000e-001  &
   2.60000e-001 2.75000e-001 2.85000e-001 3.00000e-001  &
   3.12500e-001 3.25000e-001 3.37500e-001 3.50000e-001  &
   3.60000e-001 3.70000e-001 3.85000e-001 4.00000e-001  &
   4.50000e-001 5.00000e-001 5.01000e-001 5.50000e-001  &
   5.75000e-001 5.95000e-001 5.97500e-001 6.00000e-001  &
   6.20000e-001 6.35000e-001 6.65000e-001 6.80000e-001  &
   6.90000e-001 7.00000e-001 7.20000e-001 7.35000e-001  &
   7.50000e-001 7.80000e-001 8.00000e-001 8.25000e-001  &
   8.50000e-001 9.00000e-001 9.50000e-001 1.00000e+000  &
   1.00100e+000 1.10000e+000 1.33000e+000 1.33500e+000  &
   1.40000e+000 1.50000e+000 1.60000e+000 1.66000e+000  &
   1.75000e+000 1.87500e+000 2.00000e+000 2.00100e+000  &
   2.16600e+000 2.33300e+000 2.50000e+000 2.66600e+000  &
   2.83300e+000 3.00000e+000 3.16600e+000 3.33300e+000  &
   3.50000e+000 3.65000e+000 3.80000e+000 3.90000e+000  &
   4.00000e+000 4.00100e+000 4.20000e+000 4.40000e+000  &
   4.50000e+000 4.70000e+000 5.00000e+000 5.00100e+000  &
   5.20000e+000 5.40000e+000 5.50000e+000 5.75000e+000  &
   6.00000e+000 6.00100e+000 6.25000e+000 6.50000e+000  &
   6.75000e+000 7.00000e+000 7.25000e+000 7.50000e+000  &
   7.75000e+000 8.00000e+000 8.00100e+000 8.50000e+000  &
   9.00000e+000 9.50000e+000 1.00000e+001 1.00010e+001
c
fc12 Transmitted Flux (1/cm^2-photon)
f12:p 5
ft12 inc      $ identify particles by collision (pg 3-106)
fu12 0 1 10  $ discriminate particles by collisions (3-99)
fq12 e u      $ tabulate by energy (y) & collisions (x) 3-87
fm12 4.0     $ multiply by 4 to get normalized flux
c
fc22 Transmitted H*(10) ICRP 74 pg.179   (Sv/cm^2-photon)
f22:p 5
ft22 inc      $ identify particles by collision (pg 3-106)
fu22 0 1 10  $ discriminate particles by collisions (3-99)
fq22 e u      $ tabulate by energy (y) & collisions (x) 3-87
fm22 4.0     $ multiply by to get flux (1/cm^2)   3-88
de22 1.00000e-002 1.50000e-002 2.00000e-002 3.00000e-002  &
     4.00000e-002 5.00000e-002 6.00000e-002 8.00000e-002  &
     1.00000e-001 1.50000e-001 2.00000e-001 3.00000e-001  &
     4.00000e-001 5.00000e-001 6.00000e-001 8.00000e-001  &
     1.00000e+000 1.50000e+000 2.00000e+000 3.00000e+000  &
     4.00000e+000 5.00000e+000 6.00000e+000 8.00000e+000  &
```

```
     1.00000e+001
c
df22 6.10000e-002 8.30000e-001 1.05000e+000 8.10000e-001  &
     6.40000e-001 5.50000e-001 5.10000e-001 5.30000e-001  &
     6.10000e-001 8.90000e-001 1.20000e+000 1.80000e+000  &
     2.38000e+000 2.93000e+000 3.44000e+000 4.38000e+000  &
     5.20000e+000 6.90000e+000 8.60000e+000 1.11000e+001  &
     1.34000e+001 1.55000e+001 1.76000e+001 2.16000e+001  &
     2.56000e+001
c
fc32 Transmitted Exposure   (exposure units)
*f32:p 5
ft32 inc      $ identify particles by collision (pg 3-106)
fu32 0 1 10  $ discriminate particles by collisions (3-99)
fq32 e u      $ tabulate by energy (y) & collisions (x) 3-87
fm32 4.0     $ multiply by to get flux (1/cm^2)   3-88
c  (mu_en)/rho from App. C (Table C7), Shultis & Faw
c  the star (*f31) tally multiplies flux by E for Exposure tally:
c   Exposure = Const*E*(mu_en/rho)*flux(E)  & Consts cancel w/buildup
de32 1.00000e-002 1.50000e-002 2.00000e-002 3.00000e-002  &
     4.00000e-002 5.00000e-002 6.00000e-002 8.00000e-002  &
     1.00000e-001 1.50000e-001 2.00000e-001 3.00000e-001  &
     4.00000e-001 5.00000e-001 6.00000e-001 8.00000e-001  &
     1.00000e+000 1.50000e+000 2.00000e+000 3.00000e+000  &
     4.00000e+000 5.00000e+000 6.00000e+000 8.00000e+000  &
     1.00000e+001
c
df32 4.74200e+000 1.33400e+000 5.38900e-001 1.53700e-001  &
     6.83300e-002 4.09800e-002 3.04100e-002 2.40700e-002  &
     2.32500e-002 2.49600e-002 2.67200e-002 2.87200e-002  &
     2.94900e-002 2.96600e-002 2.95300e-002 2.88200e-002  &
     2.78900e-002 2.54700e-002 2.34500e-002 1.87000e-002  &
     1.87000e-002 1.74000e-002 1.64700e-002 1.52500e-002  &
     1.45000e-002
c
fc42 Reflected Flux (1/cm^2-photon)
f42:p 6
fm42 4  $ multiply by 4 to get normalized flux (1/cm^2)   3-88
c
fc52 Reflected  H*(10) ICRP 74 pg.179   (Sv/cm^2-photon)
f52:p 6
fm52 4     $ mult by 4 to get normalized flux (1/cm^2)   3-88
de52 1.00000e-002 1.50000e-002 2.00000e-002 3.00000e-002  &
     4.00000e-002 5.00000e-002 6.00000e-002 8.00000e-002  &
     1.00000e-001 1.50000e-001 2.00000e-001 3.00000e-001  &
     4.00000e-001 5.00000e-001 6.00000e-001 8.00000e-001  &
     1.00000e+000 1.50000e+000 2.00000e+000 3.00000e+000  &
     4.00000e+000 5.00000e+000 6.00000e+000 8.00000e+000  &
     1.00000e+001
c
df52 6.10000e-002 8.30000e-001 1.05000e+000 8.10000e-001  &
     6.40000e-001 5.50000e-001 5.10000e-001 5.30000e-001  &
     6.10000e-001 8.90000e-001 1.20000e+000 1.80000e+000  &
     2.38000e+000 2.93000e+000 3.44000e+000 4.38000e+000  &
     5.20000e+000 6.90000e+000 8.60000e+000 1.11000e+001  &
     1.34000e+001 1.55000e+001 1.76000e+001 2.16000e+001  &
     2.56000e+001
c
fc62 Reflected Exposure   (exposure units)
*f62:p 6
ft62 inc      $ identify particles by collision (pg 3-106)
fu62 0 1 10  $ discriminate particles by collisions (3-99)
fq62 e u      $ tabulate by energy (y) & collisions (x) 3-87
fm62 4     $ multiply by to get flux (1/cm^2)   3-88
c  (mu_en)/rho from App. C (Table C7), Shultis & Faw
c  the star (*f31) tally multiplies flux by E for Exposure tally:
c   Exposure = Const*E*(mu_en/rho)*flux(E)  & Consts cancel w/buildup
de62 1.00000e-002 1.50000e-002 2.00000e-002 3.00000e-002  &
     4.00000e-002 5.00000e-002 6.00000e-002 8.00000e-002  &
     1.00000e-001 1.50000e-001 2.00000e-001 3.00000e-001  &
     4.00000e-001 5.00000e-001 6.00000e-001 8.00000e-001  &
     1.00000e+000 1.50000e+000 2.00000e+000 3.00000e+000  &
     4.00000e+000 5.00000e+000 6.00000e+000 8.00000e+000  &
     1.00000e+001
c
df62 4.74200e+000 1.33400e+000 5.38900e-001 1.53700e-001  &
     6.83300e-002 4.09800e-002 3.04100e-002 2.40700e-002  &
     2.32500e-002 2.49600e-002 2.67200e-002 2.87200e-002  &
     2.94900e-002 2.96600e-002 2.95300e-002 2.88200e-002  &
     2.78900e-002 2.54700e-002 2.34500e-002 1.87000e-002  &
     1.87000e-002 1.74000e-002 1.64700e-002 1.52500e-002  &
     1.45000e-002
c
fc11 Transmitted Current (1/cm^2-photon)
f11:p 5
ft11 inc      $ identify particles by collision (pg 3-106)
fu11 0 1 10  $ discriminate particles by collisions (3-99)
fq11 e u      $ tabulate by energy (y) & collisions (x) 3-87
c
fc21 Transmitted Current-H*(10) ICRP 74 pg.179   (Sv/cm^2-photon)
f21:p 5
ft21 inc      $ identify particles by collision (pg 3-106)
fu21 0 1 10  $ discriminate particles by collisions (3-99)
fq21 e u      $ tabulate by energy (y) & collisions (x) 3-87
de21 1.00000e-002 1.50000e-002 2.00000e-002 3.00000e-002  &
     4.00000e-002 5.00000e-002 6.00000e-002 8.00000e-002  &
     1.00000e-001 1.50000e-001 2.00000e-001 3.00000e-001  &
     4.00000e-001 5.00000e-001 6.00000e-001 8.00000e-001  &
     1.00000e+000 1.50000e+000 2.00000e+000 3.00000e+000  &
     4.00000e+000 5.00000e+000 6.00000e+000 8.00000e+000  &
     1.00000e+001
c
df21 6.10000e-002 8.30000e-001 1.05000e+000 8.10000e-001  &
     6.40000e-001 5.50000e-001 5.10000e-001 5.30000e-001  &
     6.10000e-001 8.90000e-001 1.20000e+000 1.80000e+000  &
     2.38000e+000 2.93000e+000 3.44000e+000 4.38000e+000  &
     5.20000e+000 6.90000e+000 8.60000e+000 1.11000e+001  &
     1.34000e+001 1.55000e+001 1.76000e+001 2.16000e+001  &
     2.56000e+001
c
fc31 Transmitted Current-Exposure   (exposure units)
*f31:p 5
ft31 inc      $ identify particles by collision (pg 3-106)
fu31 0 1 10  $ discriminate particles by collisions (3-99)
fq31 e u      $ tabulate by energy (y) & collisions (x) 3-87
c  (mu_en)/rho from App. C (Table C7), Shultis & Faw
c  the star (*f31) tally multiplies flux by E for Exposure tally:
c   Exposure = Const*E*(mu_en/rho)*flux(E)  & Consts cancel w/buildup
de31 1.00000e-002 1.50000e-002 2.00000e-002 3.00000e-002  &
     4.00000e-002 5.00000e-002 6.00000e-002 8.00000e-002  &
     1.00000e-001 1.50000e-001 2.00000e-001 3.00000e-001  &
     4.00000e-001 5.00000e-001 6.00000e-001 8.00000e-001  &
     1.00000e+000 1.50000e+000 2.00000e+000 3.00000e+000  &
     4.00000e+000 5.00000e+000 6.00000e+000 8.00000e+000  &
     1.00000e+001
c
```

```
df31 4.74200e+000 1.33400e+000 5.38900e-001 1.53700e-001  &
     6.83300e-002 4.09800e-002 3.04100e-002 2.40700e-002  &
     2.32500e-002 2.49600e-002 2.67200e-002 2.87200e-002  &
     2.94900e-002 2.96600e-002 2.95300e-002 2.88200e-002  &
     2.78900e-002 2.54700e-002 2.34500e-002 1.87000e-002  &
     1.87000e-002 1.74000e-002 1.64700e-002 1.52500e-002  &
     1.45000e-002
c
fc41 Reflected Current (1/cm^2-photon)
f41:p 6
c
fc51 Reflected  Current-H*(10) ICRP 74 pg.179   (Sv/cm^2-photon)
f51:p 6
de51 1.00000e-002 1.50000e-002 2.00000e-002 3.00000e-002  &
     4.00000e-002 5.00000e-002 6.00000e-002 8.00000e-002  &
     1.00000e-001 1.50000e-001 2.00000e-001 3.00000e-001  &
     4.00000e-001 5.00000e-001 6.00000e-001 8.00000e-001  &
     1.00000e+000 1.50000e+000 2.00000e+000 3.00000e+000  &
     4.00000e+000 5.00000e+000 6.00000e+000 8.00000e+000  &
     1.00000e+001
c
df51 6.10000e-002 8.30000e-001 1.05000e+000 8.10000e-001  &
     6.40000e-001 5.50000e-001 5.10000e-001 5.30000e-001  &
     6.10000e-001 8.90000e-001 1.20000e+000 1.80000e+000  &
     2.38000e+000 2.93000e+000 3.44000e+000 4.38000e+000  &
     5.20000e+000 6.90000e+000 8.60000e+000 1.11000e+001  &
     1.34000e+001 1.55000e+001 1.76000e+001 2.16000e+001  &
     2.56000e+001
c
fc61 Reflected Current-Exposure   (exposure units)
*f61:p 6
ft61 inc      $ identify particles by collision (pg 3-106)
fu61 0 1 10  $ discriminate particles by collisions (3-99)
fq61 e u      $ tabulate by energy (y) & collisions (x) 3-87
c  (mu_en)/rho from App. C (Table C7), Shultis & Faw
c  the star (*f31) tally multiplies flux by E for Exposure tally:
c   Exposure = Const*E*(mu_en/rho)*flux(E)  & Consts cancel w/buildup
de61 1.00000e-002 1.50000e-002 2.00000e-002 3.00000e-002  &
     4.00000e-002 5.00000e-002 6.00000e-002 8.00000e-002  &
     1.00000e-001 1.50000e-001 2.00000e-001 3.00000e-001  &
     4.00000e-001 5.00000e-001 6.00000e-001 8.00000e-001  &
     1.00000e+000 1.50000e+000 2.00000e+000 3.00000e+000  &
     4.00000e+000 5.00000e+000 6.00000e+000 8.00000e+000  &
     1.00000e+001
c
df61 4.74200e+000 1.33400e+000 5.38900e-001 1.53700e-001  &
     6.83300e-002 4.09800e-002 3.04100e-002 2.40700e-002  &
     2.32500e-002 2.49600e-002 2.67200e-002 2.87200e-002  &
     2.94900e-002 2.96600e-002 2.95300e-002 2.88200e-002  &
     2.78900e-002 2.54700e-002 2.34500e-002 1.87000e-002  &
     1.87000e-002 1.74000e-002 1.64700e-002 1.52500e-002  &
     1.45000e-002
c
e111 1e-2 10
fc111 Transmitted Current by angle (1/cm^2-photon)
f111:p 5
c111 0  0.1  0.2  0.3  0.4  0.5  0.6  0.7  0.8  0.9  1.0 t
ft111 frv 0 0 1
fq111 c e
c
e121 1e-2 10
fc121 Reflected Current by angle (1/cm^2-photon)
f121:p 6
c121 0  0.1  0.2  0.3  0.4  0.5  0.6  0.7  0.8  0.9  1.0 t
ft121 frv 0 0 -1
fq121 c e
```

C.3 NJOY input file

```
reconr
 30 31
 'pendf tape for photon interaction cross sections endl97'/
 8200 1 0
 .01/
 '82-pb'/
 0/
 gaminr
 30 31 0 33
 8200 1 3 8/
 '220 group photon library / p7'/
 220
 1.00000E+04
 1.03671E+04
 1.07600E+04
 1.12154E+04
 1.15637E+04
 1.19100E+04
 1.20998E+04
 1.22839E+04
 1.28241E+04
 1.30400E+04
 1.34185E+04
 1.38799E+04
 1.43528E+04
 1.48393E+04
 1.50000E+04
 1.52000E+04
 1.58600E+04
 1.69000E+04
 1.79300E+04
 1.89700E+04
 2.00000E+04
 2.12500E+04
 2.25000E+04
 2.37500E+04
 2.55140E+04
 2.62500E+04
 2.70000E+04
 2.72500E+04
 2.76000E+04
 2.80000E+04
 2.82000E+04
 2.85000E+04
 2.87000E+04
 2.90000E+04
 2.92500E+04
 2.95000E+04
 2.97500E+04
 3.00000E+04
 3.05000E+04
 3.10000E+04
 3.15000E+04
 3.20000E+04
 3.25000E+04
 3.31694E+04
 3.35000E+04
 3.40000E+04
 3.45000E+04
 3.47500E+04
 3.50000E+04
 3.55500E+04
 3.59846E+04
 3.62500E+04
 3.65000E+04
 3.67500E+04
 3.70000E+04
 3.72500E+04
 3.75000E+04
 3.77500E+04
 3.80000E+04
 3.82500E+04
 3.85000E+04
 3.87500E+04
 3.90000E+04
 3.92500E+04
 3.95000E+04
 3.97500E+04
 4.00000E+04
 4.05000E+04
 4.10000E+04
 4.12500E+04
 4.15000E+04
 4.17500E+04
 4.20000E+04
 4.22500E+04
 4.25000E+04
 4.27500E+04
 4.30000E+04
 4.32500E+04
 4.35000E+04
 4.37000E+04
 4.40000E+04
 4.42500E+04
 4.50000E+04
 4.60000E+04
 4.75000E+04
 4.85000E+04
 5.00000E+04
 5.10000E+04
 5.25000E+04
 5.35000E+04
 5.50000E+04
 5.75000E+04
 6.00000E+04
 6.50000E+04
 6.95250E+04
 7.61110E+04
 7.75000E+04
 8.07249E+04
 8.31023E+04
 8.60000E+04
 8.80000E+04
 9.00000E+04
 9.10000E+04
 9.20000E+04
 9.30000E+04
 9.40000E+04
```

```
9.50000E+04
9.60000E+04
9.70000E+04
9.80000E+04
9.90000E+04
1.00000E+05
1.25000E+05
1.30000E+05
1.35000E+05
1.37500E+05
1.40000E+05
1.45000E+05
1.50000E+05
1.56000E+05
1.57000E+05
1.62500E+05
1.65000E+05
1.70000E+05
1.72500E+05
1.75000E+05
1.80000E+05
1.85000E+05
1.90000E+05
1.95000E+05
2.00000E+05
2.25000E+05
2.50000E+05
2.60000E+05
2.75000E+05
2.85000E+05
3.00000E+05
3.12500E+05
3.25000E+05
3.37500E+05
3.50000E+05
3.60000E+05
3.70000E+05
3.85000E+05
4.00000E+05
4.50000E+05
5.00000E+05
5.01000E+05
5.50000E+05
5.75000E+05
5.95000E+05
5.97500E+05
6.00000E+05
6.20000E+05
6.35000E+05
6.65000E+05
6.80000E+05
6.90000E+05
7.00000E+05
7.20000E+05
7.35000E+05
7.50000E+05
7.80000E+05
8.00000E+05
8.25000E+05
8.50000E+05
9.00000E+05
9.50000E+05
1.00000E+06
1.00100E+06
1.10000E+06
1.33000E+06
1.33500E+06
1.40000E+06
1.50000E+06
1.60000E+06
1.66000E+06
1.75000E+06
1.87500E+06
2.00000E+06
2.00100E+06
2.16600E+06
2.33300E+06
2.50000E+06
2.66600E+06
2.83300E+06
3.00000E+06
3.16600E+06
3.33300E+06
3.50000E+06
3.65000E+06
3.80000E+06
3.90000E+06
4.00000E+06
4.00100E+06
4.20000E+06
4.40000E+06
4.50000E+06
4.70000E+06
5.00000E+06
5.00100E+06
5.20000E+06
5.40000E+06
5.50000E+06
5.75000E+06
6.00000E+06
6.00100E+06
6.25000E+06
6.50000E+06
6.75000E+06
7.00000E+06
7.25000E+06
7.50000E+06
7.75000E+06
8.00000E+06
8.00100E+06
8.50000E+06
9.00000E+06
9.50000E+06
1.00000E+07
1.00010E+07
-1 0/
0/
stop
dtfr
33 34 31 36
1 1 0
8 220 6 7 226 0 0
0/
'h' 100 1 0./
/
stop
```

C.4 CEPXS input file

```
title
0.5 MeV normal photons on 1mfp Pb
cutoff .01
energy 10.0005
legendre 7
electrons
 user 220
 1.00000E+01
 9.50000E+00
 9.00000E+00
 8.50000E+00
 8.00100E+00
 8.00000E+00
 7.75000E+00
 7.50000E+00
 7.25000E+00
 7.00000E+00
 6.75000E+00
 6.50000E+00
 6.25000E+00
 6.00100E+00
 6.00000E+00
 5.75000E+00
 5.50000E+00
 5.40000E+00
 5.20000E+00
 5.00100E+00
 5.00000E+00
 4.70000E+00
 4.50000E+00
 4.40000E+00
 4.20000E+00
 4.00100E+00
 4.00000E+00
 3.90000E+00
 3.80000E+00
 3.65000E+00
 3.50000E+00
 3.33300E+00
 3.16600E+00
 3.00000E+00
 2.83300E+00
 2.66600E+00
 2.50000E+00
 2.33300E+00
 2.16600E+00
 2.00100E+00
 2.00000E+00
 1.87500E+00
 1.75000E+00
 1.66000E+00
 1.60000E+00
 1.50000E+00
 1.40000E+00
 1.33500E+00
 1.33000E+00
 1.10000E+00
 1.00100E+00
 1.00000E+00
 9.50000E-01
 9.00000E-01
 8.50000E-01
 8.25000E-01
 8.00000E-01
 7.80000E-01
 7.50000E-01
 7.35000E-01
 7.20000E-01
 7.00000E-01
 6.90000E-01
 6.80000E-01
 6.65000E-01
 6.35000E-01
 6.20000E-01
 6.00000E-01
 5.97500E-01
 5.95000E-01
 5.75000E-01
 5.50000E-01
 5.01000E-01
 5.00000E-01
 4.50000E-01
 4.00000E-01
 3.85000E-01
 3.70000E-01
 3.60000E-01
 3.50000E-01
 3.37500E-01
 3.25000E-01
 3.12500E-01
 3.00000E-01
 2.85000E-01
 2.75000E-01
 2.60000E-01
 2.50000E-01
 2.25000E-01
 2.00000E-01
 1.95000E-01
 1.90000E-01
 1.85000E-01
 1.80000E-01
 1.75000E-01
 1.72500E-01
 1.70000E-01
 1.65000E-01
 1.62500E-01
 1.57000E-01
 1.56000E-01
 1.50000E-01
 1.45000E-01
 1.40000E-01
 1.37500E-01
 1.35000E-01
 1.30000E-01
```

```
1.25000E-01
1.00000E-01
9.90000E-02
9.80000E-02
9.70000E-02
9.60000E-02
9.50000E-02
9.40000E-02
9.30000E-02
9.20000E-02
9.10000E-02
9.00000E-02
8.80000E-02
8.60000E-02
8.31023E-02
8.07249E-02
7.75000E-02
7.61110E-02
6.95250E-02
6.50000E-02
6.00000E-02
5.75000E-02
5.50000E-02
5.35000E-02
5.25000E-02
5.10000E-02
5.00000E-02
4.85000E-02
4.75000E-02
4.60000E-02
4.50000E-02
4.42500E-02
4.40000E-02
4.37000E-02
4.35000E-02
4.32500E-02
4.30000E-02
4.27500E-02
4.25000E-02
4.22500E-02
4.20000E-02
4.17500E-02
4.15000E-02
4.12500E-02
4.10000E-02
4.05000E-02
4.00000E-02
3.97500E-02
3.95000E-02
3.92500E-02
3.90000E-02
3.87500E-02
3.85000E-02
3.82500E-02
3.80000E-02
3.77500E-02
3.75000E-02
3.72500E-02
3.70000E-02
3.67500E-02
3.65000E-02
3.62500E-02
3.59846E-02
3.55500E-02
3.50000E-02
3.47500E-02
3.45000E-02
3.40000E-02
3.35000E-02
3.31694E-02
3.25000E-02
3.20000E-02
3.15000E-02
3.10000E-02
3.05000E-02
3.00000E-02
2.97500E-02
2.95000E-02
2.92500E-02
2.90000E-02
2.87000E-02
2.85000E-02
2.82000E-02
2.80000E-02
2.76000E-02
2.72500E-02
2.70000E-02
2.62500E-02
2.55140E-02
2.37500E-02
2.25000E-02
2.12500E-02
2.00000E-02
1.89700E-02
1.79300E-02
1.69000E-02
1.58600E-02
1.52000E-02
1.50000E-02
1.48393E-02
1.43528E-02
1.38799E-02
1.34185E-02
1.30400E-02
1.28241E-02
1.22839E-02
1.20998E-02
1.19100E-02
1.15637E-02
1.12154E-02
1.07600E-02
1.03671E-02
1.00000E-02
photons
 user 220
1.00000E+01
9.50000E+00
9.00000E+00
8.50000E+00
8.00100E+00
8.00000E+00
7.75000E+00
7.50000E+00
7.25000E+00
7.00000E+00
6.75000E+00
```

6.50000E+00
6.25000E+00
6.00100E+00
6.00000E+00
5.75000E+00
5.50000E+00
5.40000E+00
5.20000E+00
5.00100E+00
5.00000E+00
4.70000E+00
4.50000E+00
4.40000E+00
4.20000E+00
4.00100E+00
4.00000E+00
3.90000E+00
3.80000E+00
3.65000E+00
3.50000E+00
3.33300E+00
3.16600E+00
3.00000E+00
2.83300E+00
2.66600E+00
2.50000E+00
2.33300E+00
2.16600E+00
2.00100E+00
2.00000E+00
1.87500E+00
1.75000E+00
1.66000E+00
1.60000E+00
1.50000E+00
1.40000E+00
1.33500E+00
1.33000E+00
1.10000E+00
1.00100E+00
1.00000E+00
9.50000E-01
9.00000E-01
8.50000E-01
8.25000E-01
8.00000E-01
7.80000E-01
7.50000E-01
7.35000E-01
7.20000E-01
7.00000E-01
6.90000E-01
6.80000E-01
6.65000E-01
6.35000E-01
6.20000E-01
6.00000E-01
5.97500E-01
5.95000E-01
5.75000E-01
5.50000E-01
5.01000E-01
5.00000E-01

4.50000E-01
4.00000E-01
3.85000E-01
3.70000E-01
3.60000E-01
3.50000E-01
3.37500E-01
3.25000E-01
3.12500E-01
3.00000E-01
2.85000E-01
2.75000E-01
2.60000E-01
2.50000E-01
2.25000E-01
2.00000E-01
1.95000E-01
1.90000E-01
1.85000E-01
1.80000E-01
1.75000E-01
1.72500E-01
1.70000E-01
1.65000E-01
1.62500E-01
1.57000E-01
1.56000E-01
1.50000E-01
1.45000E-01
1.40000E-01
1.37500E-01
1.35000E-01
1.30000E-01
1.25000E-01
1.00000E-01
9.90000E-02
9.80000E-02
9.70000E-02
9.60000E-02
9.50000E-02
9.40000E-02
9.30000E-02
9.20000E-02
9.10000E-02
9.00000E-02
8.80000E-02
8.60000E-02
8.31023E-02
8.07249E-02
7.75000E-02
7.61110E-02
6.95250E-02
6.50000E-02
6.00000E-02
5.75000E-02
5.50000E-02
5.35000E-02
5.25000E-02
5.10000E-02
5.00000E-02
4.85000E-02
4.75000E-02
4.60000E-02

```
4.50000E-02
4.42500E-02
4.40000E-02
4.37000E-02
4.35000E-02
4.32500E-02
4.30000E-02
4.27500E-02
4.25000E-02
4.22500E-02
4.20000E-02
4.17500E-02
4.15000E-02
4.12500E-02
4.10000E-02
4.05000E-02
4.00000E-02
3.97500E-02
3.95000E-02
3.92500E-02
3.90000E-02
3.87500E-02
3.85000E-02
3.82500E-02
3.80000E-02
3.77500E-02
3.75000E-02
3.72500E-02
3.70000E-02
3.67500E-02
3.65000E-02
3.62500E-02
3.59846E-02
3.55500E-02
3.50000E-02
3.47500E-02
3.45000E-02
3.40000E-02
3.35000E-02
3.31694E-02
3.25000E-02
3.20000E-02
3.15000E-02
3.10000E-02
3.05000E-02
3.00000E-02
2.97500E-02
2.95000E-02
2.92500E-02
2.90000E-02
2.87000E-02
2.85000E-02
2.82000E-02
2.80000E-02
2.76000E-02
2.72500E-02
2.70000E-02
2.62500E-02
2.55140E-02
2.37500E-02
2.25000E-02
2.12500E-02
2.00000E-02
 1.89700E-02
 1.79300E-02
 1.69000E-02
 1.58600E-02
 1.52000E-02
 1.50000E-02
 1.48393E-02
 1.43528E-02
 1.38799E-02
 1.34185E-02
 1.30400E-02
 1.28241E-02
 1.22839E-02
 1.20998E-02
 1.19100E-02
 1.15637E-02
 1.12154E-02
 1.07600E-02
 1.03671E-02
 1.00000E-02
photon-source
 full-coupling
material pb
print
 rows
direction
 normal
geometry 1
1 30 2.91136  50
```

C.5 Pandemonium input file

```
================================================================
GENERAL DATA
================================================================
gbNum, polyNum, sourceNum, detNum, time, criticality
 2  1  3  5  0  0
types of gloveboxes: gbType(1), gbType(2)...gbType(gbNum)
 0  1
================================================================
GLOVEBOX DATA
================================================================
glovebox positions: X, Y, Angle(degrees)
 18             48                          0
 26             42                          90
glovebox outer dimensions: Width, Height (feet)
 8              3
 8              3
glovebox shielding: Pb, Steel (cm)
 1              1
 1              1
================================================================
POLYSHIELD DATA: position & dimensions: X, Y, width, height (feet)
================================================================
24.42          42.00          0.17 8.00
================================================================
DETECTOR DATA: positions: X, Y
================================================================
23.00          42             0              0
18.00          45             0              0
12.00          43             0              0
18.00          42             0              0
20.00          39             0              0
================================================================
SOURCE DATA: positions & number densities (atoms/cm3)
================================================================
Source Number                        |
X              Y     Vx,  Vy         |
Rout           Rin   s/c  CylH        |
Pu238          Pu239       Pu240       |
Pu241          Pu242       Am241        |
U233           U235        U238          \
san1           snd1                       / FORMAT
san2           snd2                      |
san3           snd3                     |
san4           snd4                     |
ssan1          ssth1                   |
ssan2          ssth2                  |
**************************************************
Source 1
20.50          48.00          0              0
 5              0              0              0
 3.997E+18      3.733E+22      2.378E+21
 7.894E+19      3.931E+18      0
 0              0              0
 0              0
 0              0
 0              0
 0              0
 0              0
**************************************************
Source 2
26.00          42.00          0              0
 5              0              0              0
 3.997E+18      3.733E+22      2.378E+21
 7.894E+19      3.931E+18      0
 0              0              0
 0              0
 0              0
 0              0
 0              0
 0              0
 0              0
**************************************************
Source 3
26.00          40.00          0              0
 5              0              0              0
 3.997E+18      3.733E+22      2.378E+21
 7.894E+19      3.931E+18      0
 0              0              0
 0              0
 0              0
 0              0
 0              0
 0              0
 0              0
**************************************************
```

REFERENCES

1. Christenson, E., "Plutonium Processing at Los Alamos Scientific Laboratory," LA-3542, Los Alamos National Laboratory, 1969.

2. Briesmeister, J., ed., "MCNP4C – A General Monte Carlo N-Particle Transport Code," LA-13709-M, Los Alamos National Laboratory, 2000.

3. Waters, L., ed., "MCNPX User's Manual, Version 2.3.0," LA-UR-02-2607, Los Alamos National Laboratory, 2002.

4. O'Dell, R. et al., "Revised User's Manual for ONEDANT: A Code Package for One-Dimensional, Diffusion Accelerated, Neutral Particle Transport," LA-9184-M, Rev., Los Alamos National Laboratory, 1989.

5. Microshield Ver. 5 User's Manual, Grove Engineering, Rockville, MD., 1998.

6. Malenfant, R., "QAD: A Series of Point-Kernel General Purpose Shielding Programs," LA-3573, Los Alamos Scientific Laboratory, 1967.

7. Kornreich, D., Dooley, D., "A Two-Dimensional Point-Kernel Model for Dose Calculations in a Glovebox Array," *Trans. Am. Nucl. Soc.*, **81**, 249, 1999.

8. Kornreich, D., Dooley, D., "PANDEMONIUM: Bringing Order to Dose in Complicated Glovebox Arrays," LA-UR-99-2765, Los Alamos National Laboratory, 1999.

9. Los Alamos National Laboratory blueprint diagrams: LAKY-9363, LAKY-93511, LAKY-9331, 26Y-200382, Dates unknown.

10. Wilson, W., et al., "SOURCES-3A: A Code for Calculating (α,n) Spontaneous

Fission and Delayed Neutron Sources and Spectra," Los Alamos National Laboratory, LA-UR-97-4365, 1997.

11. Hetrick, D., Dynamics of Nuclear Reactors, The University of Chicago Press, Chicago, 1971.

12. Kornreich, D., "Reactivity Feedback Mechanisms in Aqueous Fissile Solutions," *Nucl. Sci. Eng.*, **115**, 50-61, 1993.

13. Sandenaw, T., Olsen, C., Gibney, R., "Heat Capacity of Plutonium Metal," LA-2398, Los Alamos National Laboratory, 1960.

14. Hansen, G., Roach, W., "Six and Sixteen Group Cross Sections for Fast and Intermediate Critical Assemblies," LAMS-2543, Los Alamos National Laboratory, 1961.

15. O'Dell, R., "Information on Hansen-Roach Cross Section Library and Use," Memo to W. Filippone, HSE-6-90-246, University of Arizona, 1990.

16. McLaughlin, T., "A Review of Criticality Accidents: 2000 Revision," LA-13638, Los Alamos National Laboratory, 2000.

17. ENDF/B-VI Nuclear Decay Data: http://t2.lanl.gov/data/decayd.html, 2001.

18. American National Standards Institute, "American National Standard for Gamma-Ray Attenuation Coefficients and Buildup Factors for Engineering Materials," Report ANSI/ANS-6.4.3-1991, American Nuclear Society, La Grange Park, Il., 1991.

19. Doggett, W.O., "Theoretical Dose Transmission and Reflection Probabilities for 0.2-10.0 MeV Photons Obliquely Incident on Finite Concrete Barriers," *Nuc. Sci. Eng.*, **39**, 92-104, 1970.

20. Fournie, E.M., Chilton, A.B., "Gamma-Ray Buildup Factors for Concrete Slab Shields Under Slant Incidence Conditions," *Nuc. Sci. Eng.*, **76**, 66-69, 1980.

21. Chen, M.F., Faw, R.E., "Build-up Factors for Gamma Rays Obliquely Incident on Slab Shields of Concrete, Iron, and Lead," *Rad. Prot. Dosim.*, **51**, 27-33, 1994.

22. Berger, M.J, Hubbell, J.H., Seltzer, S.M., Coursey, J.S., Zucker, D.S., "XCOM: Photon Cross Sections Database," http://physics.nist.gov/PhysRefData/Xcom/Text/XCOM.html, 1999.

23. Peele, R., Maienschein, F., "The Absolute Spectrum of Photons Emitted in Coincidence with Thermal-Neutron Fission of Uranium-235," ORNL-4457, Oak Ridge National Laboratory, 1970.

24. White, G., "The Penetration and Ddiffusion of ^{60}Co Gamma-Rays in Water Using Spherical Geometry," *Phys. Rev.*, **80**, 154, 1950.

25. Harima, Y., "An Historical Review and Current Status of Buildup Factor Calculations and Applications," *Radiat. Phys. Chem.*, **41**, 4/5, 631, 1993.

26. Goldstein H., Wilkins, J., "Calculation of the Penetration of Gamma Rays," NYO-3075, Nuclear Development Associates, Inc., 1954.

27. Hirayama, H., Tanaka, S., Sakamoto, Y., Subbaiah, K., Harima, Y., "Comparison of Gamma-Ray Point Isotropic Buildup Factors Including Fluorescence and Bremsstrahlung in Lead Using Discrete-Ordinates and Point Monte Carlo Methods," *J. Nucl. Sci. Tech.*, **27**, 6, 524, 1990.

28. Hirayama, H., Trubey, D., "Effects of Incoherent and Coherent Scattering on the

Exposure Buildup Factors of Low-Energy Gamma Rays," *Nucl. Sci. Eng.*, **99**, 145, 1988.

29. Kitsos, S., et.al., "Determination of Point Isotropic Buildup Factors of Gamma Rays Including Incoherent and Coherent Scattering for Aluminum, Iron, Lead, and Water by the Discrete-ordinates Method," *Nucl. Sci. Eng.*, **117**, 47-66, 1994.

30. Kitsos, S., et. al., "Improvement of Gamma-Ray S_N Transport Calculations Including Coherent and Incoherent Scatterings and Secondary Sources of Bremsstrahlung and Florescence: Determination of Gamma-Ray Buildup Factors," *Nucl. Sci. Eng.*, **123**, 215-227, 1996.

31. Harima, Y., Nishiwaki, Y., "An Approximation of Gamma-Ray Buildup Factors by Geometrical Progression," *Nucl. Eng. Des.*, **23**, 209, 1972.

32. Harima, Y., "An Approximation of Gamma-Ray Buildup Factors by Modified Geometrical Progression," *Nucl. Sci. Eng.*, **83**, 299, 1983.

33. Harima, Y., "An Approximation of Gamma-Ray Buildup Factors for Two-Layer Shields," *Nucl. Sci. Eng.*, **85**, 45, 1983.

34. Assad, A., Chrion, M., Nimal, J., Diop, C., "A New Approximating Formula for Calculating Gamma-Ray Buildup Factors in Multilayer Shields," *Nuc. Sci. Eng.*, **132**, 203, 1999.

35. Peebles, G., "Gamma Ray Transmission through Finite Slabs," R-240, Rand Corporation, 1952.

36. Hubbell, J., "Photon Mass Attenuation and Energy-Absorption from 1 keV to 20 MeV," *Int. J. Appl. Radiat. Isot.*, **33**, 1269-1290, 1982.

37. Cross Section Evaluation Working Group, "ENDF 102 Data Formats and Procedures for the Evaluated Nuclear Data File ENDF/VI," BNL-NCS-44945-01, Brookhaven National Laboratory, 2001.

38. MacFarlane, R., Muir, D., "The NJOY Nuclear Data Processing System, Version 91," LA-12740-M, Los Alamos National Laboratory, 1994.

39. Cullen, D., Hubbell, J., Kissel, L., "EPDL97: The Evaluated Photon Data Library, '97 Version," UCRL-50400 Vol. 6 Rev. 5, University of California, 1997.

40. Alcouffe, R., Baker, R., Turner, S., Dahl, J., "PARTISN Manual," LA-UR-02-5633, Los Alamos National Laboratory, 2002.

41. Daskalov, G., et. al., "Two-Dimensional Discrete-ordinates Photon Transport Calculations for Brachytherapy Dosimetry Applications," *Nuc. Sci. Eng.*, **134**, 121-134, 2000.

42. Lorence, Jr., L., Morel, J., Valdez, G., "Physics Guide to CEPXS: A Multigroup Coupled Electron–Photon Cross–Section Generating Code, version 1.0," SAND89–1685, Sandia National Laboratories, 1989.

43. Biggs, F., Lighthill, R., "Analytical Approximations for X-ray Cross Sections," SC-RR-452, Sandia Laboratories, 1967.

44. Biggs, F., Lighthill, R., "Analytical Approximations for Total Pair-Production Cross Sections," SC-RR-68-619, Sandia Laboratories, 1968.

45. Halblieb, J., Mehlhorn, T., "ITS: The Integrated TIGER Series of Coupled Electron/Photon Monte Carlo Transport Codes," SAND-84-0573, Sandia National Laboratories, 1984.

46. Kim, S., "Gauss-Lobatto F77Code," Department of Mathematics, University of Kentucky. http://www.ms.uky.edu/~skim/GRADE/basic.html, 2004.

47. Hubbell, J., Seltzer, S., " Tables of X-Ray Attenuation Coefficients 1 keV to 20 MeV for Elements Z=1 to 92 and 48 Additional Substances of Dosimetric Interest," Report NISTIR 5632, National Institute of Standards and Technology, 1995.

48. International Commission on Radiological Protection, "Conversion Coefficients for use in Radiological Protection against External Radiation," ICRP Publication 74, Pergamon Press, Oxford, 1997.

49. White, M., "Photoatomic Data Library MCPLIB04: A New Photoatomic Library Based on Data from ENDF/B-VI Release 8," LA-UR-03-1019, Los Alamos National Laboratory, 2003.

50. Chen, M., "Transmission and Reflection of Gamma and X-rays Incident on Shielding Slabs: Detailed Treatment of Fluorescence and Bremsstrahlung," Ph.D. Dissertation, Kansas State University, 1993.

51. Hirayama, H., "Calculation of Gamma-ray Exposure Buildup Factors up to 40 mfp Using the EGS4 Monte Carlo Code with a Particle Splitting," *J. Nucl. Sci. Tech.*, **32**, 12, 1201, 1995.

52. Chibani, O., "New Photon Buildup Factors," *Nuc. Sci. Eng.*, **137**, 215-225, 2001.

53. Dudziak, D., Shmucker, J., "Hydrogenous-Material Dependent Removal Cross section of Lead for Fast Neutron Biological Dose," Report TM-662, Bettis Atomic Power Laboratory, 1964.

54. Blizard, E. (ed), Reactor Handbook: Volume III, Part B, 2nd ed., Interscience Publishers, New York, 1962.